

**IMPROVED STEAM ASSISTED GRAVITY DRAINAGE (SAGD)
PERFORMANCE WITH SOLVENT AS STEAM ADDITIVE**

A Dissertation

by

WEIQIANG LI

Submitted to the Office of Graduate Studies of
Texas A&M University
in fulfillment of the requirements for the degree of
DOCTOR OF PHILOSOPHY

December 2010

Major Subject: Petroleum Engineering

**IMPROVED STEAM ASSISTED GRAVITY DRAINAGE (SAGD)
PERFORMANCE WITH SOLVENT AS STEAM ADDITIVE**

A Dissertation

by

WEIQIANG LI

Submitted to the Office of Graduate Studies of
Texas A&M University
in fulfillment of the requirements for the degree of

DOCTOR OF PHILOSOPHY

Approved by:

Chair of Committee,
Committee Members,

Head of Department,

Daulat D. Mamora
Walter B. Ayers
Jerome J. Schubert
Yuefeng Sun
Stephen A. Holditch

December 2010

Major Subject: Petroleum Engineering

ABSTRACT

Improved Steam Assisted Gravity Drainage (SAGD) Performance with Solvent
as Steam Additive. (December 2010)

Weiqiang Li, B.S., Shandong University;

M.S., Texas A&M University

Chair of Advisory Committee: Dr. Daulat D. Mamora

Steam Assisted Gravity Drainage (SAGD) is used widely as a thermal recovery technique in Canada to produce a very viscous bitumen formation. The main research objectives of this simulation and experimental study are to investigate oil recovery mechanisms under SAGD process with different injection fluids, including steam, solvent or steam with solvent.

2D simulation studies based on typical Athabasca reservoir properties have been performed. Results show that a successful solvent co-injection design can utilize the advantages of solvent and steam. There is an optimal solvent type and concentration ratio range for a particular reservoir and operating condition. Long, continuous shale barriers located vertically above or near the wellbore delay production performance significantly. Co-injecting a multi-component solvent can flush out the oil in different areas with different drainage mechanisms from vaporized and liquid components. Placing an additional injector at the top of the reservoir results only in marginal improvement. The pure high-temperature diluent injection appears feasible, although further technical and economic evaluation of the process is required.

A 2D scaled physical model was fabricated that represented in cross-section a half symmetry element of a typical SAGD drainage volume in Athabasca. The experimental results show co-injecting a solvent mixture of C7 and xylene with steam gives better production performance than the injection of pure steam or steam with C7 at the study condition. Compared to pure steam injection runs (Run 0 and 1), coinjecting C7 (Run 2) with steam increases the ultimate recovery factor of oil inside the cell from 25% to 29% and decreases the ultimate CSOR from 2.2 to 1.9 and the ultimate CEOR from 4892 J/cm^3 to 4326 J/cm^3 ; coinjecting C7 and Xylene (Run 3) increases the ultimate recovery factor of oil from 25% to 34%, and decreases the ultimate CSOR 2.2 to 1.6 and the ultimate CEOR from 4892 J/cm^3 to 3629 J/cm^3 . Analyses of the experimental results indicate that partial pressure and the near wellbore flow play important roles in production performance.

In conclusion, a successful solvent injection design can effectively improve the production performance of SAGD. Further research on evaluating the performance of various hydrocarbon types as steam additives is desirable and recommended.

DEDICATION

To my family

ACKNOWLEDGEMENTS

I would like to express heartfelt gratitude to my committee chair, Dr. D. M. Mamora, for his support and guidance through my studying at Texas A&M University in the Department of Petroleum Engineering.

I am grateful for the experience I gained during the working on this research. I would also like to thank Dr. W. B. Ayers, Dr. Jerome J. Schubert, and Dr. Y. Sun for their relentless encouragement and academic support.

I am also thankful to my friends for making my time at Texas A&M University an awesome experience.

TABLE OF CONTENTS

	Page
ABSTRACT	iii
DEDICATION	v
ACKNOWLEDGEMENTS	vi
TABLE OF CONTENTS	vii
LIST OF FIGURES.....	ix
1. INTRODUCTION.....	1
1.1 Objectives of study.....	3
2. LITERATURE	5
2.1 Gravity drainage methods	5
2.2 Shale barrier effect	10
2.3 Scaling theory of physical model	11
3. SIMULATION STUDY.....	13
3.1 Athabasca properties	13
3.2 Simulation model	14
3.2.1 Phase behavior inside vapor chamber	16
3.2.2 Solvent type and concentration ratio	29
3.2.3 Shale barrier effect	44
3.2.4 High temperature diluent injection.....	59
4. EXPERIMENTAL STUDY	75
4.1 Analytical analysis	75
4.2 Experimental apparatus	77
4.2.1 Scaled physical model.....	79
4.2.2 Fluid injection and production system	82
4.2.3 Data measurement and recording system.....	83
4.3 Experimental workflow.....	84
4.3.1 Cell preparation	84

	Page
4.3.2 Experimental procedure	85
4.4 Experiment conditions.....	86
4.5 Experimental results and discussions.....	87
4.5.1 Production performance	87
4.5.2 Discussion	92
5. CONCLUSIONS AND RECOMMENDATIONS.....	98
5.1 Conclusions	98
5.2 Recommendations	100
REFERENCES.....	101
VITA	107

LIST OF FIGURES

		Page
Figure 1	2D cross section of gravity drainage processes with horizontal well application.	3
Figure 2	Viscosity of Athabasca is reduced significantly with increase in temperature regardless of pressure between 0.1 and 10 Mpa (Mehrotra and Svrcek, 1986).	13
Figure 3	Adding more solvent (C_6) to the heated Athabasca oil can reduce the viscosity of the mixture of oil and solvent further at constant temperature (Shu, 1984).	14
Figure 4	Well pattern used for simulation study. Left: whole well pattern; right: simulated half-well pattern.	15
Figure 5	Adding C_6 to the injection steam reduces both CEOR and CSOR of the pure steam injection.	17
Figure 6	C_6 coinjection improves the oil recovery factor of pure steam injection.	18
Figure 7	The production stages under both pure steam injection and C_6 coinjection cases can be interpreted as three subproduction stages; C_6 coinjection increases the oil production rates substantially during Stage 1 and 2; and the lower production rate during Stage 3 of C_6 coinjection is because less oil remains in the reservoir.	19
Figure 8	The three subproduction stages are divided with respect to its drainage height. The oil saturation property distribution profile at 396, 1003, and 1461 days are used to illustrate the different drainage heights during different subproduction stages. Steam flows up to meet the overburden during Stage 1, steam expands laterally along the overburden during Stage 2 and the drainage height keep decreases along the side of the well pattern during Stage 3.	20
Figure 9	Property profiles used to compare the pure steam injection and C_6 coinjection cases under different subproduction stages.	21

Figure 11	The property distribution profiles at 396, 1003 and 1461 days respectively are used to describe the property distribution during Stages 1, 2 and 3; the “dome “of each property curve along the study row indicates a film of the property is built along the fluid interface; and the “dip points” along the viscosity plots indicate a significant low viscosity value.....	26
Figure 12	95% quality steam at 202°C and 1,650 kPa is injected; based on the differences in boiling points between steam and solvents, C ₃ , C ₅ , C ₆ , C ₇ , C ₁₂ , and the solvent mixture of 80% C ₆ and 20% C ₇ are chosen to investigate the effect of solvent type on oil recovery.....	30
Figure 13	Production performance comparison between different simulations with different solvent types.....	32
Figure 14	Property distribution profiles at 1551 days under different simulations with different solvent types: Different solvents create different films of water, gas solvent, and liquid solvent, which mainly attribute to the boiling points discrepancy between steam and solvents.....	35
Figure 15	With the mole ratio of C ₇ increasing, (a) the recovery factor is increasing; (b) the lowest CEOR value is given by the 7 mole% C ₇ coinjection.....	39
Figure 16	Viscosity distribution at 1003 days for different simulations with different C ₇ ratios: C ₇ coinjection reduces the heated oil to a substantial lower value compared to pure steam injection case; the lowest viscosity value along the fluid inter face is the 3 mole% C ₇ case at 1003 days, which indicate there is an optimal concentration ratio to take the advantages of both steam and solvent.....	41
Figure 17	Viscosity distribution at 1003 days for different simulations with different C ₇ ratios: C ₇ coinjection reduces the heated oil to a substantial lower value compared to pure steam injection case; the lowest viscosity value along the fluid inter face is the 3 mole% C ₇ case at 1003 days, which indicate there is an optimal concentration ratio to take the advantages of both steam and solvent.....	42
Figure 18	Profiles of homogeneous case (Case 0) and heterogeneous cases (Case 1 - 4). Red grid: sand; blue bar: shale barrier.....	45

Figure 20	Production performance comparison among different cases, including steam injection rate, oil production rate, oil recovery factor and SOR, which shows that long continuous shale barriers located vertically above or near the wellbore delay production performance significantly.....	50
Figure 21	Property profiles at 1551 days for different strategies: C_7 in vapor phase passes through the narrow flow path at the end of the shale barrier and reduces the viscosity of oil further more efficiently than steam; C_{12} coinjection can accelerate the near-wellbore flow and reduce the residual oil saturation at the wellbore vicinity; the mixture of C_7 and C_{12} flushes out the residual oil from the areas above and under the shale barrier; and the top injection application combines steam flooding mechanism from top injector and gravity drainage mechanism from bottom injector.....	53
Figure 22	Production performance comparison between different operation strategies: Coinjecting the mixture of C_7 and C_{12} in Strategy 5 delivers the highest recovery factor and the lowest CEOR among all investigated strategies.....	56
Figure 23	Phase behavior profiles in the reservoir: the high-temperature C_6 injection significantly accelerates the vapor chamber propagation compared to steam injection.....	60
Figure 24	Property distribution profiles at 1095 days along a horizontal row under both high-temperature C_6 injection and steam injection.....	61
Figure 25	Cumulative oil production and recovery factor under high-temperature C_6 injection are much higher than under steam injection.....	65
Figure 26	Oil production rate of high-temperature C_6 injection is about 1.5 to 2 times the rate of steam injection.....	66
Figure 27	Comparison between the injection solvent/oil ratio under high temperature C_6 injection and the steam oil ratio (SOR) under steam Injection.....	67
Figure 28	Circulation system proposed to reduce the solvent cost under high temperature solvent injection process.....	68

Figure 29	Effective solvent/oil ratios under high-temperature C ₆ injection with different leakage ratios, and steam oil ratio (SOR) under steam injection with no leakage.....	70
Figure 30	CEORs under high-temperature C ₆ injection and under steam injection, which shows the energy efficiency under high-temperature C ₆ injection is substantially higher than under steam injection.....	71
Figure 31	Comparison of solvent vaporization temperature with steam temperature at study pressure (from Nasr <i>et al.</i> (2003 and 2006)).....	76
Figure 32	Variation of the oil drainage rate with carbon number at study conditions (from Nasr <i>et al.</i> (2003 and 2006)).....	76
Figure 33	Photo showing the laboratory system: the drum jacket containing SAGD cell is used to isolate the surrounding infrared noise; the concrete on the top and at the bottom of the cell is used to simulate the heat loss through over burden and under burden; the data logger under the jacket is used to record the temperature distribution from thermal camera; and the other data logger on the control panel is used to monitor the injection and production data.....	78
Figure 34	Schematic diagram of experimental apparatus.....	79
Figure 35	Schematic of the scaled physical model.....	80
Figure 36	Back view of the physical model to show the distribution of the copper pins, which are used to transmit the temperature from inside of the cell to outside.....	81
Figure 37	Heat loss error introduced by boundary effects caused by the use of finite surrounding formations.....	82
Figure 38	FLIR A20M thermal video system.....	83
Figure 39	Comparison of injected solvent vaporization temperature with steam temperature.....	87
Figure 40	Comparison of oil production rates among experimental runs.....	90

Figure 41	Comparison of cumulative oil productions and oil recovery factors among experimental runs.....	90
Figure 42	Comparison of CSOR among experimental runs.....	91
Figure 43	Comparison of CEOR among experimental runs.....	91
Figure 44	Comparison of temperature distribution at 4 and 7 hours among experimental runs.....	92
Figure 45	Comparison of vapor pressure under Run 2 and Run 0 (Run 1).....	94
Figure 46	Comparison of vapor pressure under Run 3 with under Run 0 (Run 1)..	95

1. INTRODUCTION

As conventional hydrocarbon resources are being depleted rapidly, the increasing world demand for energy drives the petroleum industry to develop more unconventional oil reservoirs. World resources of bitumen and heavy oil together are estimated to be barrels, of which over 80% are located in Venezuela, Canada and USA. Over 95% of the bitumen deposits in North America are located in Alberta. The oil sands of northern Alberta are the largest bitumen sands in the world and cover a surface area exceeding 140,000 square kilometers, with an estimated initial volume in place of 270 billion cubic meters (1.7 trillion barrels), with the largest estimate being 2.5 trillion barrels. It is estimated that approximately 300 billion barrels are ultimately recoverable and over 3.0 billion barrels have been classified as proven reserves (Hein and Marsh, 2008 and Beach and Purdy, 1997).

Many production techniques have been developed to recover the Canadian heavy oil in the region of Alberta since the early 1980's. Oil sands consist of bitumen in natural reservoir conditions such that the oil is too viscous to flow into a wellbore. These techniques are diverse and can be divided into three main categories: surface mining, primary production and in-situ methods. The in-situ methods embody the last decades' technological advances to face the high viscosity of these mainly by thermal processes. The use of steam and then solvent, or both, has been combined with horizontal drilling to take advantage of gravity to deliver higher rates and recovery with lower energy required

The dissertation follows the style of *Society of Petroleum Engineers Journal*.

for oil production. Horizontal well application is used to improve reservoir contact with reduced distance for oil flow. The increased contact area between wellbore and reservoir can significantly reduce the injected fluid bypass problem (Butler, 1994).

Steam-assisted gravity drainage (SAGD) (Butler, 1994), vapor extraction or VAPEX (Nasr et al. 2003, 2005, and 2006) and steam-alternating solvent (SAS) (Zhao, 2004 and Zhao et al. 2004) methods are similar in principle (see Fig. 1). They all apply a horizontal injection well with an underlying production well. The fluid is injected through a top injection well to create a chamber in which the viscosity of bitumen is reduced. Then gravity drags it to the bottom well.

The difference among these four methods lies in the type of fluid injected and the by-product fluids. SAGD consists of steam injection which heats the oil; VAPEX involves injection of solvents that react with the bitumen and dissolve it; and ES-SAGD and SAS involve injection of both steam and solvent. The produced fluids in each process include the condensed injection fluid and the lower viscosity oil. In SAGD, large volumes of water and natural gas are required for steam generation. The production rate in VAPEX is lower than those processes that use heat such as SAGD. An advantage of VAPEX is that oil is upgraded in-situ and leaves behind a significant amount of the heavier hydrocarbons in the reservoir.

During ES-SAGD and SAS processes, the production performance is improved by co-injecting solvent and steam instead of using steam only to take advantage of the solvent effect. In the ES-SAGD process, the solvent is co-injected continuously, while the SAS process involves injecting steam and solvent alternately. Depending on the type

of solvent and the long term operating pressure, about 90% of the injected solvent can be reproduced with the bitumen, and about 75% of the solvent retained may be recovered during the following blow down phase (ConocoPhillips, 2009). This study modeled an ES-SAGD process to investigate the phase behavior of solvent and steam inside the steam chamber.

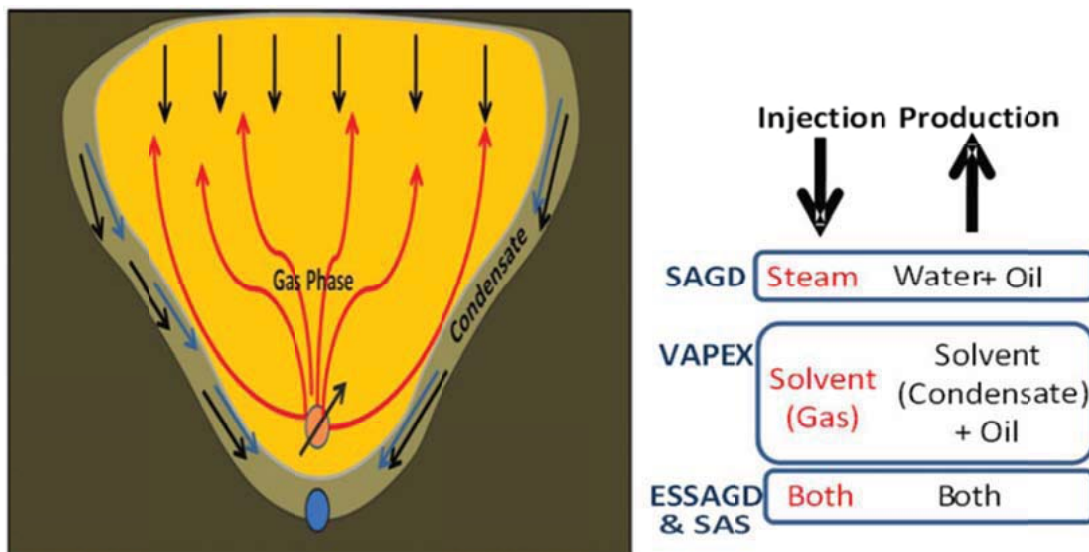


Fig. 1-2D cross section of gravity drainage processes with horizontal well application.

1.1 Objectives of study

Main research objectives of this study are to conduct experimental modeling and simulation studies to investigate oil recovery mechanisms and steam injection efficiency during production of Athabasca bitumen under Steam Assisted Gravity Drainage (SAGD). Additionally, the research will also investigate the feasibility of using a hydrocarbon solvent as a steam additive and high temperature diluent injection to

improve SAGD efficiency. The impact of shale barriers on oil recovery during SAGD will also be investigated.

The simulation study will utilize a 2D cross-sectional 31 x 1 x 30 Cartesian model to represent half a typical SAGD well-pattern in the Athabasca sands. Grid blocks are 1.7 m wide in the x-direction except for the three blocks near the z-axis where the wells are located. The grid blocks have a uniform thickness of 1 m in the z-direction. Typical rock and fluid properties and field operating conditions for Athabasca will be simulated. A 2D physical 1:131 scaled model made of 1-inch thick Teflon will be utilized that has internal cell dimensions of 15' wide x 9" tall x 1" thick. The cell will contain a mixture of Athabasca bitumen and glass beads. Expansion of the steam chamber, its shape and area, and temperature distribution will be visualized using a thermal (infra-red) video camera. Isotherms and steam chamber interface will be analyzed to study oil recovery and drainage mechanisms.

2. LITERATURE REVIEW

2.1 Gravity drainage methods

Chung and Butler (1987) experimentally investigated the effects of well spacing and steam temperature on SAGD oil recovery. They found much higher water/oil emulsion content in the produced fluid when the steam chamber was rising in experiments with bottom steam injection than in those with injection at the top. The water/oil emulsion increased the viscosity of the produced fluid and affected the oil recovery rate.

Butler and Mokrys (1991, 1993a, 1993b and 1993c) described a new recovery concept related to the steam assisted gravity drainage (SAGD) process. The process was intended to be used in thin reservoirs, where the application of SAGD alone was uneconomical due to the high heat losses to the formations above and below the reservoir. The process, called VAPEX, used a solvent, such as propane, which could form a vapor-filled chamber within the reservoir. Vapor dissolves in the oil around the chamber and the resulting solution drains, driven by gravity, to a horizontal production well placed low in the formation. A well, located at the top of the reservoir, is used to inject hot water and the solvent. Their results also showed that the process could be applied economically for heavy oil recovery. Additional advantages derived from VAPEX are a partial in-situ deasphalting and a reduction of the content of heavy metals. The resulting oil can be lighter, of a higher quality and better suited for direct refining.

Oballa and Buchanan (1996), and Elliott and Kavscek (1999) investigated single

well SAGD (SW-SAGD), in which steam is injected from the toe of the horizontal well and oil produced at the heel of the well. SW-SAGD process has advantages in thinner reservoirs where it is nearly impossible to drill two horizontal wells, but also provides a substantial cost saving associated with drilling one horizontal well rather than two. The key to apply SW-SAGD is to heat the near-wellbore region rapidly and uniformly so as to reduce the oil viscosity and promote gravity drainage. This can be performed by steam circulation within the wellbore or cyclic steam stimulation (CSS) with the horizontal well. The CSS process is the most thermally efficient early-time heating method. Although SW-SAGD is advantageous over conventional SAGD in thinner reservoirs, they suggested that the reservoir be sufficiently thick to allow significant vertical steam chamber growth.

Butler *et al.* (1997,1999,2000a, 2000b and 2001) developed the concept of steam and gas push (SAGP) process, in which a fraction of non-condensable gas is injected together with steam so that the non-condensable gas accumulates in the steam chamber, particularly near the top of the reservoir. In the SAGP process, the major heat transfer mechanism is thermal conduction. Heat transfer by diffusive steam flow and convection is significant in the region at the saturated steam temperature around the injection and production wells and becomes less important as temperature falls. SAGP has lower temperatures in the region where gas fingers rise and oil drains above the steam condensation zone. This is also a source of steam saving. Based on their test results, Butler indicated that for both uniform and layered models, SAGP produced similar oil rates as SAGD but with lower steam consumption.

Polikar *et al.* (2000) proposed fast-SAGD process, which combines the SAGD and CSS processes to help propagate the steam chamber formed by SAGD sideways. In this process, after starting the first pair of horizontal wells with the SAGD process, a set of equidistant single horizontal wells is used to propagate the steaming process down the reservoir. This process can partly solve the challenge of drilling the two horizontal wells one exactly above the other and reduce costs in a SAGD operation, and also enhance the thermal efficiency in the reservoir.

Sasaki *et al.* (2001) introduced a modified process, named SAGD-ISSLW (intermittent steam stimulation of lower well). Instead of continuous production from the lower producer, it was intermittently stimulated by steam injection, in conjunction with steam injection in the upper injector. Using this method, the time to generate a near breakthrough condition between two wells was shortened, and oil production was enhanced at the rising chamber stage as compared with that of the conventional SAGD process.

Nasr *et al.* (2001, 2003, 2005 and 2006) developed Expanding Solvent SAGD (ES-SAGD) process, which is one of the modifications of the SAGD process combining the benefits of steam and solvents in the recovery of heavy oil and bitumen. The solvent is injected with steam in a vapor phase, and then the condensed solvent around the interface of the steam chamber dilutes the oil in conjunction with heat, and reduces its viscosity. Compared to conventional SAGD, this process can improve oil production rate and decrease SOR, energy and water requirements.

Zhao *et al.* 2003 proposed wind-down process which uses the non-condensable gas

(NCG) or mixture of NCG and steam injection to maintain reservoir pressure and prolong oil production. At a certain point during the SAGD process, it is no longer economic to operate SAGD with steam injection due to high SOR. It is appropriate to start a wind-down process. Injecting NCG results in a much lower production cost compared to continued steam injection; however, the oil production is reduced. Laboratory experiments and corresponding numerical simulations were carried out to study a gas injection SAGD wind-down process. The laboratory test was conducted using a high-pressure, high-temperature 2D model. The test results showed that 12.5% of OOIP could be recovered by a non-condensable gas injection process following the SAGD operation. Temperature measurements demonstrated that the hot chamber continued to grow even after steam injection stopped.

Zhao, 2004 and Zhao *et al.* 2004 proposed a new heavy oil recovery process, Steam Alternating Solvent (SAS) process. The process is intended to combine the advantages of the SAGD and VAPEX processes to minimize the energy input per unit oil recovered. The SAS process involves injecting steam and solvent alternately, and the basic well configurations are the same as those in the SAGD process. Numerical simulations were conducted to assess the process performance under typical Cold Lake reservoir conditions using CMG STARS. Based on preliminary estimation, the energy input per unit of oil recovered using SAS process is 18% less than that using SAGD process.

Deng (2005) modeled a typical Athabasca SAGD pattern under pure steam injection and steam-propane injection. Results showed that oil recovery was accelerated

by using propane as an additive, irrespective of the amount of propane used. Ultimate oil recovery was, however, dependent on the amount of propane injected. Lower recoveries were obtained when higher concentrations of propane were injected.

Belgrave *et al.* (2007) proposed the use of air injection as a follow-up process to SAGD operations. Laboratory work has demonstrated the feasibility of maintaining a burning front in a mature steam chamber. Simulation studies indicate the potential to significantly increase the recovery factor over methane blow-down and at the same time sequester the flue gases.

Stalder *et al.* (2007) investigated the Cross SAGD (XSAGD) process. The concept is to drill the injection wells above the production wells with spacing similar to that used in SAGD, but unlike SAGD, the injectors are placed perpendicular to the producers. Portions of the wells near the crossing points are plugged after a period of steam injection, or the completion design may restrict flow near these crossing points from the start. The increased lateral distance between the injecting and producing segments of the wells improves the steam-trap control because steam vapor tends to override the denser liquid phase as injected fluids move laterally away from the injector. This allows rates to be increased while avoiding live steam production. Simulation study showed XSAGD appears to have a greater advantage over SAGD at lower pressures (1500 kPa) than at higher pressures (3000 kPa).

In N-Solv process (Nenniger, J. and Nenniger, E., 2008), propane is injected into the reservoir at its condensing condition and condenses inside the extraction chamber to take advantage of both heat and dilution effects. No published experimental results and

field applications are available, but there are many disadvantages associated with this process. For example, the temperature of propane is higher than under VAPEX but is much lower than under SAGD due to the maximum allowable saturation pressure of propane. Considering the heat capacity and saturation temperature of propane is much lower than steam, an accelerated production rate of this process over SAGD is skeptical. Meanwhile, the difficulties to apply a subcool strategy to retain the injected propane inside the extraction chamber are expected because of the high injection pressure and low temperature of propane. To purify propane from the produced fluid and reduce the propane lost at the surface also are difficult due to the small relative volatility of propane and methane. Solvent leakage from reservoir will be another critical issue to significantly increase the solvent cost because of the high pressure inside the extraction chamber.

In recent years, Alberta Research Council (ARC) conducted extensive studies with either ethane (C₂) or propane (C₃) (Frauenfeld *et al.* 2006, 2007, 2009 and Ivory, *et al.* 2010) as the injected solvent at non-condensing condition. Their results show much lower production rate and recovery factor than with steam injection. The main reasons are that the heat delivered by a solvent under non-condensing conditions is too small and the solubility of the solvent in the bitumen is too low to significantly reduce the oil viscosity.

2.2 Shale barrier effect

Real reservoirs are always heterogeneous due to their long and frequently complex histories of geological evolution. In particular,, vertical flow in a gravity drive process,

such as the SAGD process, is significantly affected by horizontal shale barriers distributed in the reservoir. Richardson *et al.* (1978) showed that the time required for oil drainage from a barrier is proportional to its width squared and viscosity, and inversely proportional to the horizontal permeability and density difference. Yang and Butler (1989) found that a short horizontal barrier does not significantly affect the general performance; a long barrier will decrease the production rate. Kisman and Yeung (1995) concluded that the effect of the barriers on performance is expected to be small unless they are both continuous over distances significantly greater than 15 m and stable under steam conditions.

Farouq-Ali (1997) showed that the observed steam chamber was oblate and expanded sideways rather than vertically to the top of the formation in Phase A of the Underground Test Facility (UTF) project. They attributed this to small differences in formation characteristics, as well as to convection in the lower part of the formation. Chen *et al.* (2007) showed that the drainage and flow of hot fluid within the near-wellbore area is of short characteristic length and is very sensitive to the presence and distribution of shale, while the area above the wellbore affects the (vertical and horizontal) expansion of the steam chamber that is of characteristic flow length on the order of half of formation height.

2.3 Scaling theory of physical model

Stegemeier *et al.* (1980) proposed a low-pressure model that uses vacuum and lower-than-ambient temperatures to scale steam injection. This technique requires

scaling of the fluid viscosities; therefore, synthetic oil with the scaled viscosity has to be used. The results showed that the quantity of steam injected was the most important factor affecting the amount of oil recovered.

Pujol and Boberg (1972) examined the scaling accuracy of laboratory steam flooding models, especially with regard to the scaling of capillary pressure. They found that, for highly viscous oils, accurate scaling of capillary pressure was not crucial.

Farouq Ali and Redford (1977) provided a thorough analysis of notable scaled laboratory thermal recovery studies. They examined the scaling groups derived for steam injection and in-situ combustion processes by various investigators.

Kimber *et al.* (1988, 1989, and 1991) studied new scaling criteria for steam and steam-additive injection experiments. In these studies, five different approaches were adopted, with each approach scaling a selected mechanism of the recovery process while relaxing the remaining mechanisms.

Chung and Butler (1987) carried out two-dimensional scaled reservoir models to investigate the SAGD theory. They found approximate agreements between experimental results and field performances.

3. SIMULATION STUDY

3.1 Athabasca properties

Viscosity of Athabasca oil is reduced from the initial value of 2×10^6 cp to 10 cp when it is heated to 200°C (Fig. 2). Because of the large latent heat of vaporization, steam can be used as an efficient medium to deliver heat to the vicinity of the oil interface to reduce the oil viscosity and so mobilize the heavy oil. The disadvantages of steam injection include (1) large amounts of water are required combined with limitation of water resources in the field, (2) large investment needed to build a facility to heat water for steam generation, and (3) cost of treatment of disposal water to meet the environmental regulations.

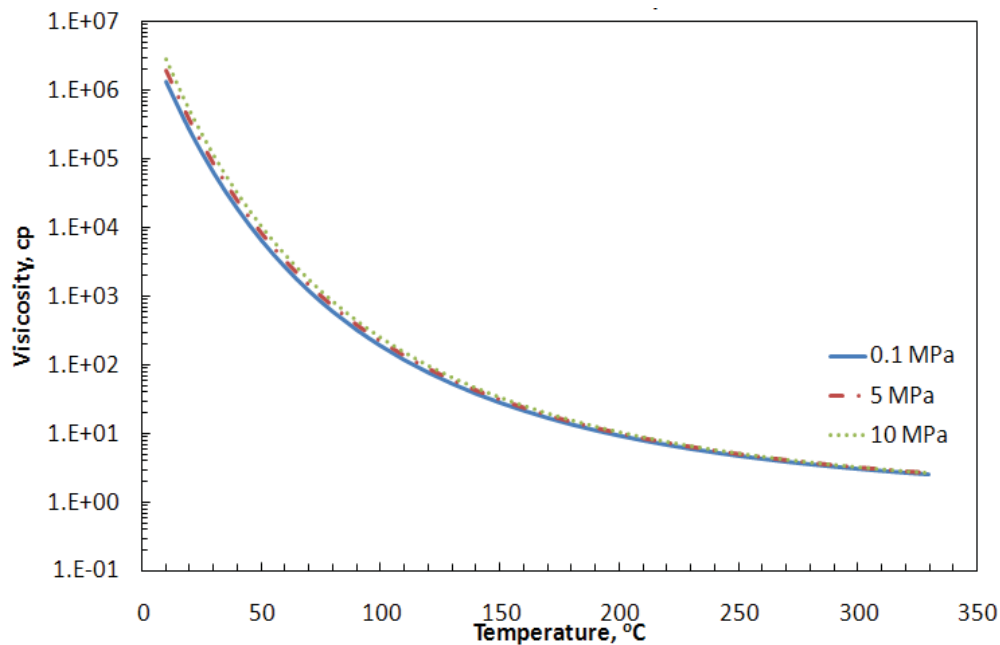


Fig. 2-Viscosity of Athabasca is reduced significantly with increase in temperature regardless of pressure between 0.1 and 10 Mpa (Mehrotra and Svrcek, 1986).

Fig. 3 shows that the viscosity of Athabasca oil is reduced further with solvent mixing the heated oil at constant temperature. Along with the 200°C curve, the oil viscosity is reduced to 4 cp with a solvent volume ratio of 0.1, and is only about 1 cp with the solvent volume ratio increased to 0.3. Therefore, combining both heat and solvent dilution effects reduces the oil viscosity much more efficiently than only using heat.

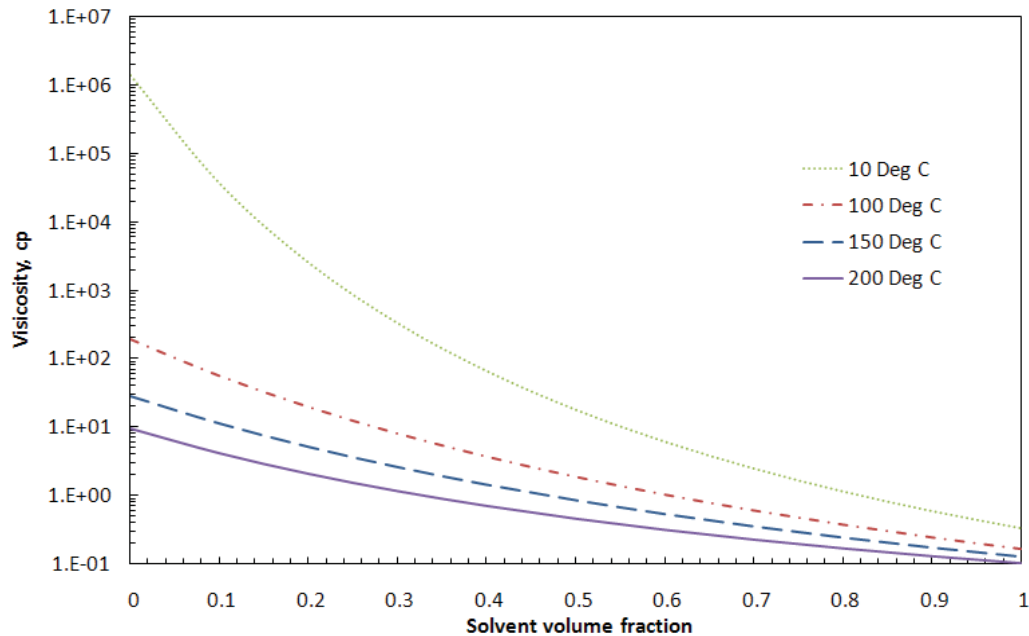


Fig. 3-Adding more solvent (C_6) to the heated Athabasca oil can reduce the viscosity of the mixture of oil and solvent further at constant temperature (Shu, 1984).

3.2 Simulation model

Assuming no pressure drop and flow resistance along the horizontal wellbore, a 2D simulation model is sufficient for studying reservoir phase behavior reservoir and production performance. The 2D prototype well pattern selected for this simulation

study is for an Athabasca reservoir with a horizontal section length of 500 m. The reservoir thickness is 30 m, and one whole well pattern width is 100 m. The producer is 1.5 m from the bottom of the reservoir and the space between injector and producer is 5 m. The well pattern is symmetrical, so only half the well pattern is used for this study (Fig. 4).

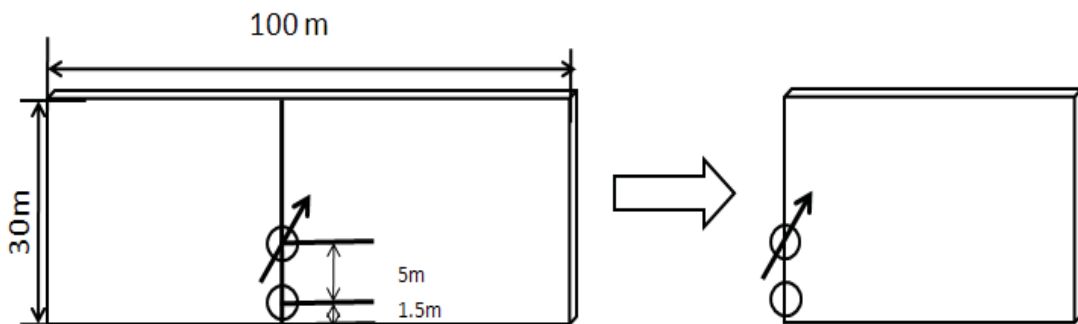


Fig. 4-Well pattern used for simulation study. Left: whole well pattern; right: simulated half-well pattern.

We used CMG STARS simulator for this simulation study. The 2D grid system includes 31 blocks along the horizontal direction with widths of 0.5 m, 0.7 m, and 1.2 m for the first three columns and all others of 1.7 m. The smaller grid widths of the first 3 columns permit better resolution at the wellbore vicinity. The model is divided into 30 blocks in the vertical direction, each 1 m high. The initial Athabasca reservoir conditions; properties of rock, water, and oil; and relative permeability data are those used by Law *et al.* (2000). The only difference is that the horizontal permeability is 6 darcy and the vertical permeability is 3 darcy in this study.

For steam injection, we inject 95% quality 202°C steam at 1,650 kPa at the injector, which is slightly higher than the initial reservoir pressure at 1,500 kPa. The production period for steam injection case is 10 years. The maximum water injection rate at surface is 500 m³/day and the subcool temperature difference between injector and producer is 20°C. The K-value correlation coefficients and pressure/volume/temperature (PVT) properties of solvents are the default values built in the CMG STARS library or from Poling *et al.* (2000). The produced oil volume is altered by the surface separation condition. In this study, the production of solvent and original oil is discussed separately with no solvent contained in the produced oil.

3.2.1 Phase behavior inside vapor chamber

A suitable solvent should be selected in such a way that it would evaporate and condense at the same conditions as the water phase in the ES-SAGD process. The selected hydrocarbon solvent would condense with condensed steam at the boundary of the steam chamber (Nasr, 2006). It is usual to inject a mixture of solvents in the field due to cost considerations and refinery limitations. In this study, we chose C₆ as the surrogate solvent since it has the closest boiling point to steam at injection conditions in this study. The concentration of C₆ in the total injected fluid stream is 5 mole%.

Cumulative steam/oil ratio (CSOR) and oil recovery factor are common parameters to evaluate the economic performance of a steam injection process. When solvents are coinjected with steam, cumulative energy required for cumulative produced oil volume (CEOR) is a better parameter than CSOR to assess the energy efficiency of the process.

Fig. 5 shows the CSOR and CEOR plots and Fig. 6 shows the oil recovery factor curve for both pure steam injection and solvent coinjection cases. From Fig. 5, solvent co-injection reduces CSOR by 10 to 15% compared to the pure steam injection for the whole production period. The CEOR value of the solvent coinjection case is about 5 to 10% less than the pure steam injection case during the early phase. The ultimate CEOR values of both cases are similar for a long production period, which is 10 years in this study. The observations indicate that solvent coinjection can save steam and natural gas required for oil production in the field.

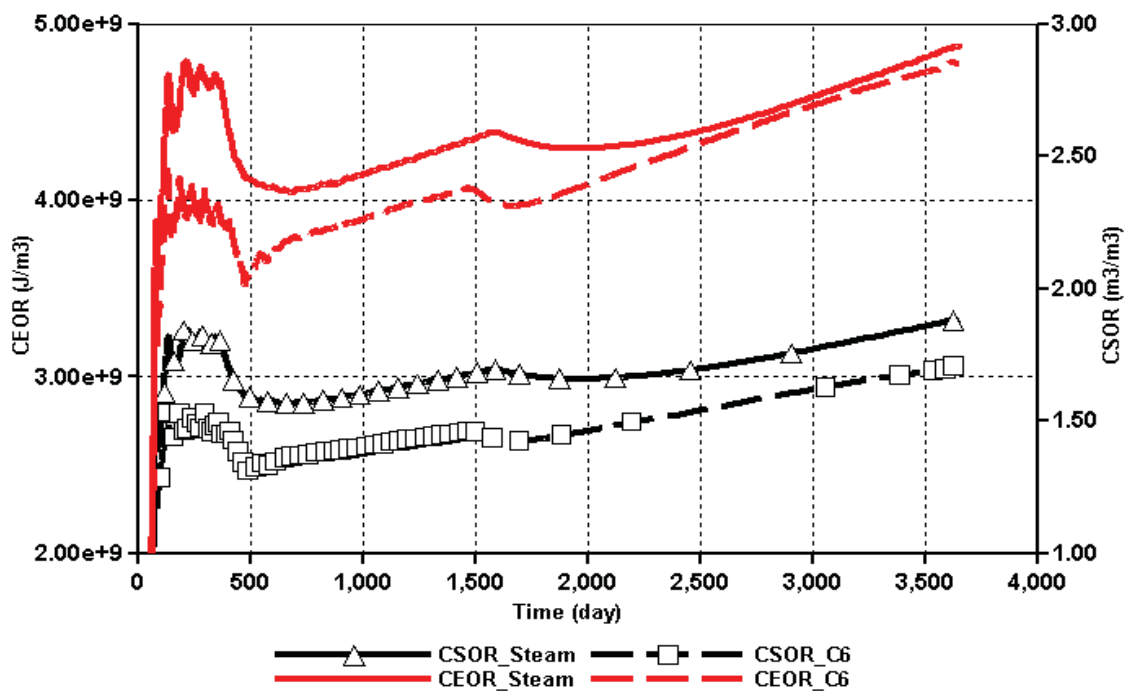


Fig. 5-Adding C_6 to the injection steam reduces both CEOR and CSOR of the pure steam injection.

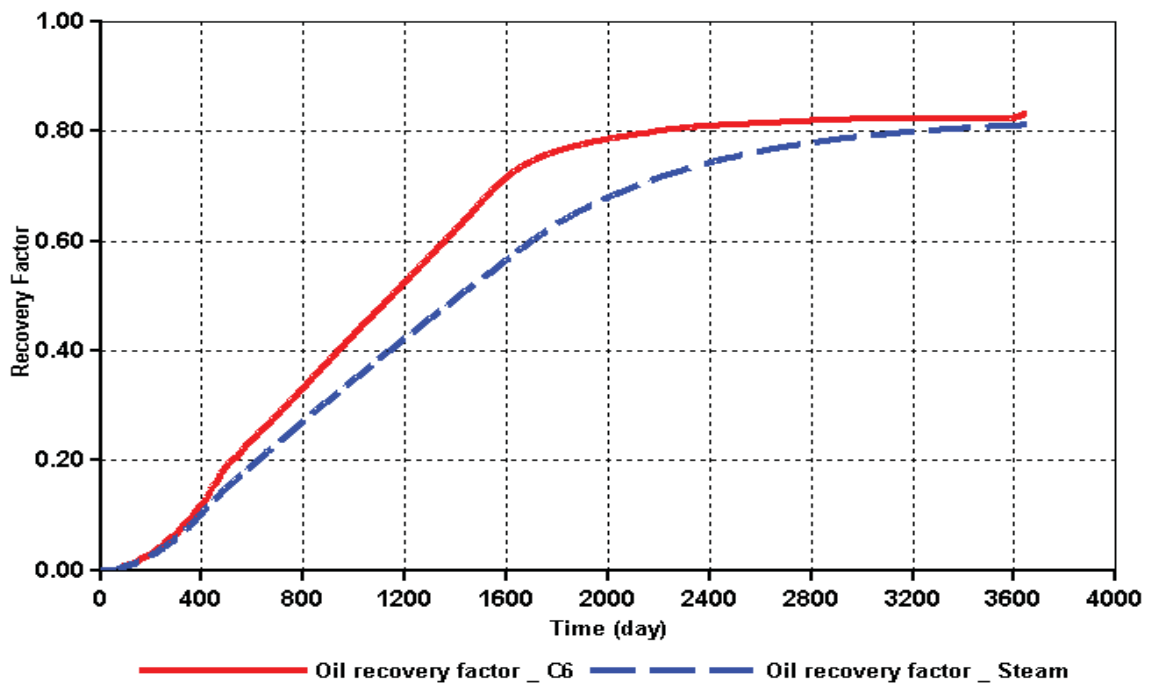


Fig. 6-C₆coinjection improves the oil recovery factor of pure steam injection.

The oil recovery factor for solvent coinjection is higher than for pure steam injection. In this study, the same set of permeability curves with the same end points are used for both cases. Inside the steam chamber, most C₆ stays in the vapor phase and so the difference of residual oil saturation under both cases is very small. All these lead to similar ultimate oil recovery factors under both cases (Fig. 6). Considering the accelerated production during the early production period, solvent coinjection delivers higher oil recovery factor and so returns a higher net present value (NPV).

Fig. 7 shows the production rate plots for both solvent coinjection and pure steam injection cases. The oil saturation distribution profiles at 396, 1,003, and 1,461 days for both cases are shown in Fig. 8. The oil drainage rate is proportional to the square root of drainage height based on Butler's theory. From Fig. 7 and Fig. 8, the entire production

period can approximately be divided into three subproduction stages with respect to its drainage height.

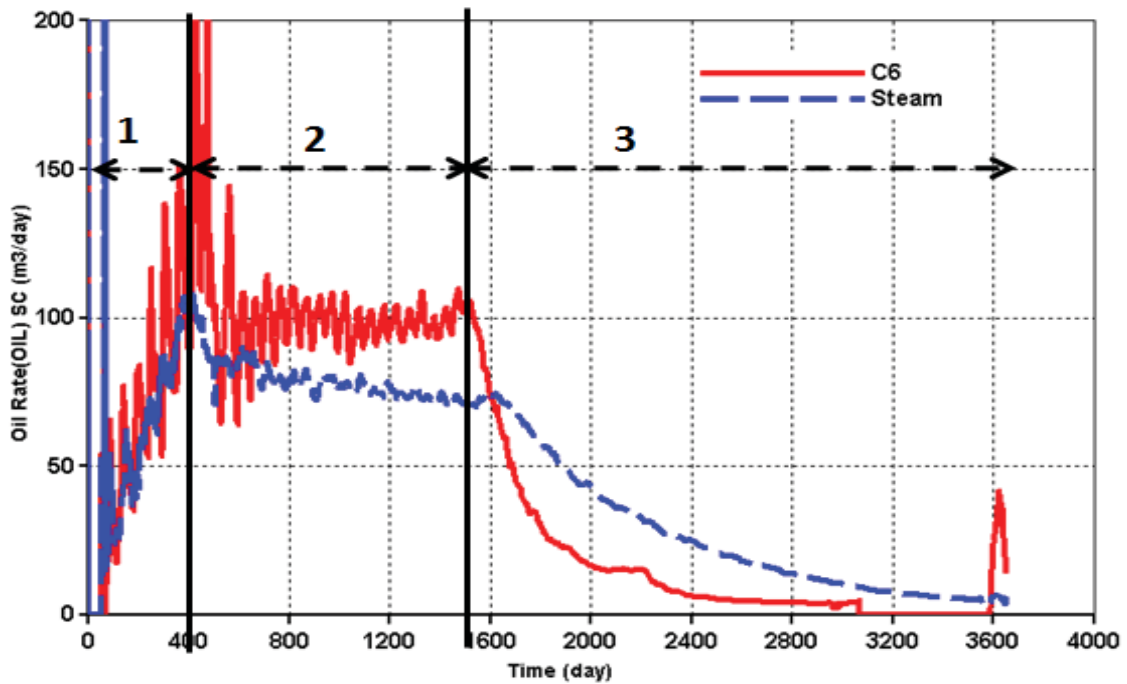


Fig. 7-The production stages under both pure steam injection and C₆ coinjection cases can be interpreted as three subproduction stages; C₆ coinjection increases the oil production rates substantially during Stage 1 and 2; and the lower production rate during Stage 3 of C₆ coinjection is because less oil remains in the reservoir.

Stage 1 (from 0 to 396 days): The oil production rate increases to a maximum value until the steam chamber reaches the overburden. Stage 2 (from 396 to 1,461 days): The oil production rate decreases to a roughly stable level until the steam chamber meets the side boundary. Stage 3 (after 1,461 days): The oil production rate and the drainage height decrease along the side boundary until the production period is finished.

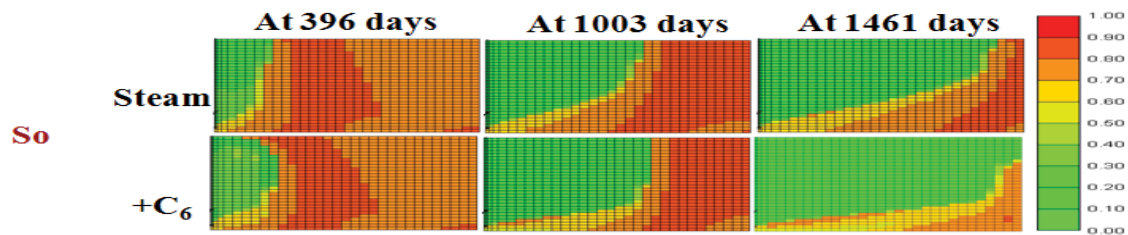


Fig. 8-The three subproduction stages are divided with respect to its drainage height. The oil saturation property distribution profile at 396, 1,003, and 1461 days are used to illustrate the different drainage heights during different subproduction stages. Steam flows up to meet the overburden during Stage 1, steam expands laterally along the overburden during Stage 2 and the drainage height keep decreases along the side of the well pattern during Stage 3.

The production rate of C_6 coinjection during Stages 1 and 2 is higher than that of pure steam injection, which illustrates the additional oil viscosity reduction by the solvent. The slightly decreasing trend during Stage 2 under both cases, which is more obvious under pure steam injection, is due to the increasing heat loss when the steam chamber expands more laterally along the overburden. The reason for the lower production rate during Stage 3 under solvent coinjection is less oil remains in the reservoir.

The property distribution profiles at 396, 1003, and 1461 days for both cases are shown in Fig. 9. The following should be noted:

- The color scale shown here is used only to represent how the color range changes from high values to low values. No actual values are assigned due to the different resolution of different properties.

- Color scales of the same property under both cases are the same for convenient comparison.
- The cut-off value for water or oil flow is $1 \text{ m}^3/\text{day}$.
- The color scale for viscosity is a log scale to get better resolution for the values in low ranges.

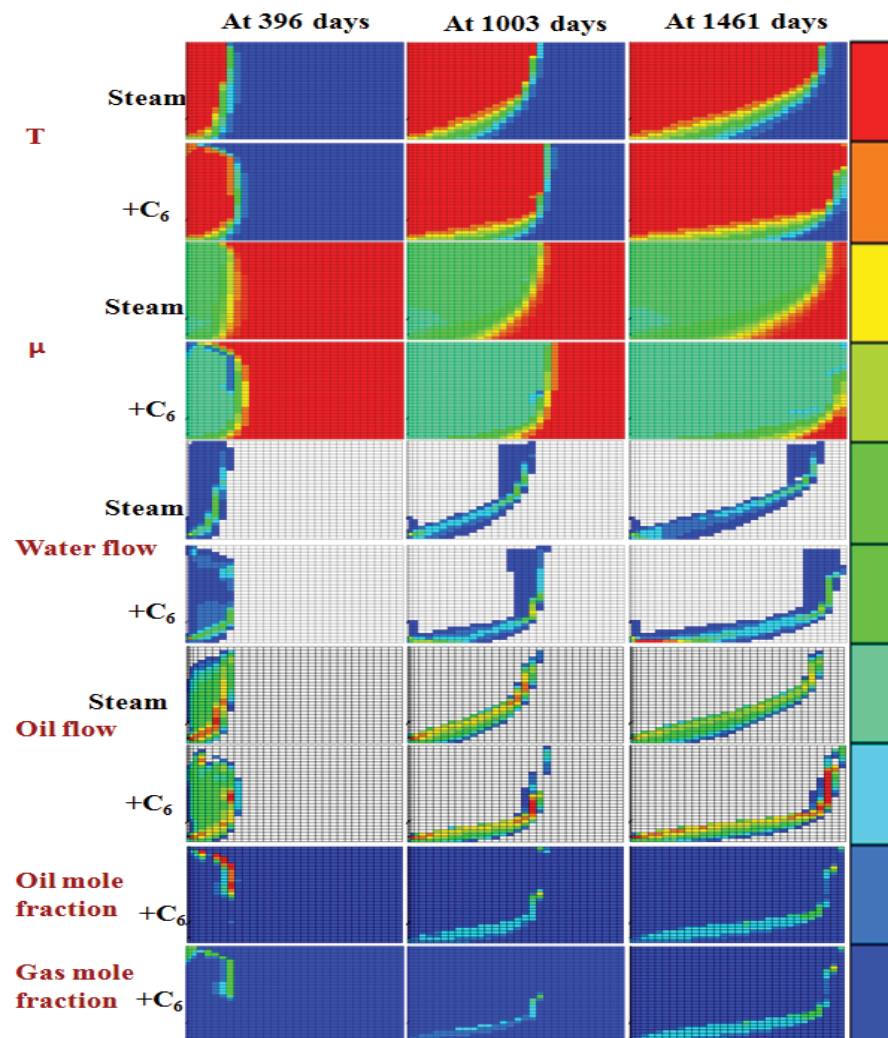


Fig. 9-Property profiles used to compare the pure steam injection and C_6 co-injection cases under different subproduction stages.

From the profiles of pure steam injection, the temperature and viscosity distribution is stable inside the steam chamber because of the dominant gravity drainage mechanism. Steam releases its latent heat inside the steam chamber by convection; outside the steam chamber, the heat is transferred only through conduction since the in-situ bitumen is immobile (refer to the temperature profile). The transition zone of the temperature profile is thicker at the lower area than the upper area. The reason is that more latent heat is released at the near wellbore area. The bitumen along the steam chamber is heated to a higher temperature and so has lower viscosity (refer to the viscosity profile). When the viscosity of the heated oil is low enough, gravity drains it along the wall of the steam chamber to the bottom producer (refer to the oil flow profile). Once the mobile oil is drained away, lower-temperature bitumen is exposed to the steam chamber and then is heated up. During this continuous process, the bitumen along the boundary remains hot and is drained continuously to the producer by gravity (refer to the water and oil flow profiles). The production performance therefore depends on two critical issues: viscosity reduction efficiency of in-situ oil and drainage efficiency of mobile oil from the side of the steam chamber to the bottom producer.

From the profiles of solvent coinjection, the vaporized C_6 travels with steam throughout the steam chamber. Since the boiling point and density of C_6 are lower than steam, C_6 will travel ahead of steam to build one gas solvent film with higher concentration ratio at the top of steam chamber during Stage 1 and along the slope boundary of the steam chamber during all stages (refer to the gas mole fraction of C_6). Once the injected hot fluid meets the surrounding lower-temperature bitumen, C_6

dissolves into the heated oil zone mainly by condensing from vapor phase to oil phase (refer to the profiles for the oil mole fraction and the gas mole fraction of hexane) to mix and reduce the mobility oil viscosity further (refer to the viscosity profiles). For the same production constraints, the lower the viscosity of the oil along the fluid interface, the higher is the oil drainage efficiency (refer the oil flow profiles).

The gas solvent front built along the steam chamber boundary would impede heat transfer from the steam chamber to the surrounding reservoir. The gas film built at the ceiling of the steam chamber during Stage 1 significantly reduces the heat transformation (refer to the temperature profiles at 396 days) from inside the steam chamber to the surrounding formation. Similarly, the solvent gas film built along the slope edge of steam chamber will likely impede heat transfer, which is not very significant in this study. A more detail discussion can be found from Deng (2005), which shows that light solvents, such as C_3 , build a very thick gas film along the fluid interface and significantly impede heat transformation.

As the injected fluid travels from the injector to the far-wellbore area, the temperature inside the steam chamber steam remains roughly the same, with steam quality decreasing by convection flow. Between the steam chamber and the surrounding reservoir, the transition condensation zone can be described with three different films built along the fluid interface, which include the film of condensate water, the film of C_6 in the gas phase, and the film of C_6 in the oil phase. These three films work together to reduce the viscosity of condensate along the fluid interface in a complex relationship.

A horizontal block row (its location is shown in Fig. 10) illustrates the detailed phase behavior during different production stages. The phase behavior at the time points of 396, 1,003 and 1,461 days respectively is interpreted as the phase behavior throughout Stages 1, 2 and 3. The property distribution profiles along the study row at 396, 1,003 and 1,461 days under pure steam injection are shown in Fig. 11(a), while the profiles under C_6 co-injection are shown in Fig. 11(b).

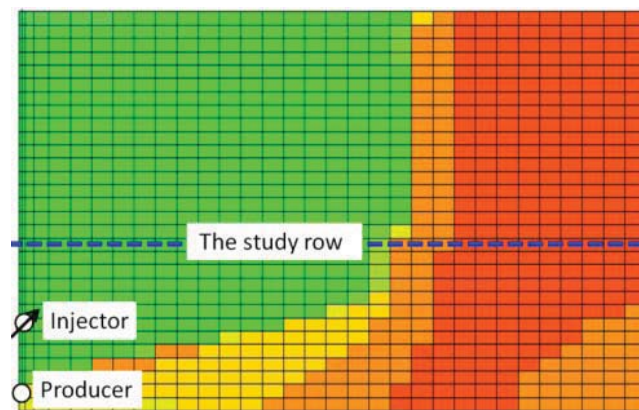


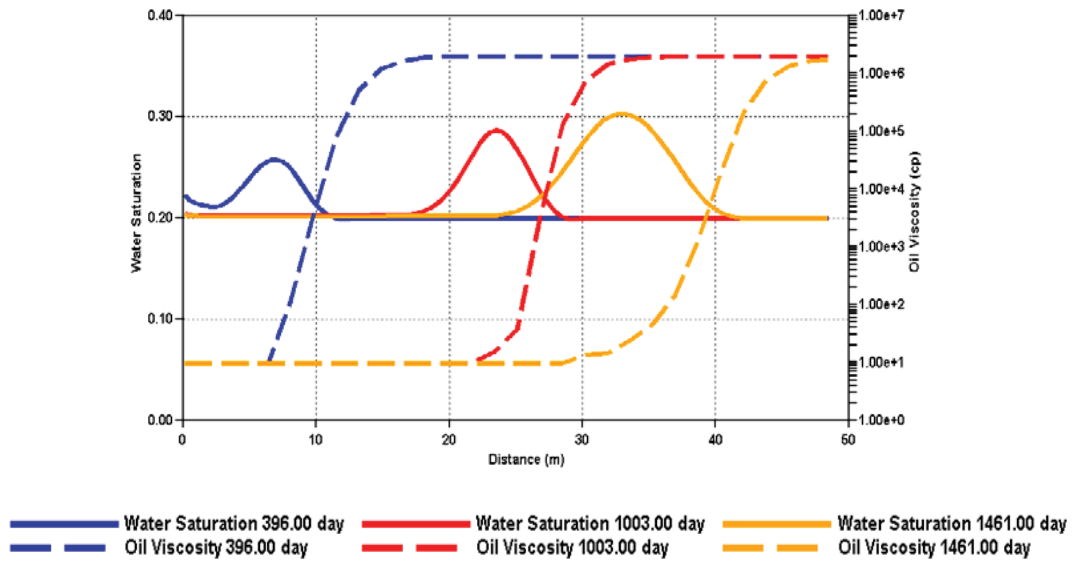
Fig. 10-Illustration showing location of the study block row overlaying on the oil saturation distribution profile under C_6 co-injection case at 1003 days.

The viscosity plots under C_6 co-injection dip in comparison to those under pure steam injection (refer to the viscosity plots of both cases in Fig. 11(a)). The “dip points” indicate much lower in-situ viscosity values. The reason is that a film of C_6 in the oil phase is built along the fluid interface (refer to the oil mole fraction of C_6 in Fig. 11(a)). The C_6 in the oil phase can mix with the heated oil and reduce its viscosity significantly. The water saturation of the water film is higher under steam injection than under C_6 coinjection (refer to the water saturation plots of both cases in Fig. 11(a)) for all three

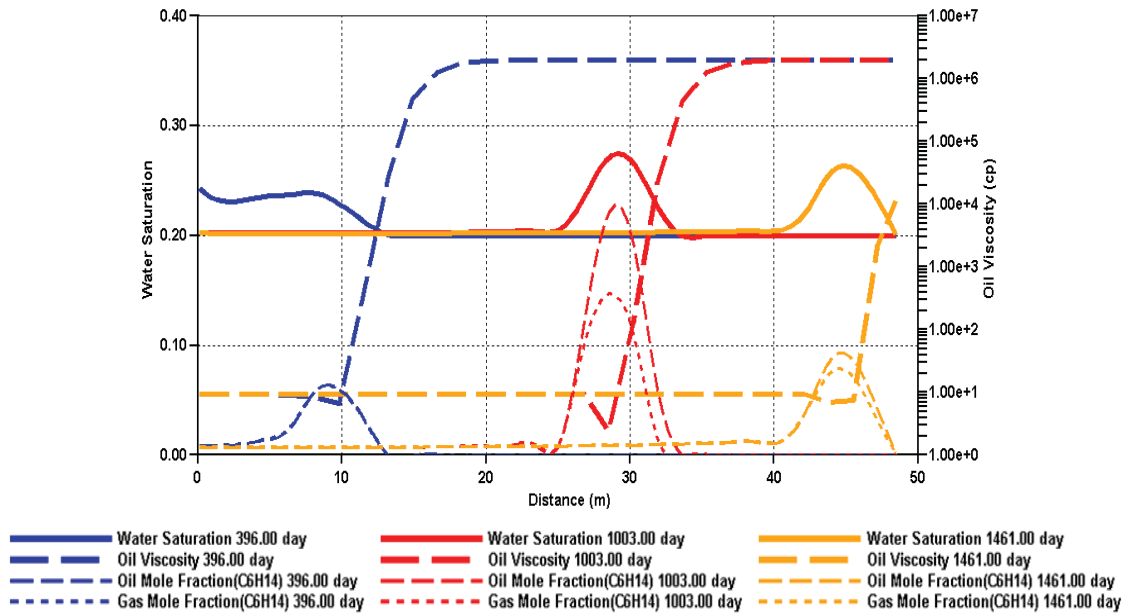
stages. The main reason is that the condensate is drained more efficiently due to its lower viscosity under C_6 co-injection.

From Fig. 11(b), the gas mole fractions and the oil mole fractions of C_6 are significantly different for the three subproduction stages. The solubility of solvent depends on its K-value. At a given injection pressure and temperature, the K-value of C_6 can be interpreted as the function of $K = \frac{y}{x}$, where y is the mole fraction of C_6 in the gas phase and x is the mole fraction of C_6 in the oil phase. The higher the K-value, the lower is the solubility of the solvent. The calculated K-values of C_6 at the fluid interface along the study row at different stages follow the order of Stage 1, Stage 3, and Stage 2.

The water saturation values of the water film created are different for different stages (Fig. 11(b)). The higher the water saturation along the fluid interface, the lower is the relative permeability of oil phase. It also expected the water film created is likely to impede the diffusion of solvent. Altering the injection strategy to create a thinner water film to reduce its dilution effect to solvent may be beneficial and needs to be investigated in future study.



(a) Water saturation, oil viscosity and oil flow rate under pure steam injection



(b) Water saturation, oil viscosity , oil mole fraction of C₆ and gas mole fraction of C₆ under C₆ co-injection

Fig. 11-The property distribution profiles at 396, 1003 and 1461 days respectively are used to describe the property distribution during Stages 1, 2 and 3; the “dome” of each property curve along the study row indicates a film of the property is built along the fluid interface; and the “dip points” along the viscosity plots indicate a significant low viscosity value.

Because of the refining limitations and cost considerations, it is usual to inject a mixture of solvents in the field. It is difficult to find one solvent with exactly the same phase behavior as steam in the field. The phase behavior differences inside the steam chamber can be generalized from the discussions of C_6 in this study for field application. The solvent and steam effects are not the same for different production stages and are not uniform along the fluid interface, which suggests some directions for future research to investigate altering operation strategies for different subproduction stages, including changing steam additive type and ratio, and injection pressure and temperature, instead using one fixed strategy for the whole production period.

This study focuses on the solvent coinjection and C_6 is used as a surrogate to investigate the phase behavior of solvent coinjection process. Different components of solvents show different phase behaviors inside the steam chamber. The light solvents, such as C_3 , would build too thick a gas film long the steam-oil interface and impede heat transfer. The advantage of the light solvents is that they can easily be delivered by steam throughout the steam chamber, even to areas where oil is trapped, due to its lower density. The high density solvents with heavy components and higher boiling points enter the reservoir with difficulty and only affect the near-wellbore area. Their sweep efficiency depends on the reservoir thickness, well spacing and geological complexity. The advantages of solvents with heavy components are that they can build a thick film of solvent in the oil phase to mix with the mobile oil much more efficiently and reduce the residual oil saturation significantly. Suitable solvent mixture should be designed

carefully to take advantage of both light and heavy solvents to improve production performance.

Furthermore, there is an optimal ratio of solvent to steam for a particular reservoir and operational conditions. If the solvent-to-steam injection ratio is small, the solvent effect is small. If the solvent-to-steam ratio is too high, the partial pressure of steam is reduced, the saturation temperature of steam is lowered and the temperature gradient from the steam chamber to the surrounding reservoir is lowered. The lower temperature gradient leads to lower heat transfer efficiency across the transition zone, so the viscosity reduction effect from the heat will be lower. The optimal concentration ratio of solvent is a tradeoff between viscosity effects from solvent and from steam.

Summaries

The main conclusions from this part of the simulation study are as follows:

1. In this simulation study, C_6 is used as a surrogate solvent to investigate the phase behavior of solvent and steam inside the steam chamber. The results indicate that a successful solvent co-injection design can deliver higher oil production rate and higher oil recovery factor with lower CSOR and CEOR values than pure steam injection.

2. Due to the similar boiling points of steam and C_6 , C_6 is vaporized by steam and travels into the steam chamber. Once the injected solvent and steam reach the lower temperature areas just beyond the boundary of the steam chamber, the steam releases its latent heat to reduce the adjacent oil viscosity, and the solvent dissolves into the heated oil to reduce the heated oil viscosity further. The key to designing a successful solvent coinjection is to take advantage of the solvent without losing the heating effect of steam.

3. Due to the difference in boiling points of solvent and steam, the vaporizing and condensing dynamics of solvent and steam inside the steam chamber is different at different locations and stages. The resulting gas solvent film, liquid solvent film, and water film created along the steam-oil interface work together to affect the viscosity reduction effects of steam and solvent.

3.2.2 Solvent type and concentration ratio

We chose C_3 , C_5 , C_6 , C_7 , and C_{12} because of the boiling point difference between these hydrocarbons and steam at the injection condition (Fig. 12). Since a solvent mixture of 80 mole% C_6 and 20 mole% C_7 has almost the same boiling point as steam at the injection condition, this solvent mixture is also included in the simulation study. The sensitivity study of the solvent type is based on simulation of 5 mole% solvent in the injected fluid. The plots of oil recovery factor, CEOR, oil production rate, and fraction of solvent produced with oil for different solvents are plotted in Fig. 13.

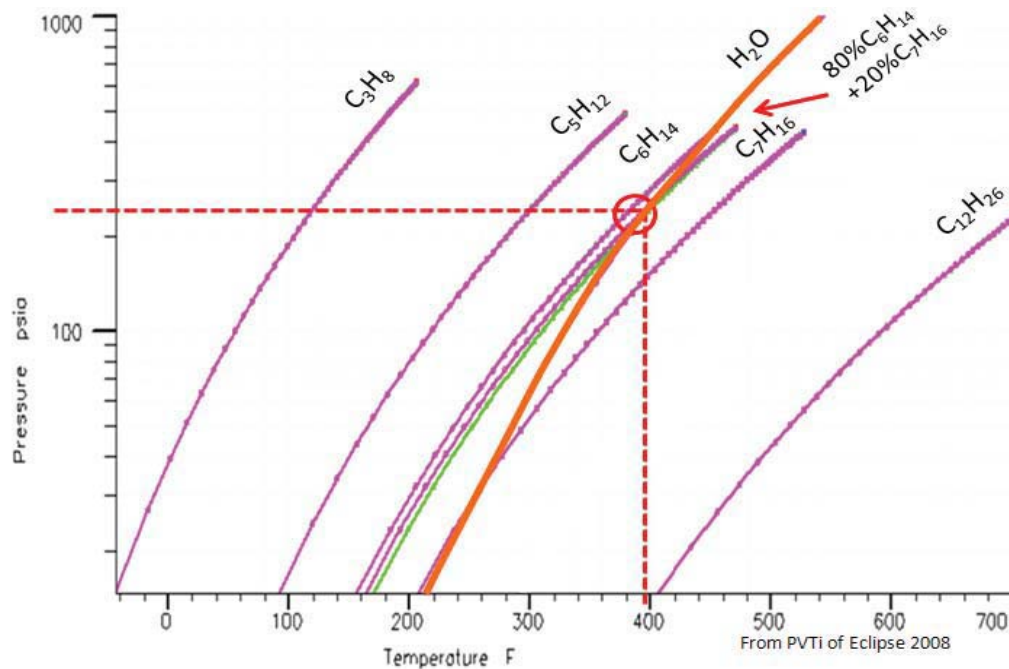
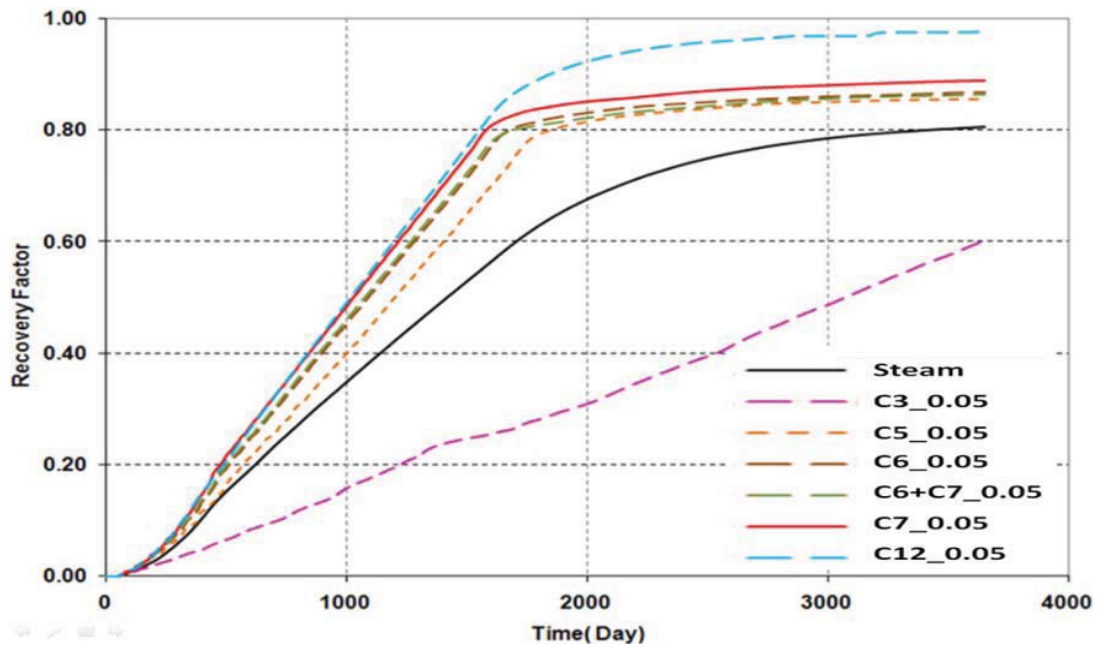


Fig. 12-95% quality steam at 202°C and 1,650 kPa is injected; based on the differences in boiling points between steam and solvents, C₃, C₅, C₆, C₇, C₁₂, and the solvent mixture of 80% C₆ and 20% C₇ are chosen to investigate the effect of solvent type on oil recovery.

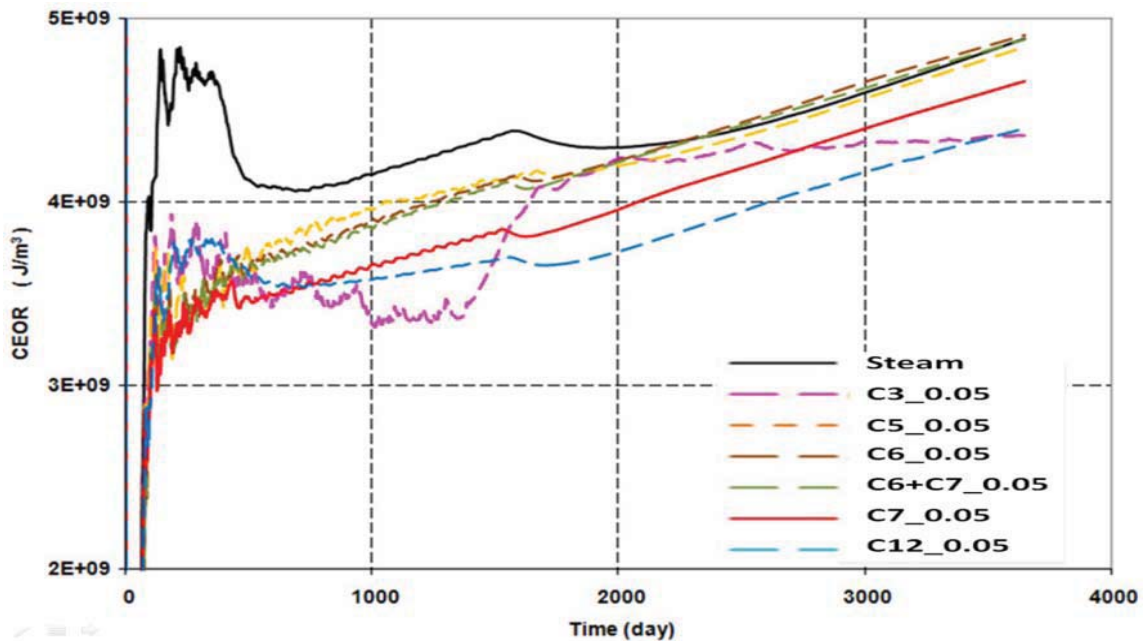
Oil recovery factor increases with increase in the carbon number of the solvent. C₁₂ gives the highest recovery factor, which is more than 96% oil initially-in-place (OIIP). Recovery factor for co-injection of steam and a mixture of C₇ and C₆ is between those of steam co-injection with C₆ and C₇. Recovery factor with steam co-injection with C₃ is lower than under the pure-steam injection case (Fig. 13(a)). During the early stage, steam co-injection with C₃ gives the lowest CEOR and then starts to increase once its volume of vapor phase inside the steam chamber is too large to reduce the injectivity of steam. During steam chamber expanding, CEOR for steam co-injection with other solvents decreases as follows: pure steam, C₅, C₆, mixture of C₆ and

C_7 , C_7 , and C_{12} . The ultimate CEOR values of steam co-injection with C_7 and C_{12} cases are lower than steam co-injection with other solvents, and steam co-injection with C_{12} gives the lowest CEOR for the simulated thin reservoir (Fig. 13(b)).

At early stages, the oil production rate under steam co-injection with solvent decreases with the solvent type in the following order: C_{12} , C_7 , mixture of C_7 and C_6 , C_6 , C_5 , pure steam, and C_3 . The reason for the fluctuation of C_{12} plots at the end of production is that C_{12} remains mainly in the liquid phase. The reason for the higher production rate of C_3 during the later stages is that its earlier production rate is too low and most of the oil has not been produced (Fig. 13(c)). During the early stages, the gas phase of C_3 occupies a larger volume and so is produced more than the other solvents. With more steam and C_3 injected into the reservoir, C_3 flows upwards and accumulates at the top area, so less can be produced. Once the steam chamber matures, the fraction of vapor solvent produced with oil mainly depends on its initial concentration ratio. The fraction of vaporized solvents produced with oil, including the C_3 , C_5 , C_6 , mixture of C_6 and C_7 , and C_7 , is around 92 to 95% of amount injected. C_{12} is produced more in the earlier period and less at the later period because it exists mainly as a liquid. About 18% of injected C_{12} is retained in the steam chamber, which may be more difficult to recycle by the blowdown process due to its high boiling point (Fig. 13(d)).

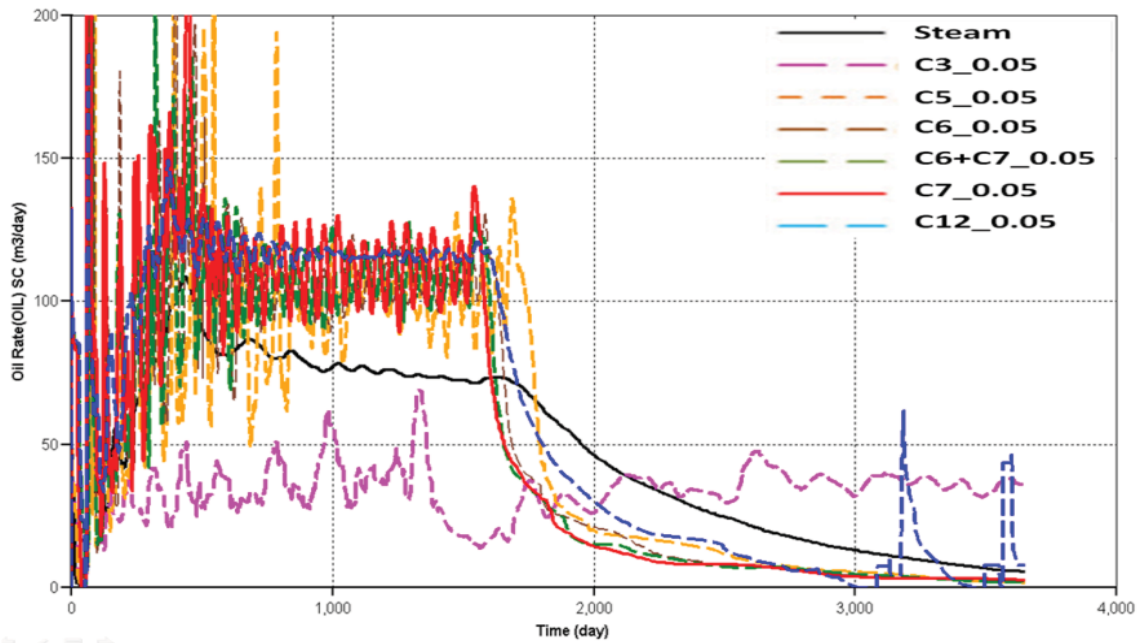


(a) Oil recovery factor

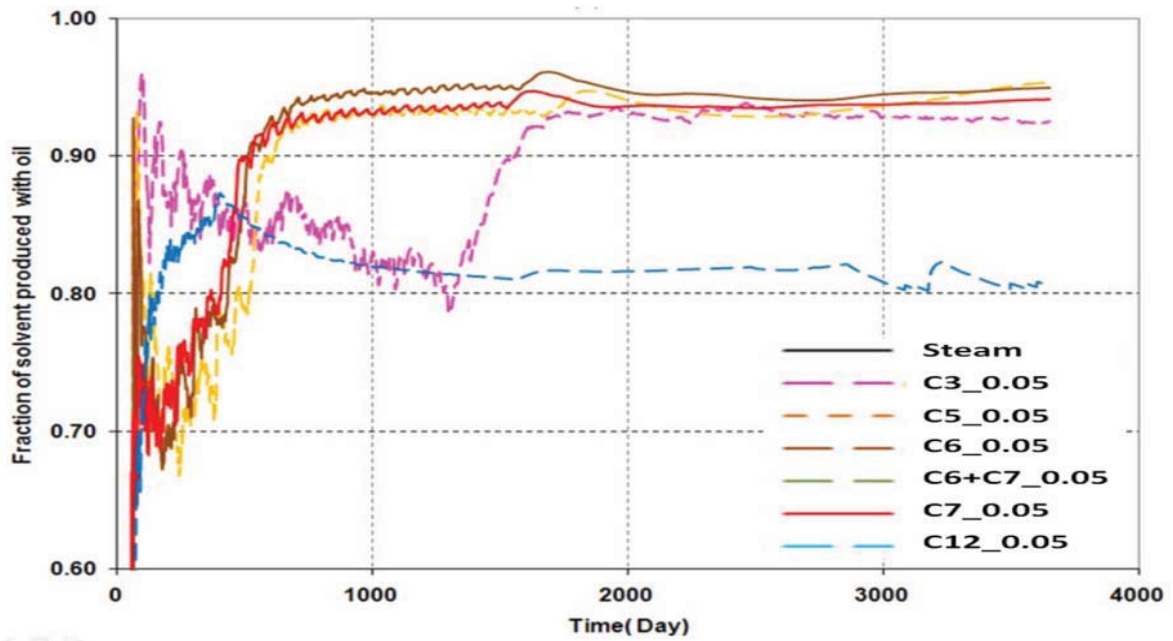


(b) CEOR

Fig. 13-Production performance comparison between different simulations with different solvent types.



(c) Oil production rate



(d) Recovery factor of the injected solvent

Fig. 13 – Continued

The suitable solvent type in the ES-SAGD process should be vaporized and condensed with steam simultaneously along the steam chamber boundary to dilute the bitumen. Under conditions studied, only C_5 , C_6 , a mixture of C_6 and C_7 , and C_7 are suitable for ES-SAGD processes. Since their boiling points are similar to that of the injected steam, applying blowdown at a later stage can successfully recycle most of the retained solvents. More than 90% of these solvents are produced with oil and can be reinjected again. It is also easy to re-vaporize these solvents from the produced oil and then reuse it, which can significantly reduce the operational cost in the field. The recycling of C_{12} from the produced fluid by reheating or from the depleted reservoir through the blowdown phase is expected to be much more difficult due to its much higher boiling point compared to other solvents.

The property distribution profiles at 1551 days are shown in Fig. 14. The following should be noted:

1. The color scale shown here is used only to represent how the color range changes from high values to low values. No actual values are assigned due to the different resolution of different properties.
2. Color scales of the same property under both cases are the same for convenient comparison.
3. Only the pure steam, C_3 , C_6 , C_7 , and C_{12} cases are compared.
4. The cut-off value for total oil and water flow is $5 \text{ m}^3/\text{day}$.
5. The color scale for the C_{12} solvent fraction in the gas phase is in the range of 0 to 0.05 instead of 0 to 1 for better resolution.

6. The color scale for viscosity is a log scale to have better resolution for the values in the low ranges.

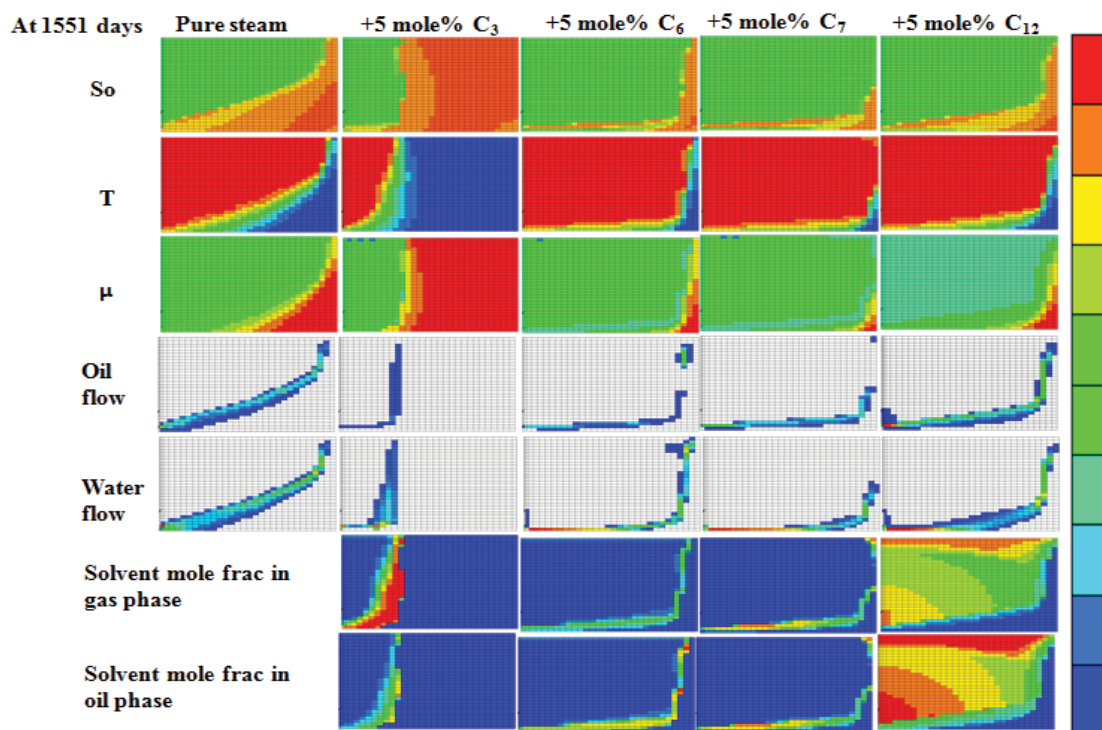


Fig. 14-Property distribution profiles at 1551 days under different simulations with different solvent types: Different solvents create different films of water, gas solvent, and liquid solvent, which mainly attribute to the boiling points discrepancy between steam and solvents.

From the comparison, relative condensation time is important for solvent solubility. If the solvent condenses after or with steam, the water film built along the fluid interface would dilute the solvent condensate and so reduce the solubility effect of solvent. The boiling point of C₃ is very low and so most stays in the gas phase, which reduces the steam partial pressure significantly. The temperature inside the steam

chamber is decreased to a much lower value, and so steam condenses much earlier than under pure steam injection to build a very thick water film. Although the steam condition under steam co-injection with C_{12} is similar to that for pure steam due to its small partial pressure effect, the water film thickness under steam co-injection with C_{12} is thinner than pure steam injection due to the accelerated flow at near-wellbore area. C_7 condenses ahead of steam because of its higher boiling point than that of steam, while C_6 condenses after steam because of its lower boiling point. The dilution effect of the water film is less for C_7 than for C_6 (refer to the oil and water flow profiles, Fig. 14).

The gas solvent film along the steam chamber boundary would impede heat transfer from the steam chamber to the adjacent reservoir. The gas film thickness of C_6 and C_7 is similar and the difference between the two cases is ignored for discussion in this study. The C_{12} solvent fraction in the gas phase is much lower than the other solvents and so a much thinner gas film is built for C_{12} case than for the other cases. The low density of the C_3 gas phase allows it to flow up and accumulate to build one very thick gas film along the steam chamber boundary (refer to the profile of solvent mole fraction in gas phase, Fig. 14).

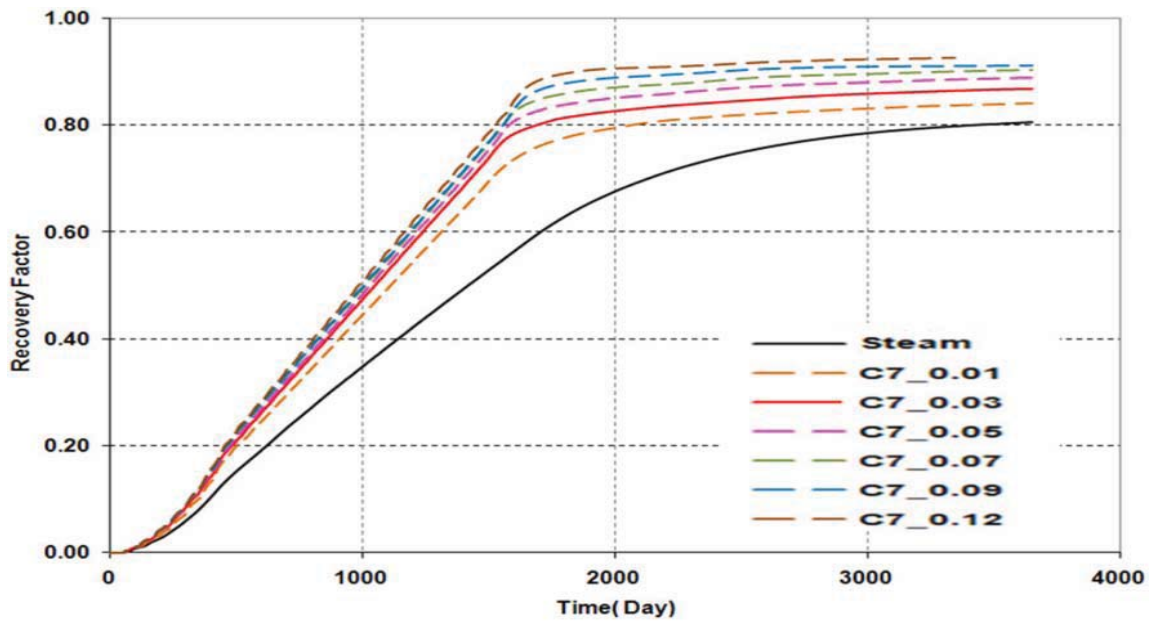
The solubility of vapor solvent depends on its K-value. The solubility of C_3 is small due to rather its low boiling point. C_7 builds a thicker liquid solvent film than C_6 at the near wellbore area because of its higher boiling point. Since C_{12} is unsaturated in the injection stream, a small fraction of C_{12} is vaporized into the gas phase. At the top of the reservoir, the temperature is lowered by the heat loss to the overburden, and the gas phase C_{12} condenses to an oil phase to flush a greater fraction of residual oil at that

zone. A successful subcool control can build a condensate liquid leg between the injector and producer. The liquid leg works as a flow resistor to impede liquid C_{12} to flow directly from injector to producer. The density of liquid C_{12} is lower than that of the condensate, so C_{12} mainly accumulates on the top of the liquid leg. When the subcool temperature limitation is triggered, the condensate at the bottom of the liquid leg is produced first. Liquid C_{12} accelerates the near-wellbore flow and reduces the residual oil saturation in the wellbore vicinity significantly. Theoretically, liquid solvent can flush out all residual oil. In addition, in this study the reservoir is quite thin. All these lead to more than 96 % oil recovery for the C_{12} case (refer to profiles of solvent mole fraction in oil phase and oil flow, Fig. 14).

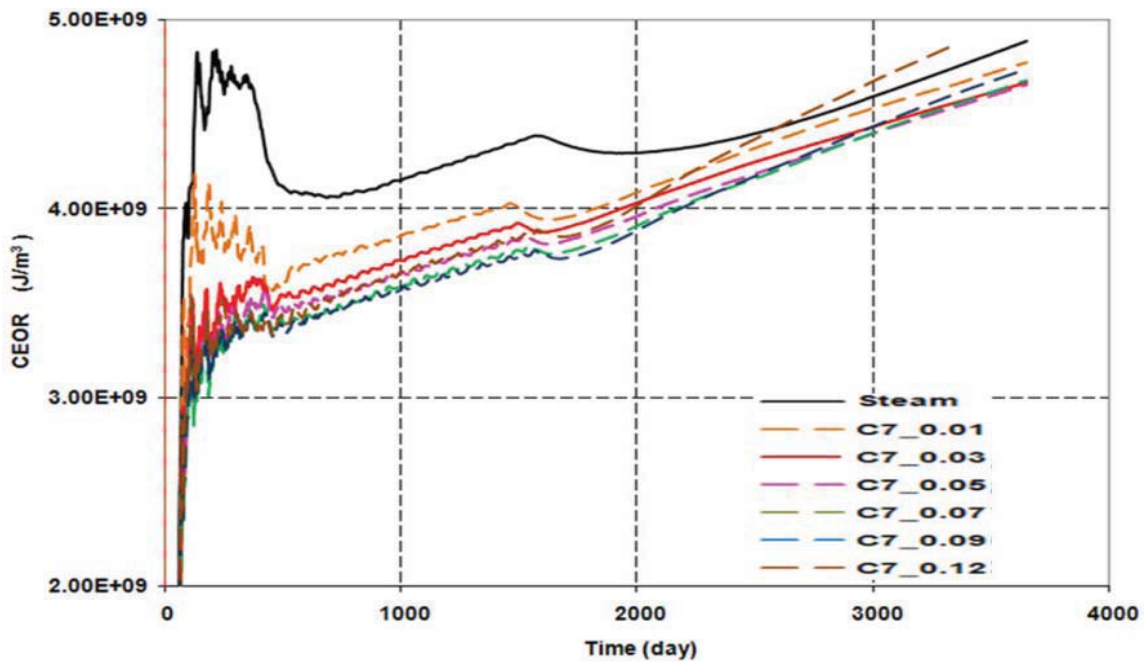
For a very thick formation, C_{12} should be injected with other lighter solvents simultaneously to ensure better sweep efficiency. Further, steam co-injection with C_{12} will be uneconomical for high solvent concentration, which may leave an uneconomical fraction of solvent in the pores and a great amount of C_{12} would be produced directly from injector to producer. For the heterogeneous cases, solvents with lower molar weight, such as C_6 and C_7 , can take advantage of their lower density and lower boiling point to be delivered by steam to the trapped area. The trapped area is only heated by conduction, the temperature inside is lower, so the vaporized solvent may condense to liquid phase inside the trapped area to flush out more residual oil out. The heavier solvents are suitable to improve near-wellbore flow and may reduce the residual saturation there due to its liquid phase, as discussed earlier.

In a real reservoir, the oil is typically saturated with natural gas, such as C_1 , at reservoir pressure. When the gas/oil ratio (GOR) is high, the extraction of in-situ C_1 reduces the production performance greatly by reducing the partial pressure effect of steam and accumulation of a thick gas film to reduce heat transfer efficiency, similar to the negative effect of C_3 in this study. In addition, it is usual to inject a mixture of solvents in the field, which also include various volatile components, such as C_1 , C_2 and C_3 , which also reduce production performance through same mechanism as the extracted C_1 from the reservoir. Coinjecting heavier components to mix with the volatile components can result in a higher dew point of the solvent mixture inside the steam chamber. The higher dew point accelerates the solvent condensation dynamics, i.e. more solvent condensing from gas phase to liquid phase, along the fluid interface with less gas solvent accumulated to build the gas film. The accelerated condensation process of solvent also is helpful to remove the volatile components from the steam chamber by the production of solvent condensate.

The simulation study of solvent concentration focuses on the solvent suitable for the ES-SAGD process. We used 1, 3, 5, 7, 9 and 12 mole% C_7 to investigate the effect of solvent concentration on oil recovery. The oil recovery factor, CEOR, viscosity, oil mole fraction profiles along the horizontal direction at the producer, and the temperature profiles along the vertical direction at the producer at 1003 days are plotted in Figs. 15 to 17.



(a) Oil recovery factor



(b) CEOR

Fig. 15-With the mole ratio of C_7 increasing, (a) the recovery factor is increasing; (b) the lowest CEOR value is given by the 7 mole% C_7 coinjection.

In Fig. 15, as C_7 concentration increases, the recovery factor increases (Fig. 15 (a)). C_7 in the range of 1 to 9% has a lower CEOR than pure steam injection. Although the solvent concentration increases by steps of 2% from 1% to 9% and 3% from 9% to 12%, the CEOR values for different solvent cases decrease slower than for higher solvent concentrations. When the ratio is increased from 7% to 9%, the decrease of CEOR is very small at early stages but finally starts to increase to a higher value than the 7% solvent concentration case. The CEOR value for 12% C_7 concentration is always higher than the value for 7% C_7 concentration and finally is even higher than for pure steam injection. The optimal concentration ratio range of C_7 is around 7% for entire production period (Fig. 15 (b)).

The drainage efficiency of the condensate depends on the viscosity reduction along the entire fluid interface. From Fig. 16, the 3% C_7 case has the lowest oil viscosity along the horizontal direction at the producer at 1003 days, which indicate there is an optimal concentration ratio to take the advantages of both steam and solvent. With the concentration of C_7 increasing, more fraction of C_7 in oil phase mixes with oil along the fluid interface (Fig. 17a), but the partial pressure of steam decreases, the steam temperature decreases (Fig. 17b) inside the steam chamber, and so the heat effect from steam is less. So, the solvent effect is too small if the solvent concentration is too low, or the heat effect of steam will be significantly lost if the concentration is too high.

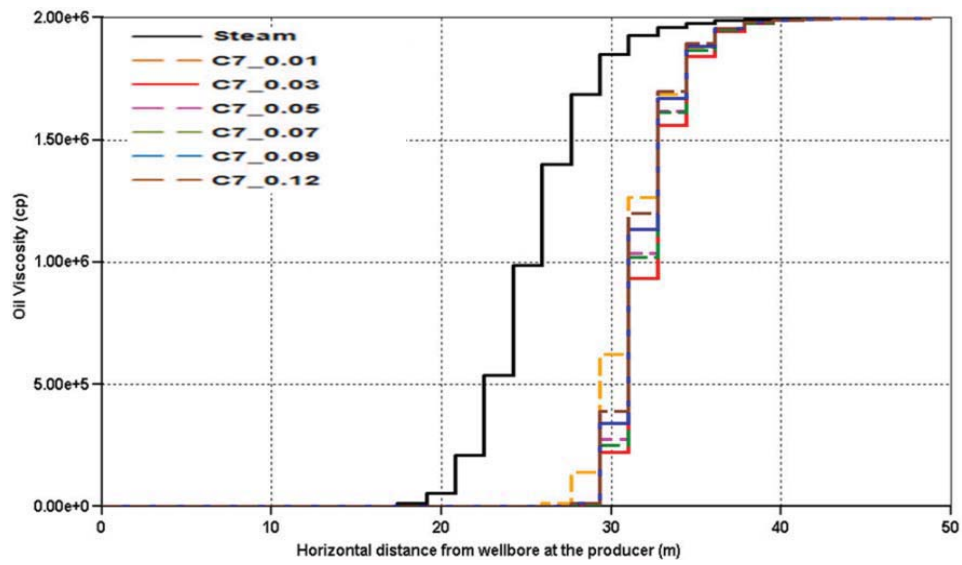
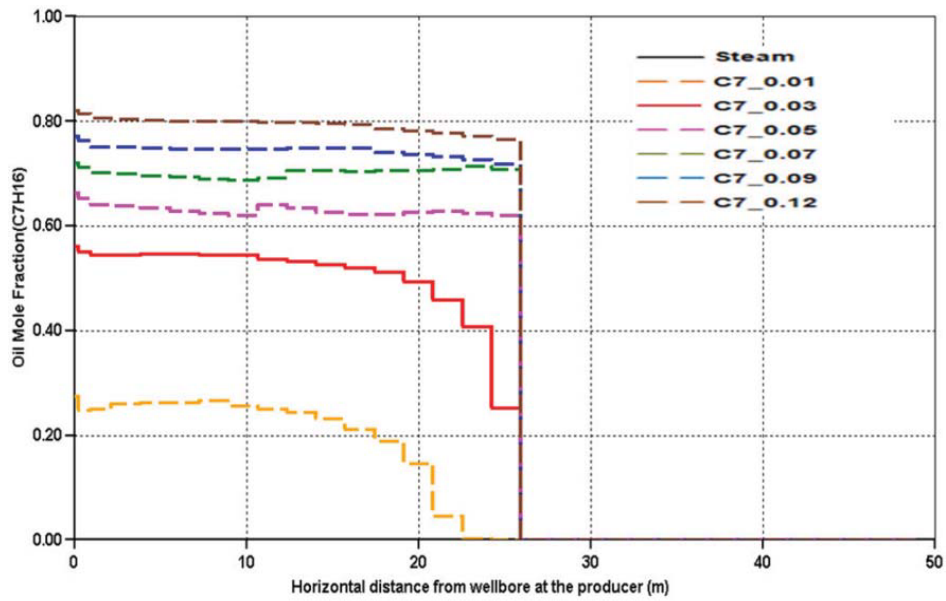
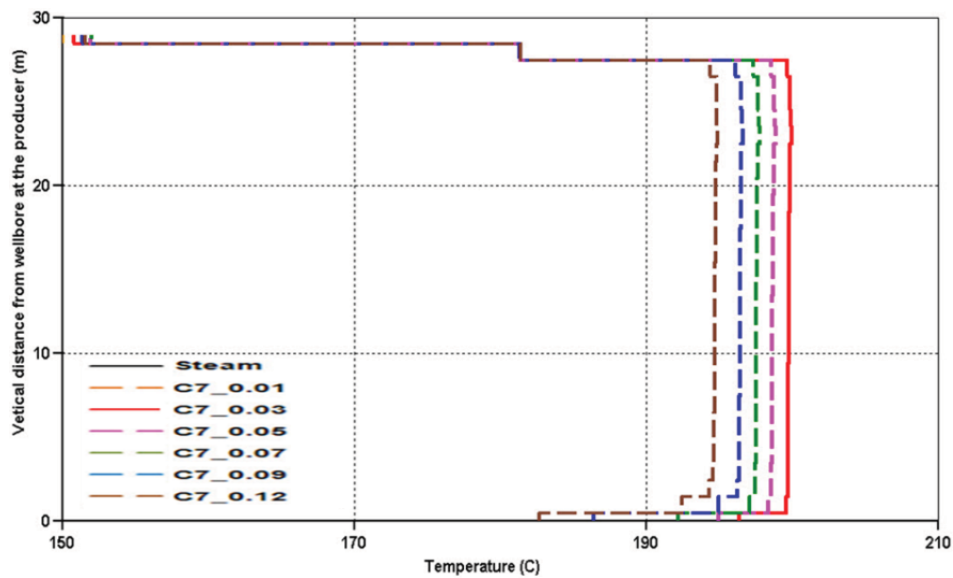


Fig. 16 -Viscosity distribution at 1003 days for different simulations with different C_7 ratios: C_7 coinjection reduces the heated oil to a substantial lower value compared to pure steam injection case; the lowest viscosity value along the fluid inter face is the 3 mole% C_7 case at 1003 days, which indicate there is an optimal concentration ratio to take the advantages of both steam and solvent.



(a) Oil mole fraction of C_7 along horizontal direction at the producer location



(b) Temperature along vertical direction at the producer location

Fig. 17 -Viscosity distribution at 1003 days for different simulations with different C_7 ratios: C_7 coinjection reduces the heated oil to a substantial lower value compared to pure steam injection case; the lowest viscosity value along the fluid inter face is the 3 mole% C_7 case at 1003 days, which indicate there is an optimal concentration ratio to take the advantages of both steam and solvent.

Summaries

The following main conclusions can be drawn from this part of the simulation study:

1. The relative condensation times of solvent and steam create different films of gas solvent, liquid solvent, and water. A gas solvent film impedes heat transfer, while a liquid solvent film increases solvent solubility, and a water film dilutes the solvent effect.
2. If most of the injected solvent is in the gas phase (C_3 in this study), production performance under the steam-solvent co-injection is even worse than that with pure steam injection.
3. For the solvents to meet the requirement of ES-SAGD, such as C_6 and C_7 in this study, the solvent that condenses before steam (C_7 in this study) results in better production performance than the solvent that condenses after steam (C_6 in this study).
4. Injected solvents that consist of heavier compounds, such as C_{12} , accelerate the fluid flow and reduce the residual oil saturation significantly at the near-wellbore area. The liquid condensate leg built by sub-cooling acts as a flow resistor to retain solvent in the steam chamber. Otherwise, the injected heavy solvent will be produced directly from injector to producer.
5. For a thin homogeneous formation, C_{12} coinjection increases production performance significantly due to its liquid phase. For a thick formation or in a heterogeneous reservoir, the sweep efficiency of pure C_{12} may be too low. In such situations, co-injection of lighter components with C_{12} can achieve better performance.

6. Coinjecting heavier components is helpful to reduce the negative effect of volatile components by accelerating the condensation dynamic inside the steam chamber.

7. In the ES-SAGD process, the optimal solvent ratio range, which is in a low concentration range (around 7 mole% in this study), depends on the tradeoff between the heat effect from steam and the solubility effect from solvent.

3.2.3 Shale barrier effect

If shale barriers are distributed continuously and laterally across the whole formation, well stimulation is needed to build a fluid flow path, or the sub-reservoirs should be drained separately with several well pairs if the formation is thick enough. If the shale has limited dimensions, fluids may meander around them and be produced. If the shale barrier is distributed partly continuously in the reservoir, some oil maybe trapped inside and steam may have difficulty reaching the trapped areas. This study focuses on the partially continuous shale barrier with different lengths and locations to investigate the shale barrier effects.

Profiles of the simulated homogeneous case (Case 0) and heterogeneous cases (Cases 1 to 4) are shown in Fig. 18. We simulated two different interpretations of shale barrier with respect to their different impacts on steam vertical flow. In Cases 1, 2, and 4, the shale barrier directly blocks the steam vertical flow to meet the top of formation. This is called “blocking” shale barrier. The “unblocking” shale barrier (Case 3) means the shale barrier allows steam to flow vertically until the top of the formation and then expands laterally. Cases 1 to 4 also can be categorized by two other different

interpretations of shale barriers with respect to their vertical locations or length dimensions. The “far-wellbore” shale barrier is located 14.5 m from the injector while the “near-wellbore” shale barrier is located 6.5 m from the injector. The shale barrier lengths are 38.1 m for “long” shale barriers and 14.3 m for “short” ones. Typical shale permeability is in the range of 10^{-6} to 10^{-3} md (Pooladi-Darvish *et al.* 2002). The shale permeability is set as 10^{-5} md in this study. Water saturation of shale is 100%, porosity of shale is 10%, and shale barrier thickness is 2 m.

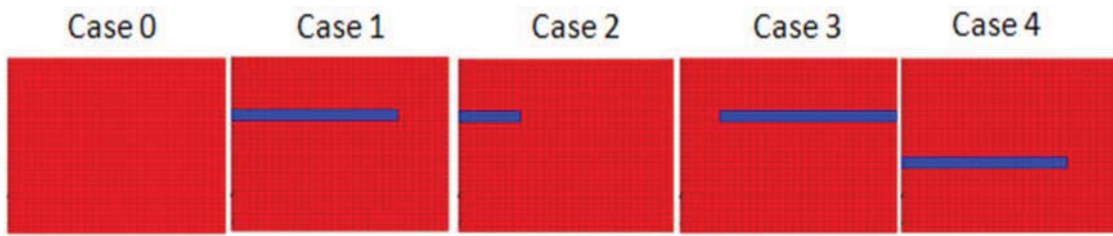


Fig. 18-Profiles of homogeneous case (Case 0) and heterogeneous cases (Case 1 - 4). Red grid: sand; blue bar: shale barrier.

The property profiles at 1,551 days for different cases are shown in Fig. 19. The following should be noted:

- The color scale used here is only to show how the color range changes from high value to low value. No actual values are assigned due to the different resolutions of different properties.
- Color scales of the same property for all cases are the same to compare the property distribution profiles.

- The color scale for viscosity is in log scale to get better resolution for the values in a low range.
- Cut-off values for oil and steam flow are $2 \text{ m}^3/\text{day}$.

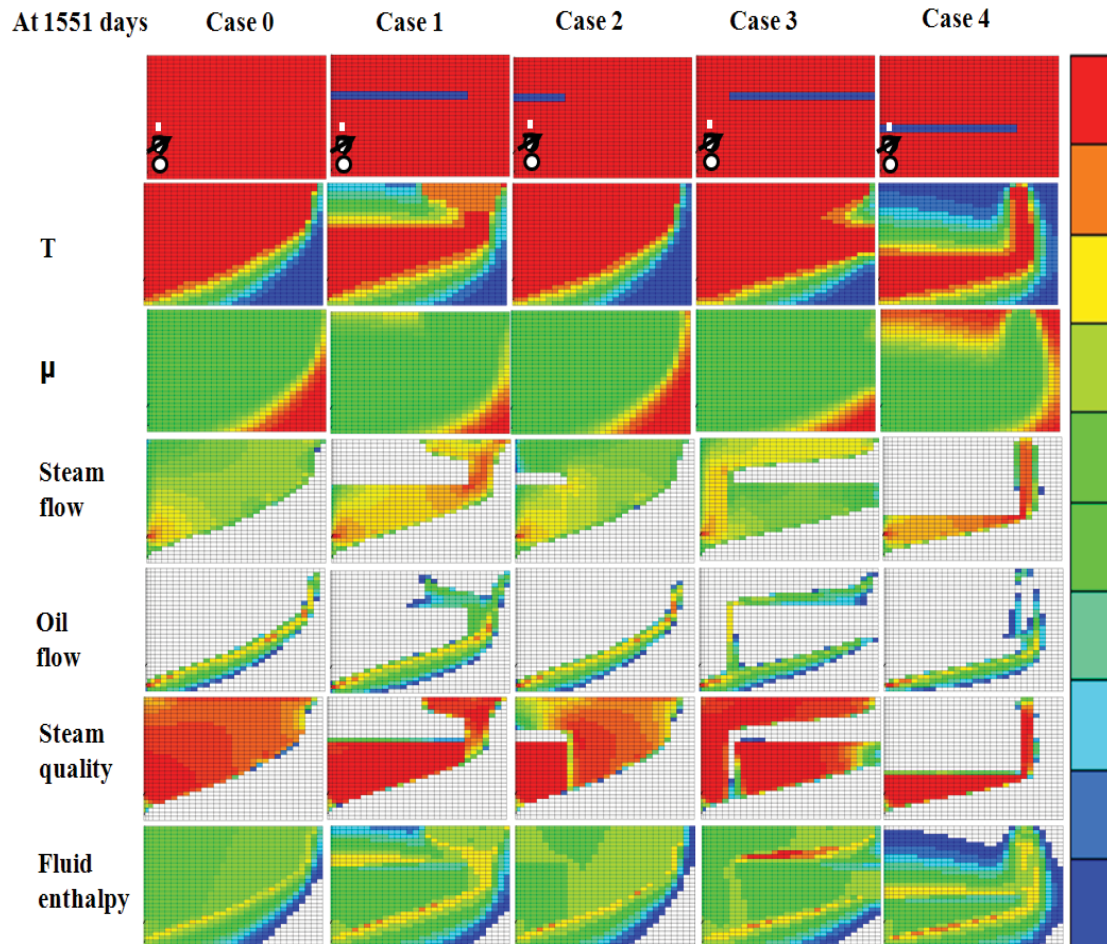


Fig. 19-Property profiles at 1551 days for different cases: the flow resistance at the end of shale barriers and the extra heat absorbed by the residual water inside the unproductive shale barrier are the main reasons for the shale barrier effects.

From the profiles of pure steam injection, the temperature and viscosity distribution is stable inside the steam chamber because of the dominant gravity drainage

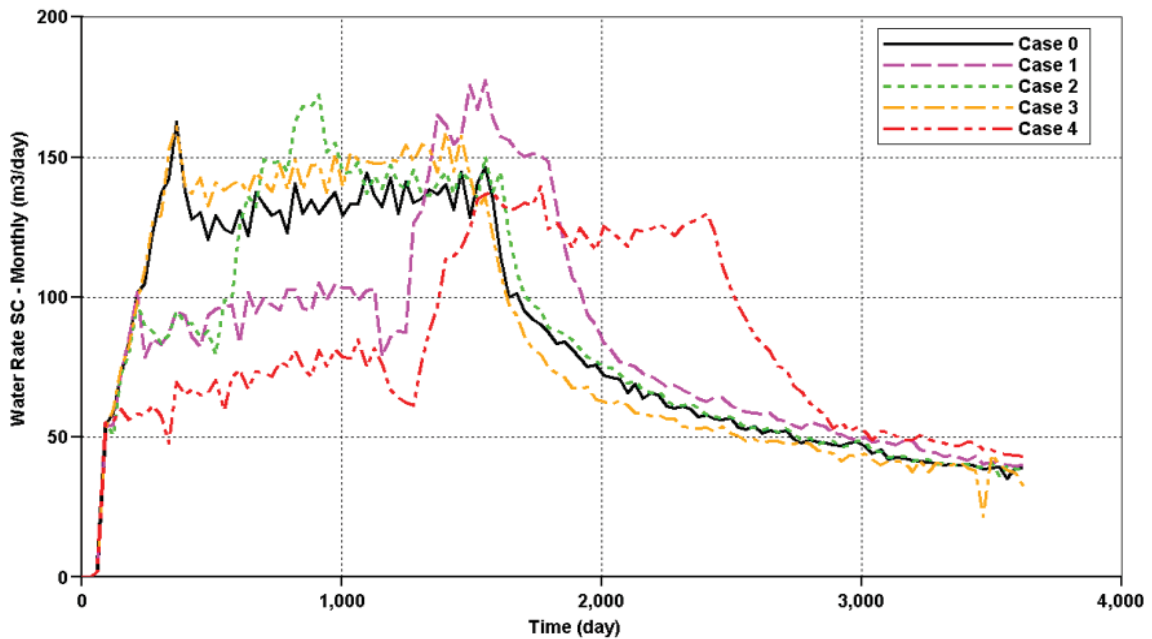
mechanism. Steam releases its latent heat along the fluid interface through convection; outside the steam chamber, the heat is transferred only through conduction since the in-situ bitumen is immobile (refer to the temperature, steam-quality and fluid enthalpy profiles, Fig.19). The bitumen along the fluid interface is heated to a higher temperature and so with lower viscosity (refer to the viscosity profile, Fig.19). When the viscosity of the heated oil is low enough, gravity drains it along the wall of the steam chamber to the bottom producer. Once the mobile oil is drained away, lower-temperature bitumen is exposed to the steam chamber and then is heated up. During this continuous process, the bitumen along the boundary remains hot and is drained continuously with the condensed water to the producer by gravity (refer to the water and oil flow profiles, Fig.19). The production performance therefore depends on two critical factors: viscosity reduction efficiency of in-situ oil and drainage efficiency of mobile oil from the sides of the steam chamber.

For Case 1, steam expands more laterally to build one steam chamber under the blocking shale barrier during early phase (refer to the steam flow profile under Case 1, Fig.19). Besides the heat transfer processes discussed in Case 0, the bitumen above the shale barrier is heated only by conduction from the underneath steam (refer to the temperature profile under Case 1, Fig.19), but the initial flow path at the end of the shale barrier is very narrow (refer to the steam and oil flow profile under Case 1, Fig.19). Steam condenses to water quickly when it meets the low-temperature bitumen (refer to the steam quality profile under Case 1, Fig.19). The condensate's downward flow impedes steam flow upward (refer to the steam quality and oil flow profiles under Case 1,

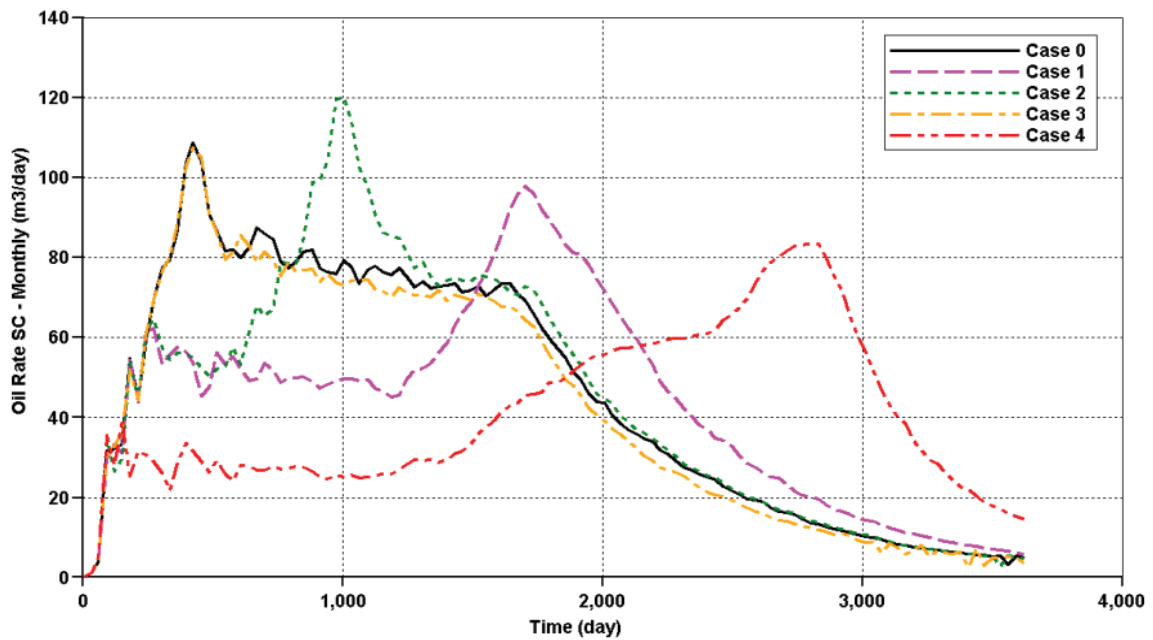
Fig.19). Before the heated oil at the edge of shale barrier is drained away, the steam cannot flow upward. This is same situation as the preheating period to connect both wells and will significant delay the entire steam chamber propagation. Once the flow path is wide enough to allow the steam flow upward, the flow resistance of countercurrent flow will disappear, and the steam can release its latent heat efficiently to heat the adjacent bitumen. When a large steam chamber is built around the shale barrier, the shale barrier effect disappears since the thermal properties of shale and sand mixing with bitumen are similar.

A shorter blocking shale barrier has less flow resistance since steam can pass through the end of shale barrier earlier, which can be observed from the comparison between Case 1 and Case 2 (refer to the steam and oil flow profiles of Case 1 and Case 2, Fig.19). A similar discussion can be applied to the comparison between Case 1 and Case 4: Nearer to the wellbore, the shale barrier shows a greater flow resistance. In Case 4, the drainage height below the shale barrier is smaller than in Case 1, so the oil production rate is lower (refer to the oil flow profiles of Case 1 and Case 4, Fig.19) at early stage, which further reduces the steam injectivity (refer to the steam flow profiles of Case 1 and Case 4, Fig.19). There is almost no flow resistance for the unblocking shale barrier if the steam can flow upward to meet the overburden and then expand sideways, such as in Case 3 (refer to the steam and oil flow profiles of Case 3, Fig.19). The detail discussions of Case 3 based on experimental study can be found from Butler (1994) and Yang and Butler (1992).

The plots of steam injection rate, oil production rate, oil recovery factor and steam-to-oil ratio (SOR) for different cases are shown in Fig. 20. The ultimate production performances of all cases approach similar values for a long 10-year production period, since the shale barrier effects finally disappears. For the blocking shale barriers in Cases 1, 2, and 4, the production performances are delayed more significantly by the longer shale barrier (refer to Case 1 and Case 2) or the near-wellbore shale barrier (refer to Case 1 and Case 4) due to the related greater flow resistance at the end of shale barrier. The flow resistance from a blocking shale barrier is much greater than from an unblocking shale barrier (refer to Case 1 and Case 3). The production performance under unblocking shale barrier case, *i.e.* Case 3, is similar to under the homogeneous case, *i.e.* Case 0. The small differences between Case 3 and Case 0 are mainly attributed to the extra heat needed to heat the residual water in the shale barrier, which can be implied from the higher SOR in Case 3. From above discussions of Fig. 19 and Fig. 20, the long continuous shale barriers located vertically above or near the wellbore delay the production performance much more significantly than other types of shale barriers before a steam chamber is built around the entire shale barrier.

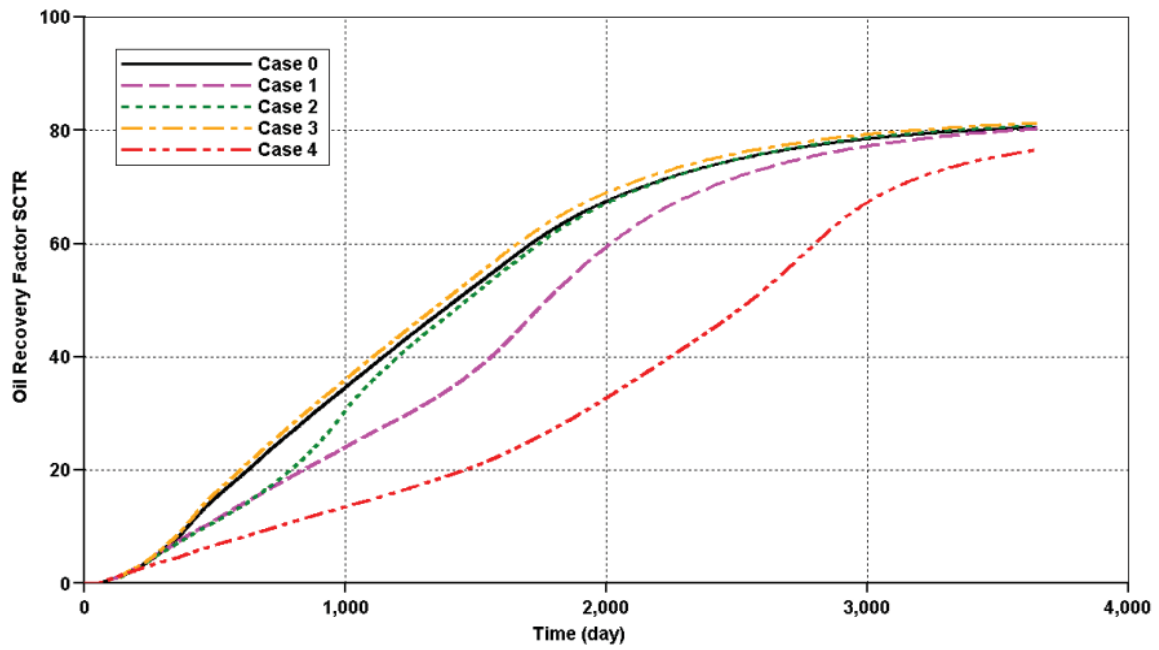


(a) Steam injection rate

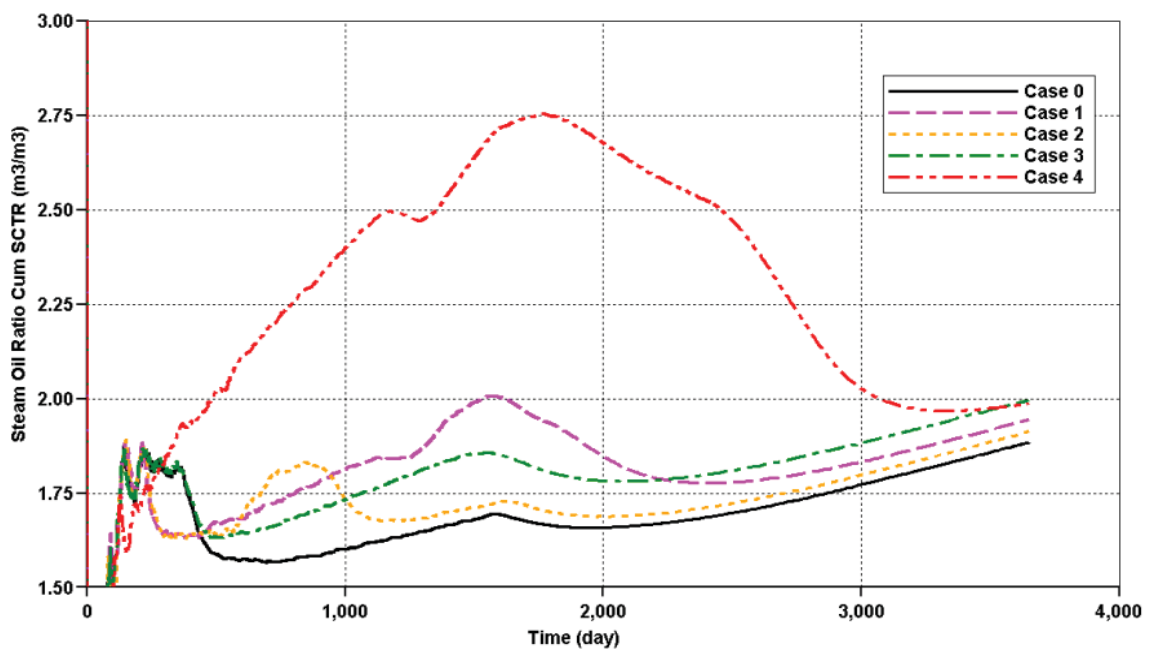


(b) Oil production rate

Fig. 20-Production performance comparison among different cases, including steam injection rate, oil production rate, oil recovery factor and SOR, which shows that long continuous shale barriers located vertically above or near the wellbore delay production performance significantly.



(c) Oil recovery factor



(d) SOR

Fig. 20- Continued

To reduce the flow resistance at the end of the shale barrier, the viscosity reduction efficiency should be increased and the heated bitumen should be drained away quickly to allow steam upward flow. A top injector above the shale barrier could be helpful to push the trapped oil through the end of the shale barrier. Meanwhile, coinjecting the solvent at low concentration ratio may remove the flow resistance at the end of shale barrier due to the additional solvent dilution effect (Li and Mamora, 2010).

Based on these considerations, we investigated the following potential injection strategies focusing on Case 4:

1. Pure steam injection, which is a pure SAGD process (base case).
2. Pure steam injection with top injector application.
3. 3 mole% C_7 coinjection with steam, which is an ES-SAGD process.
4. 3 mole% C_{12} coinjection with steam.
5. Coinjection of solvent mixture, which includes 3 mole% C_7 and 3 mole% C_{12} .
6. 3 mole% C_7 coinjection with steam plus top injector application.

The top injector starts to inject fluid at 1034 days, when the lower steam chamber meets the end of the shale barrier. The bottom injector keeps injecting to maintain the lower steam chamber warm; otherwise, the viscosity of the heated bitumen increases quickly. The same injection constraints are applied for both top and bottom injectors. For brief discussion, the strategies above are referred to as Strategy 1, 2, 3, 4, 5, and 6 respectively in following discussions.

The property distribution profiles of the different injection strategies at 1551 days are showed in Fig. 21.

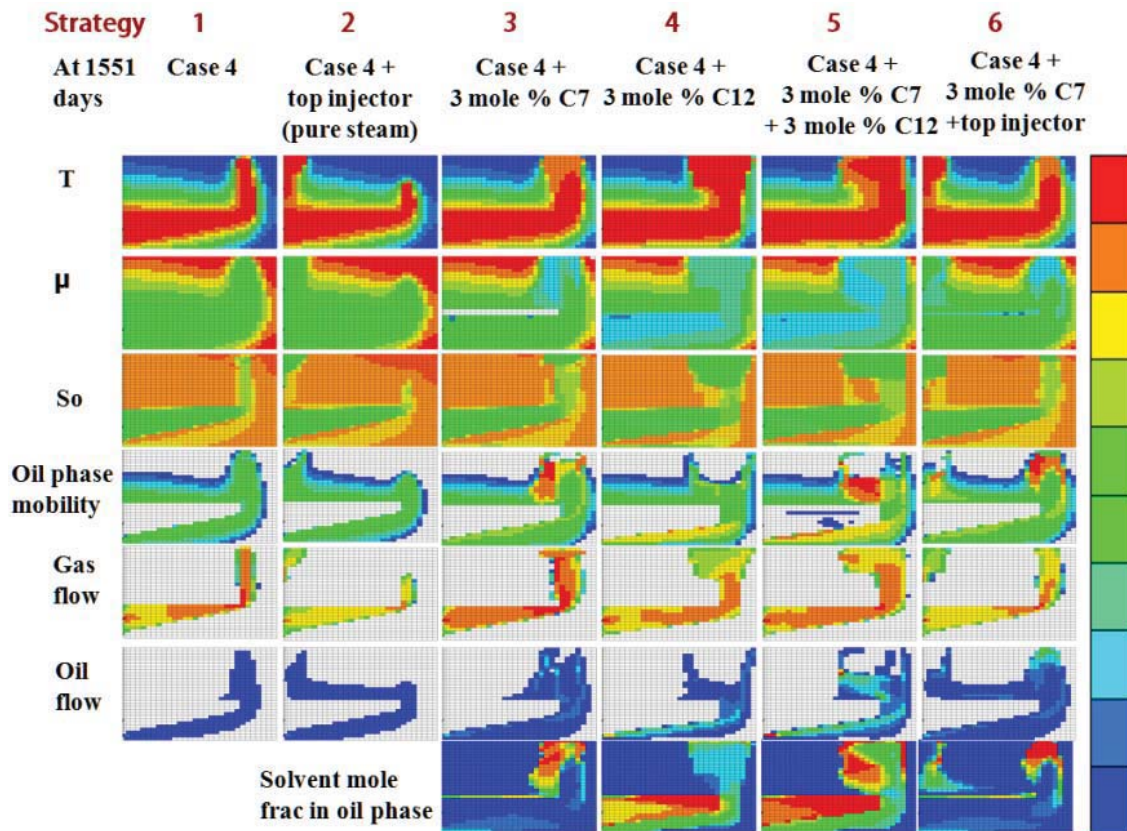


Fig. 21-Property profiles at 1551 days for different strategies: C₇ in vapor phase passes through the narrow flow path at the end of the shale barrier and reduces the viscosity of oil further more efficiently than steam; C₁₂ coinjection can accelerate the near-wellbore flow and reduce the residual oil saturation at the wellbore vicinity; the mixture of C₇ and C₁₂ flushes out the residual oil from the areas above and under the shale barrier; and the top injection application combines steam flooding mechanism from top injector and gravity drainage mechanism from bottom injector.

It should be noted that the cut-off value of oil phase mobility is set to 0.001 darcy/cp. From the property profiles of Strategies 2 and 1, top injection application under the SAGD process essentially is one hybrid process combining steam flooding and gravity drainage mechanism. From the oil-flow profiles, the heated oil along the top of the shale barrier is first pushed through the end of the shale barrier by

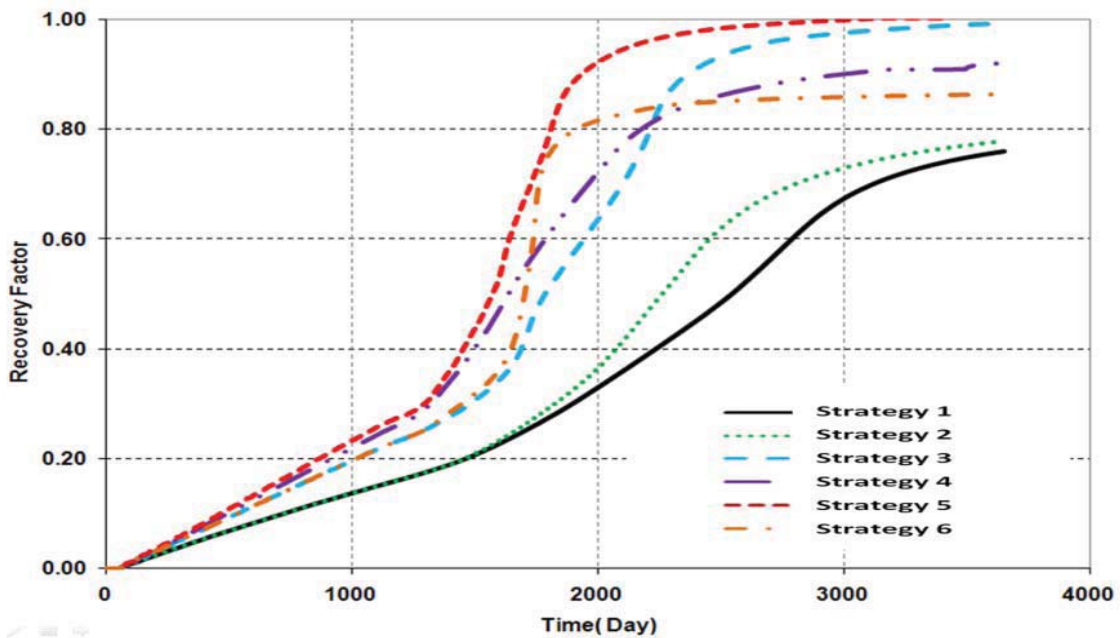
steamflooding from top injector. Then the empty space left behind is filled by steam, a large steam chamber is quickly built around the shale barrier and then gravity drainage mechanism will dominate the production. Similar discussion can be applied to Strategy 3 and 6. It should be noted that the fraction of C_7 condensed to liquid phase inside the trapped area in Strategy 6 is much less than in Strategy 3. The reason is that the top area is heated by the top steam injection.

Strategy 3 shows that the vaporized C_7 is delivered to and passes through the narrow flow path at the end of the shale barrier more easily than steam. Since the temperature at the end of the shale barrier is low (refer to the temperature profiles of Strategies 3 and 1, Fig.21), C_7 condenses from the vapor phase to the liquid phase, which significantly reduces the viscosity of the heated bitumen (refer to the viscosity profiles of Strategies 1 and 3, Fig.21). The mobile oil at the end of shale barrier is drained away much more efficiently under Strategy 3 than under Strategy 1, a wider flow path at the end of shale barrier is opened under Strategy 3 to allow more steam to flow upward (refer to the oil saturation, oil flow and gas flow profiles of Strategies 1 and 3, Fig.21). Meanwhile, the vaporized C_7 is liquefied again once reaches the low-temperature area above the shale barrier (refer to the profile of the mole fraction of solvent in oil phase under Strategies 3, Fig.21), which can reduce the residual oil saturation significantly (refer to the oil saturation profiles of Strategies 3 and 1, Fig.21).

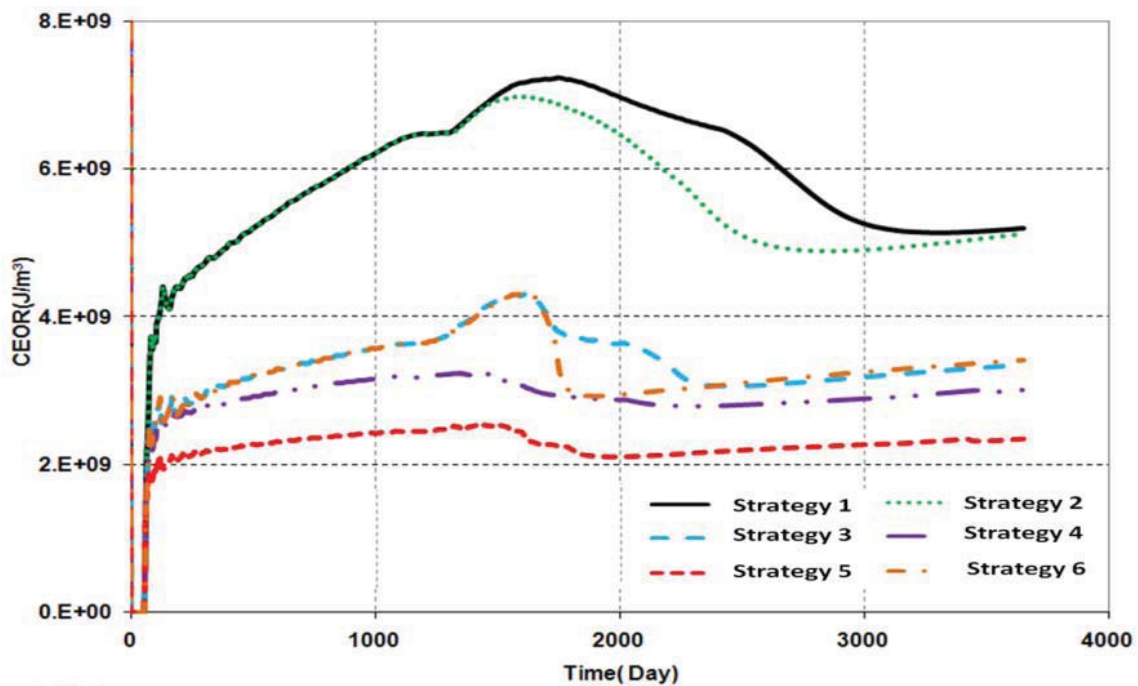
In Strategy 4, the liquid leg between injector and producer built by subcool control retains most of the liquid C_{12} in the steam chamber (refer to the profile of the solvent mole fraction in oil phase under Strategies 4, Fig.21). The liquid C_{12} reduces the

condensate viscosity and residual oil saturation much more efficiently than the vaporized C_7 in Strategy 3 at the wellbore vicinity (refer to the viscosity profiles in Strategies 3 and 4, Fig.21), which would substantially increase the oil drainage efficiency (refer to the oil flow profiles in Strategies 1 and 4, Fig.21). The solvent mixture used in Strategy 5 can take advantages of both C_7 and C_{12} . Most of C_{12} stays in liquid phase and significantly accelerates the drainage efficiency at the near-wellbore area, which further improves the injectivity of C_7 and steam. The phase change of C_7 , from vapor to liquid, takes effect inside the trapped area, where is with lower temperature, to flush out the oil.(refer to the profiles of the solvent mole fraction in oil phase and the gas flow under Strategies 5, Fig.21). The comparison of oil flow and oil phase mobility profiles among Strategies 3, 4, and 5 shows Strategy 5 accelerated the oil flow throughout the entire steam chamber instead of only at the area above shale barrier in Strategy 3 or only at the area under the shale barrier in Strategy 4 (refer to the oil flow profiles under Strategies 3, 4, and 5, Fig.21).

The plots of oil recovery factor and cumulative energy to oil ratio (CEOR) for different strategies are plotted in Fig. 22. The ultimate recovery factors of different strategies from high to low follow the order of Strategies 5, 3, 4, 6, 2 and 1, while the ultimate CEOR values of different strategies from high to low follow the order of Strategies 1, 2, 6, 3, 4 and 5. So, coinjecting the mixture of C_7 and C_{12} in Strategy 5 delivers the highest recovery factor with the lowest CEOR among all the investigated strategies.



(a) Oil recovery factor



(b) CEOR

Fig. 22-Production performance comparison between different operation strategies: Coinjecting the mixture of C₇ and C₁₂ in Strategy 5 delivers the highest recovery factor and the lowest CEOR among all investigated strategies.

Solvent coinjections show better performance than pure steam injection from the comparison between pure steam injection strategies (Strategies 1 and 2) and the solvent coinjection strategies (Strategies 3, 4, 5 and 6). The reason is the additional dilution effect of the solvent. Strategy 4 gives a higher recovery factor at the early phase but finally is lower than Strategy 3 because most of C_{12} stays in the liquid phase and mainly affects the near-wellbore area. Under Strategy 5, almost all residual oil is washed out by the liquid C_{12} at the near-wellbore area and the liquefied C_7 inside the trapped area above shale barrier, which is theoretically correct. Solvent in liquid phase can mix with bitumen efficiently at any proportion and flush all the residual oil out.

Top injector applications include Strategies 2 and 6. The top-injector application marginally decreases the CEOR from Strategy 1 to 2. The reason is that the heated oil above the shale barrier is produced quickly by steamflooding from top injection. After the steam pass through the end of shale barrier, the shale barrier effect disappears and the advantage of top injection starts to disappear. Strategy 6 gives higher recovery factor and lower CEOR than Strategy 3 once top injection starts. The ultimate recovery factor of Strategy 3 is higher than Strategy 6 with lower ultimate CEOR. The reason is that more fractions of C_7 condensate from vapor phase to liquid phase inside the trapped area above the shale barrier under Strategy 3 than under Strategy 6. Solvent coinjection decreases CEOR significantly compare to pure steam injection (refer to Strategies 1, 3, 4, and 5). The lower CEOR in Strategy 4 than in Strategy 3 is because the simulated reservoir is very thin. Liquid C_{12} only affects the near-wellbore area. For a thicker

formation, the sweep efficiency of C_{12} would be lower and the CEOR value under C_{12} will be higher.

Summaries

Main conclusions from this part of the simulation study are as follows:

1. The flow resistance at the end of the shale barrier and the extra heat absorbed by the residual water in the shale barrier lead to the following effects.

- The blocking barriers (Case 1, 2, or 4) with long length or with a location near the wellbore delay the oil production significantly and lead to high SOR value.

- The flow resistance of the unblocking shale barrier (Case 3) is very small.

2. Solvent coinjection can reduce the flow resistance at the end of shale barrier.

- Vaporized solvent (C_7 in this study) can pass through the narrow flow path at the end of the shale barrier more efficiently than steam to accelerate the steam chamber propagation at the end of shale barrier.

- The phase change of solvent (C_7 in this study) from vapor to liquid efficiently reduces the flow resistance at the end of the shale barrier and flushes more oil out from the trapped area above the shale barrier.

- The liquid solvent (C_{12} in this study) can be trapped inside the steam chamber by the sub-cool control strategy to accelerate the near-wellbore flow.

- Multicomponent solvent (the mixture of C_7 and C_{12} in this study) coinjection takes the advantages of both vapor and liquid solvents and flush out the residual oil at different area with different drainage mechanism. In this study, the solvent

mixture coinjection strategy, *i.e.* Strategy 5, delivers the highest recovery factor and the lowest CEOR among all the investigated strategies.

3. Top-injector application shows only marginal improvement by combining steam flooding and gravity drainage mechanisms. Considering additional drilling cost, top-injector application may be not economic for field application.

3.2.4 High temperature diluent injection

It is logical to suggest injecting high-temperature solvent to deliver heat and solvent dilution effects simultaneously. However, the latent heat delivered by the solvent is much less than the amount delivered by the same mass of steam and the price of solvent is much higher than that of the produced oil. It appears that the high-temperature solvent injection is not feasible for commercial field application. However, the cost of solvent may be significantly reduced if the solvent is recovered from the produced fluid and reinjected.

For steam injection, we inject 95% quality 202°C steam at 1,650 kPa at the injector, which is slightly higher than the initial reservoir pressure at 1,500 kPa. The production period for steam injection case is 10 years. Under thermal solvent injection, C₆ is injected near its saturation condition with pressure of 1,650 kPa and temperature of 195°C. The entire production period for solvent injection case is only 1642 days due to the accelerated production rate. After 1642 days, we inject high-temperature gas (N₂ in this study) at 202°C and 1650 kPa to recover the solvent left in the depleted reservoir. For both cases, the subcool temperature difference between injector and producer is 10°C to trap the vapor phase inside the reservoir. In this simulation study, the total

dispersions are used to simulate both diffusion and dispersion, and are set as $0.006 \text{ cm}^2/\text{min}$ for C_6 in the oil phase and $0.0006 \text{ cm}^2/\text{min}$ for oil in the oil phase.

The phase behavior profiles in the reservoir under both high-temperature C_6 and steam injection cases are shown in Fig. 23, including the oil saturation and temperature distribution profiles at different times. It should be noted the oil phases discussed in Fig. 23 include both the original oil-in-place and the C_6 in the oil phase.

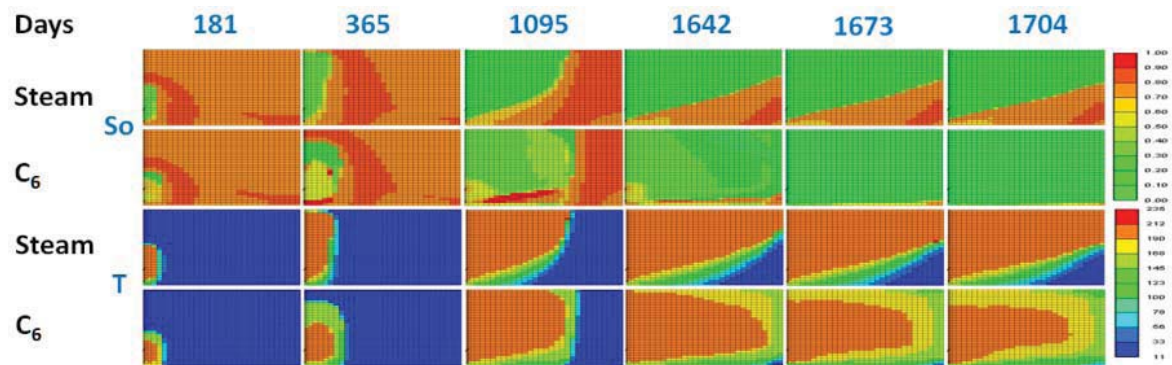


Fig. 23-Phase behavior profiles in the reservoir: the high-temperature C_6 injection significantly accelerates the vapor chamber propagation compared to steam injection.

The property distribution profiles along a horizontal row (Fig. 24) at 1095 days are used to quantitatively compare the detailed property differences under both cases. The location of the study horizontal row is shown by the dashed line, which is sketched on the oil saturation profile overlaid on Fig. 24.

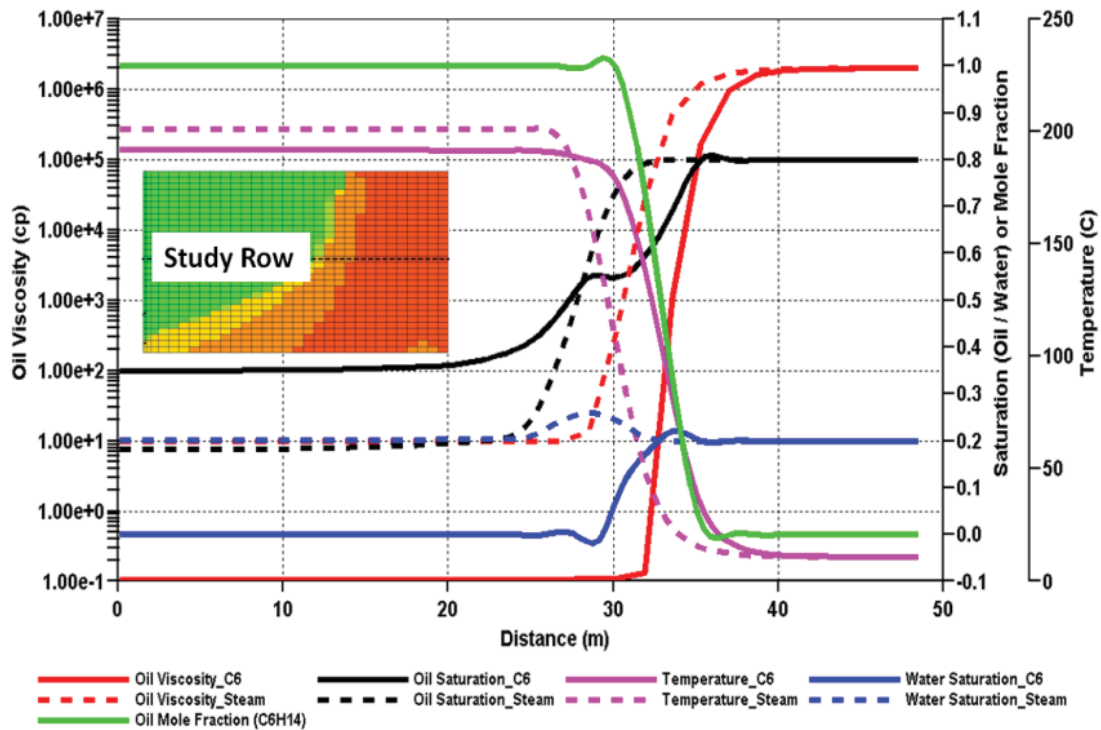


Fig. 24-Property distribution profiles at 1095 days along a horizontal row under both high-temperature C_6 injection and steam injection.

The property profiles include the profiles for oil viscosity, oil saturation, temperature, and water saturation under both cases, and the mole fraction of C_6 in the oil phase under high-temperature C_6 injection.

The vapor chamber propagation processes for two cases are illustrated by the oil saturation distribution profiles, which show that injecting C_6 at high temperature significantly accelerates the vapor chamber propagation compared to steam injection. Under high-temperature C_6 injection, the sweep efficiency is almost 95% at the 1642 days, while the sweep efficiency under steam injection is only about 60% at the same time period (refer to oil saturation profiles under both cases, Fig. 23).

The oil saturation and temperature profiles under C_6 injection are not overlaid together as under steam injection, which implies different drainage mechanism under different case (refer to comparison between oil saturation and temperature profiles under both cases, Fig. 23). For the steam injection, the oil flow along the fluid interface is dominated by the amount of heat released by steam. The oil along the fluid interface is heated to a higher temperature resulting in a lower viscosity. Once the viscosity of the oil along the fluid interface is lower enough, gravity drains it along the wall of the steam chamber to the bottom producer. Once the mobile oil is drained away, lower-temperature bitumen is exposed to the steam chamber and then is heated up. During this continuous process, the bitumen along the boundary remains hot and is drained continuously to the producer by gravity.

From the left to the right of Fig. 24, the temperature decreases from the respective saturation temperature of injected fluid to the initial reservoir value. Inside the vapor chamber, the temperature distribution is roughly constant. The temperature inside the vapor chamber is 202°C under steam injection and is 195°C under C_6 injection (refer to temperature profiles under both cases, Fig. 24). With the temperature decreasing along the edge of the vapor chamber, the injected fluids release their latent heat. Since less latent heat is delivered by C_6 (about 193 kJ/kg) than by steam (about 1928 kJ/kg), the temperature gradient along the fluid interface under C_6 injection is much smaller than under steam injection (refer to temperature profiles under both cases, Fig. 23). The smaller temperature gradient under high-temperature C_6 injection can reduce the heat

loss to the overburden and less heat is used to warm the vapor chamber, but the heat transformation efficiency along the fluid interface is lower.

Under high-temperature C_6 injection, the oil viscosity is reduced by both the heat effect and the dilution effect from C_6 simultaneously. The solubility of C_6 depends on its K-value. The lower temperature along the fluid interface, the more fractions of C_6 in vapor phase condense to liquid phase. The solubility of C_6 is higher. A liquid solvent will mix with the oil and reduce the oil viscosity much more efficiently than if the solvent were in the vapor phase. Along the fluid interface, C_6 mixes with the heated oil (refer to the mole fraction profiles of C_6 in oil phase, Fig.24) to reduce its viscosity further and offsets the lower latent heat effect delivered by C_6 . Under steam injection, the oil along the fluid interface has a viscosity of about 10 cp; under high-temperature C_6 injection, the oil viscosity along the fluid interface is only about 0.1 cp, which is about 2 orders of magnitude lower than under steam injection (refer to oil viscosity profiles under both cases, Fig. 24). Since the total dispersions for C_6 input to the simulator cannot capture the high solvent concentration ratio phenomena created at the fluid interface by the solvent phase change, the dilution effect of solvent in the field may be even more effective.

Under steam injection, oil and the water saturation inside the vapor chamber is about 20%, which may be attributed to the end points of the relative permeability plots (refer to profiles of the oil and water saturation under steam injection, Fig. 24). Under high-temperature C_6 injection, oil saturation inside the vapor chamber is about 35% before 1642 days and then decreases to zero after the 2 months blow down phase from

1642 days to 1794 days. This means all the retained C_6 are successfully revaporized and flushed out by the high-temperature N_2 (refer to the oil saturation profiles under C_6 injection, Figs. 23 and 24). Water saturation inside the vapor chamber is reduced to zero due to the low partial pressure of water phase inside the vapor chamber (refer to the water saturation profile under C_6 injection, Fig. 24). The lower water saturation can lead to higher relative permeability of the oil phase and higher oil flow inside the vapor chamber. In conclusion, the oil drainage mechanism under high-temperature C_6 injection consists of three main stages: first, heat is released by the high-temperature solvent; second, the solvent dilution effect; and third, the lower residual oil left behind after the blow down stage.

Fig. 25 shows the cumulative oil production and recovery factor under high-temperature C_6 injection and steam injection. The ultimate recovery factor is about 100 %OIIP at 1704 days under high-temperature C_6 , which is significantly higher than the value of 76 %OIIP at 3650 days under steam injection.

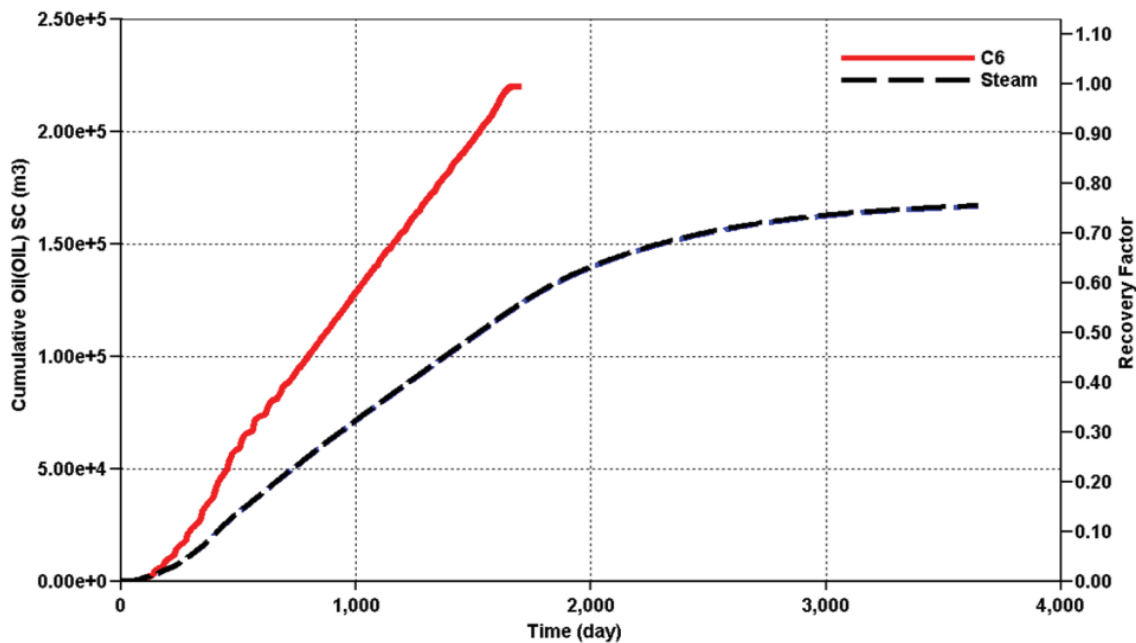


Fig. 25-Cumulative oil production and recovery factor under high-temperature C₆ injection are much higher than under steam injection.

Fig. 26 compares the oil production rates under both cases. Under steam injection, the producer starts to produce oil at 53 days instead of 90 days under high-temperature C₆ injection. Before fluid flows between the injector and the producer, the area between both wells is mainly heated by thermal conduction. Since more heat is released from steam than solvent, the time to connect both wells is shorter under steam injection than under high-temperature solvent injection.

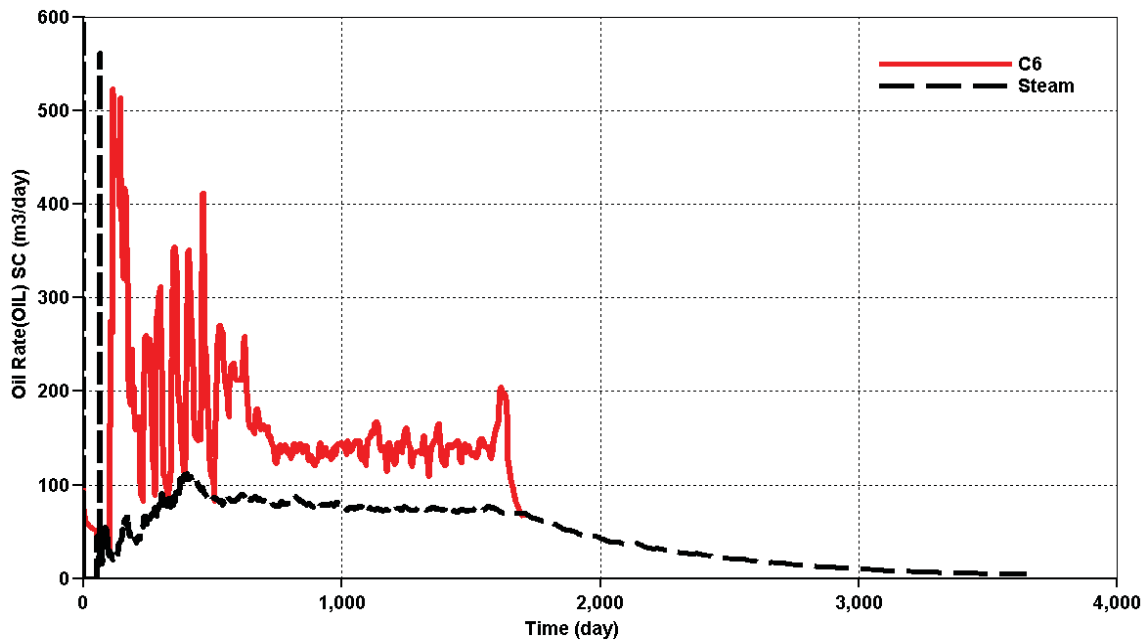


Fig. 26-Oil production rate of high-temperature C₆ injection is about 1.5 to 2 times the rate of steam injection.

The oil production rate under high-temperature C₆ injection is about 1.5 to 2 times the rate under steam injection. The fluctuation of oil rate under both cases is due to the production control by the subcool temperature. Since less latent heat is delivered by C₆ and the injection rate of C₆ is much higher, more volume of liquid phase accumulates at the bottom of the vapor chamber before the producer opens under high-temperature C₆ injection. The viscosity of the condensate near the producer under high-temperature C₆ injection is much lower than under steam injection due to the accumulation of liquid C₆. Once the producer is open, the drainage efficiency of condensate is much higher under high-temperature C₆ injection than under steam injection, and results in the higher fluctuation of oil production. The ratio of the cumulative injected solvent volume to the

cumulative oil production volume under high-temperature C_6 injection, which is called injection solvent/oil ratio, is shown in Fig. 27.

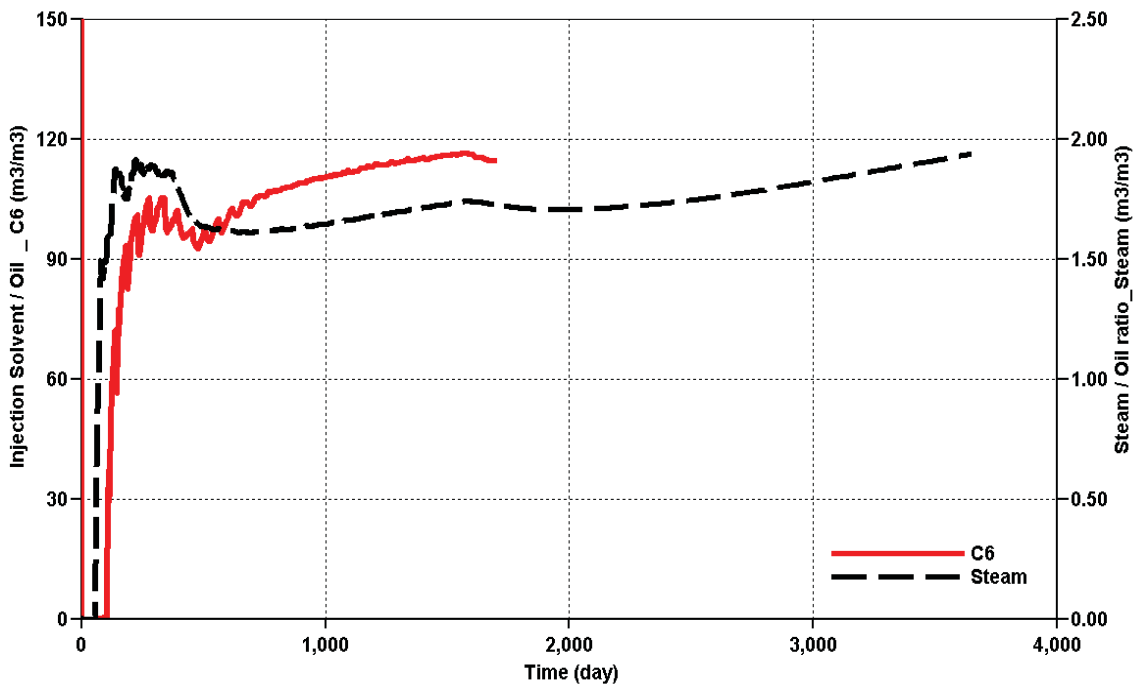


Fig. 27-Comparison between the injection solvent/oil ratio under high-temperature C_6 injection and the steam oil ratio (SOR) under steam injection.

For a convenient comparison, the steam oil ratio (SOR) under steam injection is also displayed. The ultimate injection solvent/oil ratio under high-temperature C_6 injection at 1704 days is about 115, which means injecting 115 m³ of solvent produces 1 m³ of oil. Compared to the SOR value (between 1.5 and 2) under the steam injection, it seems that the high-temperature solvent injection is uneconomic for field application. Recycling the effective solvent from the production fluid and then reinjecting the solvent into the reservoir may reduce the operational cost to an acceptable level.

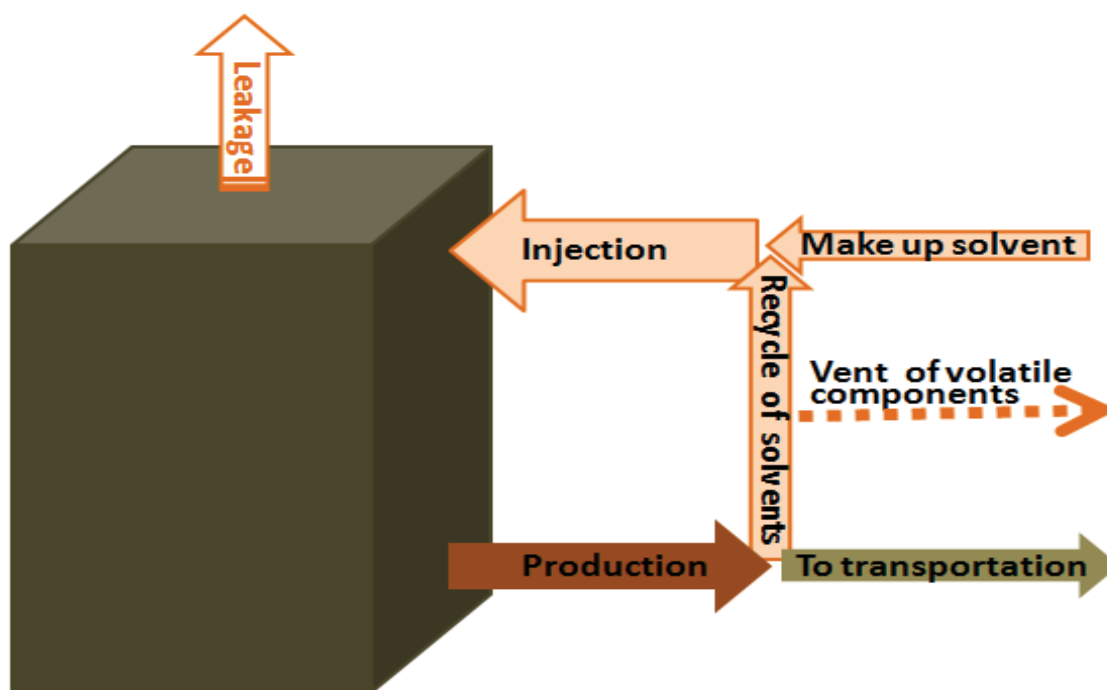


Fig. 28-Circulation system proposed to reduce the solvent cost under high-temperature solvent injection process.

Fig. 28 describes a proposed solvent circulation loop for field application. Once the condensed solvents are produced with oil, we can distill the solvents from the produced fluid and then inject them into the reservoir again. During the distillation process, most of the volatile components in the range of $C_1 \sim C_3$ need to be vented out to reduce the negative gas film effect. The diluents used in the field are usually in the range of $C_5 \sim C_{12}$ with a boiling point much higher than the volatile components. The intermediate heavy hydrocarbons from C_5 to C_8 can be easily distilled from the produced oil and separated from the volatile components. Since some fractions of diluents are needed to mix the produced oil for convenient transportation, the solvents left in the produced oil should not be considered as waste. All the operational costs associated with

operation of solvent circulation can be considered as the equivalent leaked solvent with the same enthalpy. Based on above discussions, the effective solvents lost at the surface would be very small and may be neglected, which is assumed to be 0.1 volume% of produced C_6 in this study.

The total leaked solvents include the solvents leaked at surface and from the vapor chamber in the reservoir. So, the solvent cost under high-temperature C_6 injection should be evaluated by the effective solvent/oil ratio, which is calculated as the cumulative volume of leaked solvents (at surface or from vapor chamber) to the cumulative volume of oil production. The leakage ratio of solvent from the reservoir is calculated by the volume of leaked solvent from the vapor solvent chamber to the volume of solvent in the vapor chamber. Because the injection pressure (1650 kPa) of C_6 is just slightly higher than the reservoir pressure (1500 kPa), the leakage ratio of solvent from the reservoir is very small. The effective solvent/oil ratios with different solvent leakage ratios, including 0.05, 0.10, and 0.20, under high-temperature C_6 injection are shown in Fig. 28.

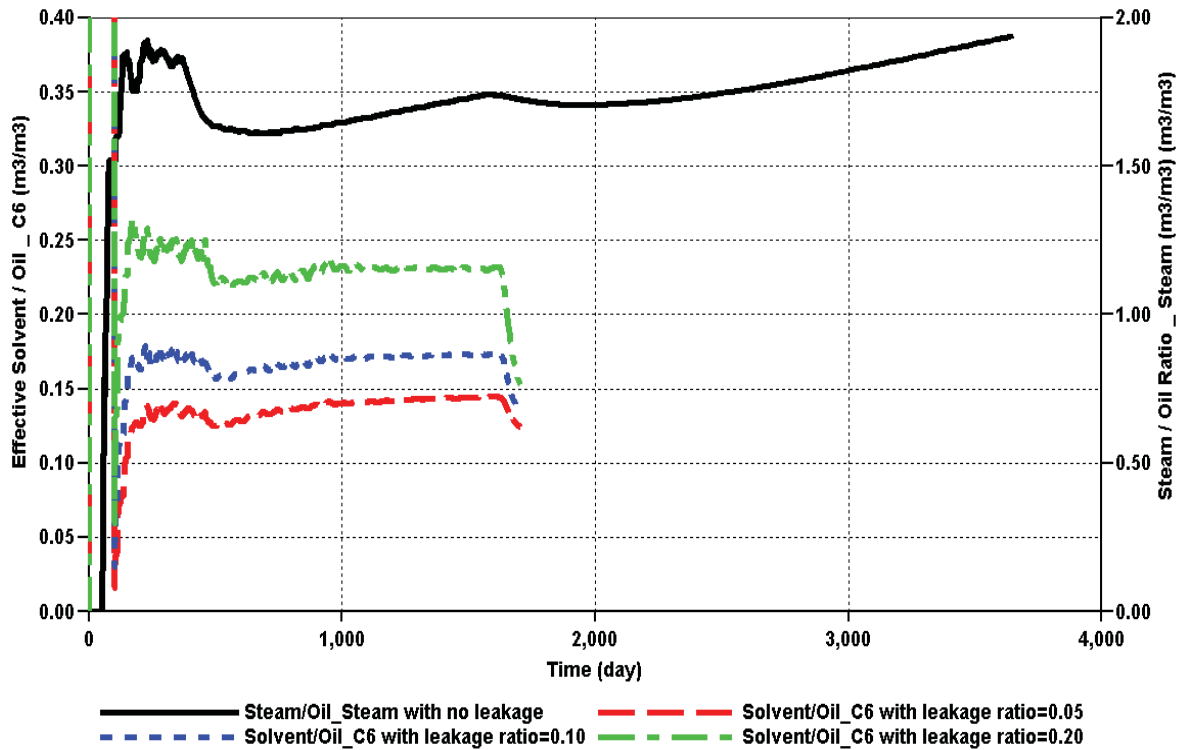


Fig. 29-Effective solvent/oil ratios under high-temperature C₆ injection with different leakage ratios, and steam oil ratio (SOR) under steam injection with no leakage.

The steam/oil ratio (SOR) under steam injection with no leakage also is displayed for convenient comparison. For the case of the leakage ratio 0.05, the effective solvent/oil ratio under high-temperature C₆ injection is about 0.14 before the blow down stage, which means 0.14 m³ of solvent can produce 1 m³ of oil. Even for the much worse situation with leakage ratio of 0.20, the effective solvent/oil ratio is about 0.23 before the blow down stage and is only about 0.15 after the blow down stage, which may be still economic for commercial application with better return during the later production period.

The cumulative energy required for oil production (CEOR) is a better parameter to evaluate the energy efficiency under both cases. Under steam injection, all the energy included in the produced hot water is lost. Under high-temperature C_6 injection, the produced solvents are recycled and most of the heat included in the produced C_6 condensate reenters into the vapor chamber. In this study, we first assume all the heat included in the produced C_6 is successfully reinjected to the reservoir.

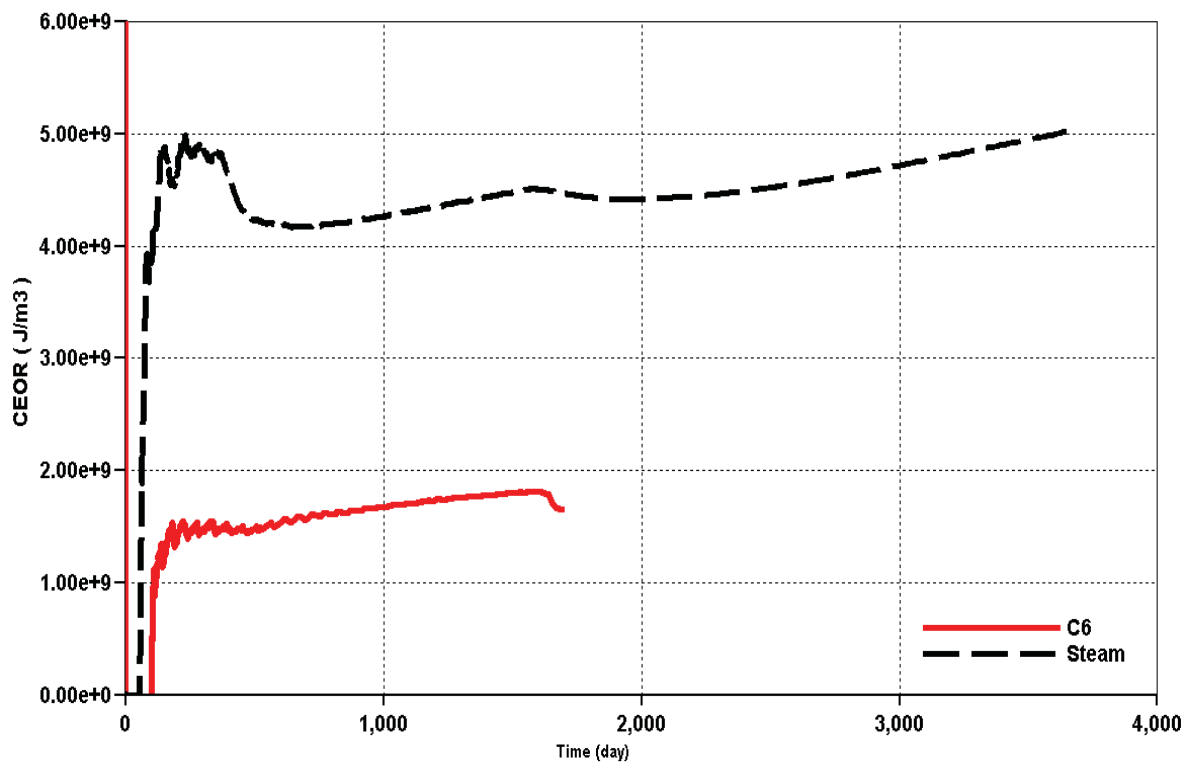


Fig. 30-CEORs under high-temperature C_6 injection and under steam injection, which shows the energy efficiency under high-temperature C_6 injection is substantially higher than under steam injection.

Fig. 30 shows the comparison between CEOR values under both cases. At the end of production, the ultimate CEOR value under steam injection is about $5 \times 10^9 \text{ J/m}^3$. Under high-temperature C_6 injection, the ultimate CEOR value is about $1.80 \times 10^9 \text{ J/m}^3$ before blow down stage and is only about $1.65 \times 10^9 \text{ J/m}^3$ after the blow down stage. Therefore, the energy efficiency under high-temperature C_6 injection is about 64% ~ 67% higher than under steam injection. If only 80% of the energy in the produced solvent is recycled, the energy efficiency under high-temperature C_6 injection still is about 56% ~ 60% higher than under steam injection.

The shorter production period under high-temperature solvent injection implies that a larger well pattern may be utilized. A simple heat transfer can meet revaporization requirement and the surface facility investment is much lower than steam injection system. For field application, we can simultaneously reduce the injection pressure and inject nitrogen at a temperature higher than the bubble point of the injected diluents to recycle the residual diluents as much as possible. Considering the extensive requirement of water and natural gas and the additional costs needed for investment of surface facility, high-temperature solvent injection appears economical.

Downhole electrical heaters located at the wellbores can reduce the communication period under high-temperature solvent injection. After the well pair is connected, the heater at the injector can continue to regulate the temperature of injected solvent to maintain a stable condensing condition, but the other heater at the producer should be shut down to avoid revaporizing the volatile components from the condensate. The accumulation of volatile components inside the vapor chamber has several negative

impacts on production performance: altering the condensing condition by partial pressure effect, reducing the heat transfer from vapor chamber to surrounding oil, impeding the heavier hydrocarbon entering into the reservoir, and blocking the contact between the heavier hydrocarbon and bitumen, as described by Li and Mamora (2010).

Since this simulation study is a preliminary study to compare production performance, the simulator may not capture all the details of phase behavior and drainage mechanisms within the reservoir. It should be noted that the assumption of the equivalent solvent leaked at surface is only 0.1 volume% of produced C_6 maybe too optimistic. If more solvent leaked from reservoir, more additional solvent is needed to make up the injection volume and more energy is required to produce same volume of oil. A higher solvent leakage ratio at the surface would significantly reduce the economics of high-temperature solvent application since the circulation rate of solvent is very large. When the circulation rate of solvent at the surface is increased, the operational costs of equipment would increase also. Further experimental work and more detailed economic evaluation are necessary to assess the feasibility of high-temperature solvent injection.

Summaries

1. High-temperature solvent injection at the solvent condensing condition can take advantages of both the heat and dilution effect of the solvent to reduce the oil viscosity efficiently with no steam required. The phase change of solvent under the condensing condition can deliver more heat into the reservoir and mix with oil more efficiently than under non-condensing condition. In the field, the key to designing a successful high

temperature solvent injection process is to choose an injection solvent including more fractions of components near their condensing conditions at suitable injection condition.

2. In this study, the reason to choose C6 as the surrogate component is based on the simulated reservoir and injection conditions. Under high-temperature C6 injection, the production rate is about 1.5 to 2 times the rate under steam injection; the production period is about half that with steam injection; and the oil recovery factor is almost 100 %OIP.

3. A preliminary economic evaluation is discussed with the blow down process and a solvent circulation loop to reduce solvent cost. Under these conditions, the evaluation appears to indicate that high-temperature solvent injection is economical for field application. Further technical study and a more detailed economic evaluation are necessary.

4. EXPERIMENTAL STUDY

4.1 Analytical analysis

Nasr *et al.* (2003; Nasr and Ayodele 2005, 2006) developed the expanding solvent SAGD (ES-SAGD) process, which is one of the modifications of the SAGD process combining the benefits of steam and solvents. The solvent is injected with steam in the vapor phase. The solvent condenses at or near the vapor-bitumen interface. This dilutes the oil and in conjunction with heat reduces viscosity of the bitumen at the vapor-bitumen interface. Compared to conventional SAGD, this process can improve oil production rate with less energy and water requirements.

A suitable hydrocarbon additive used in ES-SAGD should be selected in such a way that it can vaporize and condense at the same pressure-temperature conditions as the water phase. By selecting the hydrocarbon solvent in this manner, the phase change of solvent is expected to be the same as steam along the vapor-bitumen interface. As shown in Figs. 31 and 32, hexane (C_6) has the closest vaporization temperature to steam at the experimental pressure of 2.2 MPa. This results in a higher drainage rate than other pure solvents. However, Fig. 32 also indicates that coinjecting a diluent (mainly C_4 to C_{10}) with steam results in a drainage rate comparable to or even slightly higher than that from C_6 co-injection. Since diluents include other components besides C_6 , the observation of the higher drainage rate under diluent injection is not fully understood. We thus conducted a study to better understand the drainage mechanism under solvent mixture co-injection.

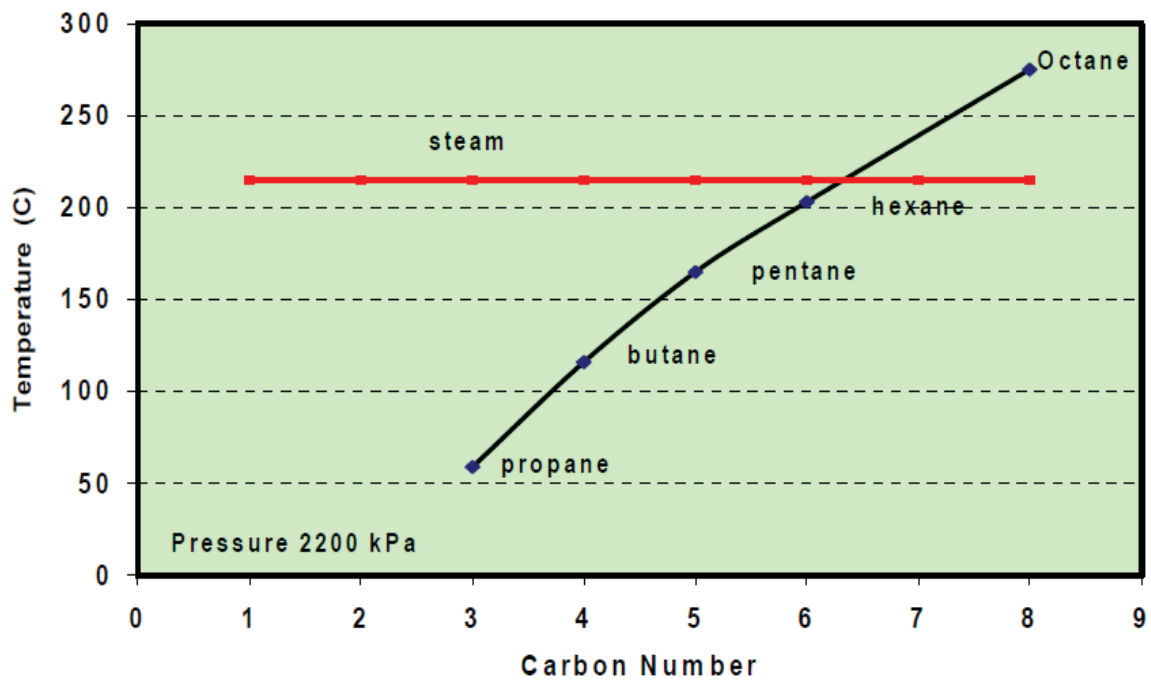


Fig. 31-Comparison of solvent vaporization temperature with steam temperature at study pressure (from Nasr *et al.* (2003 and 2006)).

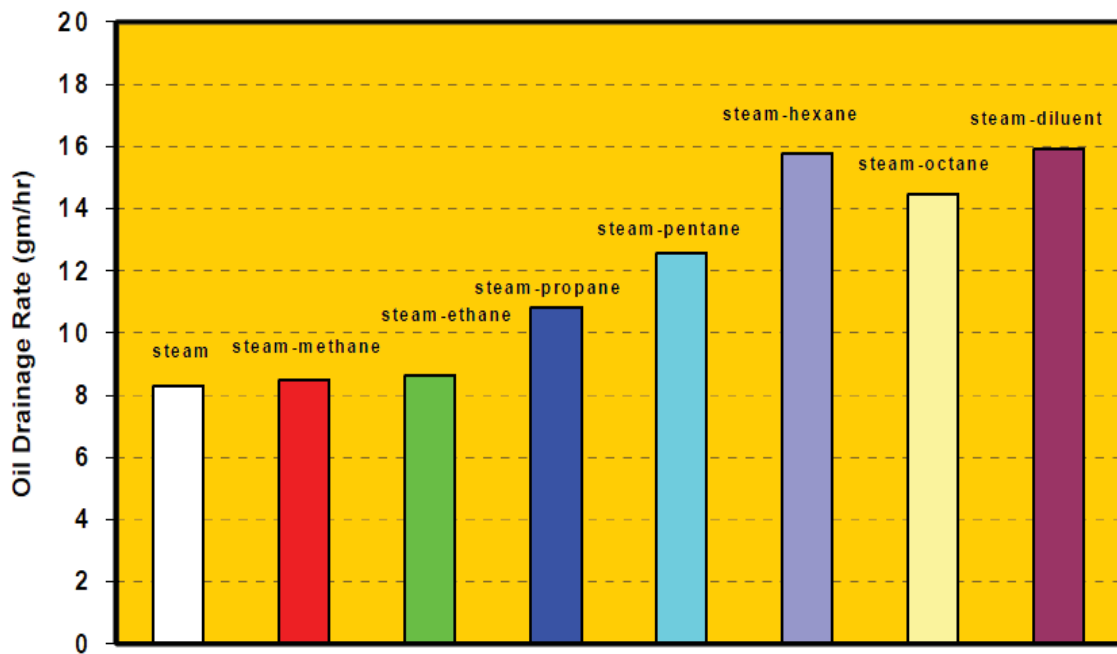


Fig. 32-Variation of the oil drainage rate with carbon number at study conditions (from Nasr *et al.* (2003 and 2006)).

4.2 Experimental apparatus

Certain Athabasca reservoirs have low pressures because they have been depleted by production of overlying gas. Other reservoirs are naturally occurring low-pressure shallow bitumen reservoirs (Ayodele *et al.* 2009). One of the challenges for SAGD research is to investigate low-pressure applications in these reservoirs. For this experimental study, a low-pressure scaled model was constructed representing a 2D cross section normal to the horizontal well pair. Low Athabasca field conditions were used in the scaling, except when it was operationally impossible to represent them in the laboratory with our experimental setup.

The experimental apparatus consists of three main systems (Fig. 33): the scaled physical model; the fluid injection and production system; and the data measurement and recording system. A schematic diagram showing the entire experimental setup is presented in Fig. 34.



Fig. 33-Photo showing the laboratory system: the drum jacket containing SAGD cell is used to isolate the surrounding infrared noise; the concrete on the top and at the bottom of the cell is used to simulate the heat loss through over burden and under burden; the data logger under the jacket is used to record the temperature distribution from thermal camera; and the other data logger on the control panel is used to monitor the injection and production data.

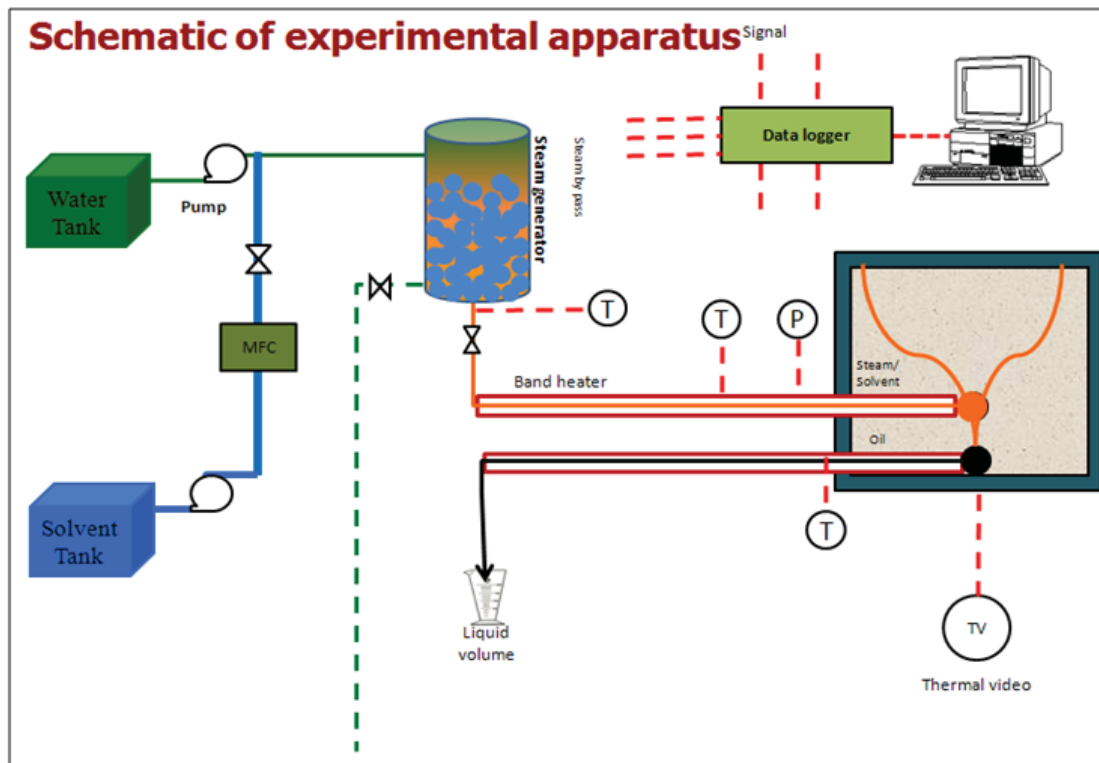


Fig. 34-Schematic diagram of experimental apparatus.

4.2.1 Scaled physical model

Certain Athabasca reservoirs have low pressures because they have been depleted due to production of over-laying gas. Other reservoirs are naturally occurring low-pressure shallow bitumen reservoirs (Ayodele *et al.* 2008). The current interesting challenge for SAGD research is to investigate low pressure application in these reservoirs. For this experimental work, a low pressure physical model is designed to scale down a 2D cross section along the low pressure SAGD horizontal well pairs. Low Athabasca field conditions will be used in the scaling, except when it is operationally impossible to represent them in the laboratory with our experimental setup.

Modeling scaling is based on Butler's theory, which is suitable to scale pure steam injection under gravity drainage processes but is less reliable for solvent coinjection processes. The detailed scaling process can be found from Chung and Butler (1987). The scaling factor chosen is 1:131.2. In laboratory condition, one hour represents about 1.68 years in the field. The resulting internal dimensions of the cell are 15 in. long by 9 in. wide by 1 in. thick with well spacing between injector and producer of 1.5 in. The location of the producer is 0.45 in. from the bottom of cell. The walls of the cell are constructed of 1-in.-thick Teflon PTFE (polytetrafluoroethylene) sheets. Since the walls of the cell represent a no-flow boundary for mass and energy, Teflon was chosen because of its low thermal conductivity, high operating temperature rating, and compressive strength. A schematic diagram of the cell is shown in Fig.35.

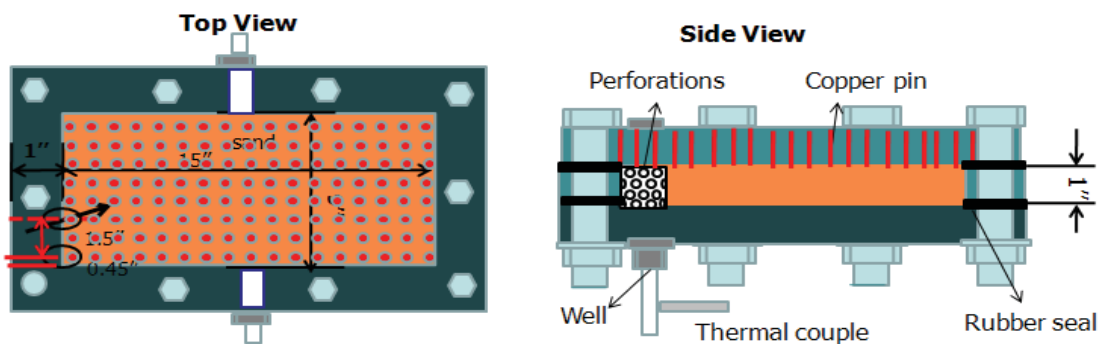


Fig. 35-Schematic of the scaled physical model.

To monitor the traveling front profile of the high-temperature vapor during the experiments, about 490 thermal copper pins (with 0.9-mm diameter) are placed in holes

drilled through the bottom Teflon plate (Fig. 36). They are arranged in 17 rows and 29 columns with spacing of 0.5 in. Heat inside the model is conducted to the outside through these copper pins with minimum temperature drop. Thus the inside cell temperature is measured by the infrared thermal camera. To avoid ambient infrared data noise, the physical model is placed in a metal drum (see Fig. 33).



Fig. 36-Back view of the physical model to show the distribution of the copper pins, which are used to transmit the temperature from inside of the cell to outside.

The over-burden is simulated using a concrete block placed on top of the model. The under-burden is represented by the thick concrete platform molded at the entrance of the drum (see Fig. 33). To determine whether the use of finite concrete slabs would cause errors introduced by boundary effects, the corresponding cumulative heat losses were calculated and then compared to the heat losses for a hypothetical boundary

concrete block. Following the calculation method of Stegemeier (1980), a 5-inch concrete block introduces less than 2% error for the maximum expected experimental run time of 6 hours (Fig. 37).

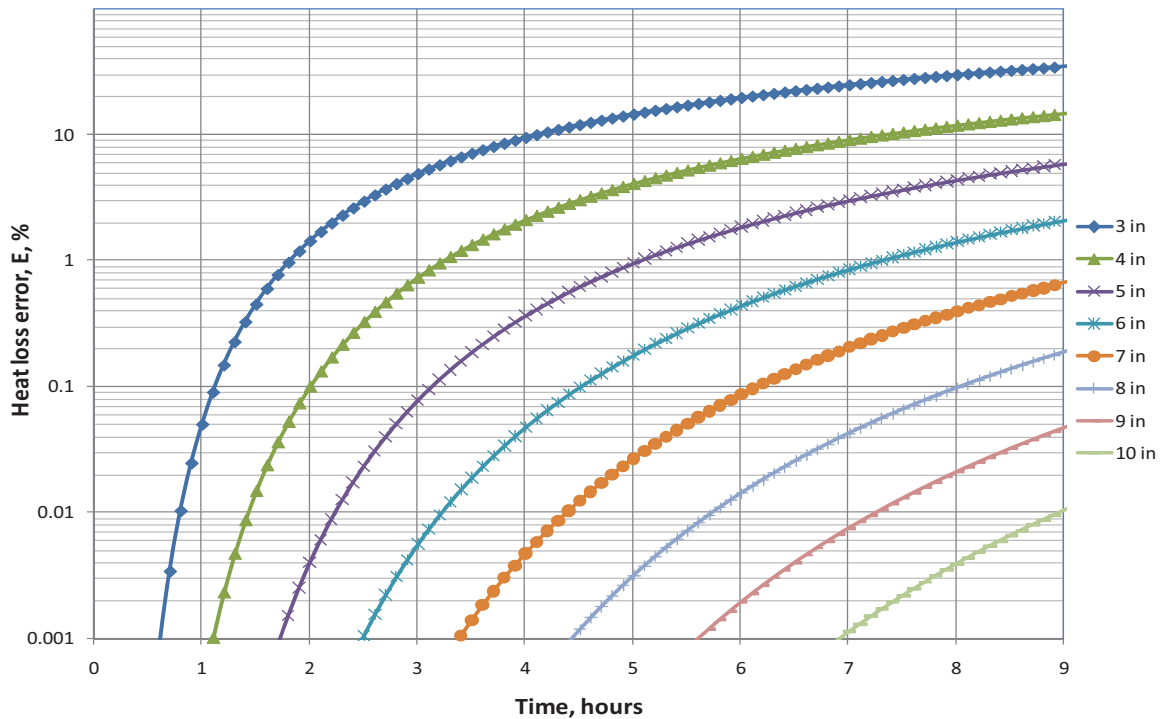


Fig. 37-Heat loss error introduced by boundary effects caused by the use of finite surrounding formations.

4.2.2 Fluid injection and production system

The fluid Injection system consists of a steam generator, water and solvent reservoir, two high-performance liquid-chromatography (HPLC) pumps, and two back-pressure regulators. The distilled water from the water reservoir is fed by one HPLC pump at a constant rate into the steam generator. The pump outlet pressure is maintained constant at about 1000 psi minimize pulsation. For steam with solvent

additive injection, the solvent is fed by a second HPLC pump and then mixed with the injected water. One production system is used for all study conditions, which is controlled manually to maintain the cell outlet pressure.

4.2.3 Data measurement and recording system

A data logger and a personal computer are used to record and monitor the following parameters: time, fluid injection temperature, and injection pressure. The parameters are recorded at 30-second intervals. An FLIR A20M thermal video system (Fig.38) is used during the experiment to record the cell temperature distribution with the data being recorded by another data logger (see Fig. 33).



Fig. 38-FLIR A20M thermal video system.

4.3 Experimental workflow

4.3.1 Cell preparation

We followed the procedure below to prepare the cell for testing:

1. Dis-assemble the physical model. Brush away any glass beads left on the cell, clean every part with xylene and acetone, and dry all the components with air.
2. Assemble the model. While assembling the model, follow the number sequence of the bolts to tighten the nuts. Always use a torque wrench to tighten nuts. Apply 50~60 lbs-in of torque on each nut while tightening.
3. Apply 18 psig pressure to the model using nitrogen. If the model holds pressure for more than 30 minutes proceed to Step 4. If the pressure drops, check for leaks and reapply pressure. Measure and record the weight of the empty model.
4. Fill model with 2 mm glass beads. Repeatedly shake the model while filling to ensure uniform packing of the model. Measure the weight of the model again.
5. Connect the top of the physical model to the top of the transfer oil vessel and connect the bottom of the transfer vessel to the transfer vacuum flask.
6. Preheat the model and oil reservoir to 60°C in the oven for 6 hours.
7. Open the valve between the transfer oil vessel and model, and apply the vacuum. If the vacuum drops, check for leaks and reapply vacuum.
8. When no leak is detected, open the valve between the transfer oil vessel and model, apply vacuum to suck heated oil from the transfer oil reservoir to the model until 1.5 pore volumes are fed to make sure the model is fully saturated.

9. Leave the model in the oven for 24 hours to ensure the model has the same temperature as the environment. Record the weight of model to calculate the weight of oil in the model.

10. Put the model inside the drum jacket; connect the fluid injection and production system.

11. Connect the fluid injection system to the outlet of the steam generator.

4.3.2 Experimental procedure

1. The steam generator is set and conditioned to 130°C to make sure the injected steam is 100% dry.
2. During the start period, a band heater is used to heat both wells to 130°C until injector and producer are hydraulically connected. We then set the band heater at the producer to 90°C to reduce the flow resistance inside the producer. The pressure in the model is maintained at 8 to 10 psig by manually controlling the production valve (a needle valve).
3. Produced fluid is collected in a preweighed glass flask at 20-minute intervals. Once the experimental time of 6 to 7 hours is reached, all equipment is turned off.
4. The sample-filled glass flasks are heated in an oven whose temperature is set higher than the boiling point of the injected solvent. The vaporized water and solvent are blown out by nitrogen, and then the glass flasks are weighed again to calculate the produced oil weight.
5. Experimental results are analyzed based on the collected data.

4.4 Experiment conditions

Fig. 39 compares injected solvent vaporization temperature with steam temperature. Based on the difference between solvent vaporization temperature and steam temperature, three types of runs are conducted to investigate mechanisms controlling the production performance.

1. Type 1 (Runs 0 and 1): Both of these runs are pure steam injection runs and used to simulate conventional SAGD process and to make sure the experimental results are repeatable. The constant steam injection rate is 3 cc/min.
2. Type 2 (Run 2): C_7 is chosen as the injected solvent used to simulate a conventional ES-SAGD process. At injection conditions, the vaporization temperature of C_7 is almost same as the value of steam (see Fig. 39) and so can be vaporized by steam. The injection rate of C_7 is 0.6 cm³/min with the same steam injection rate as Run 0 and 1 (3 cc/min).
3. Type 3 (Run 3): At injection conditions, xylene has a much higher vaporization temperature than steam (see Fig. 39) and is difficult to vaporize by steam. The solvent mixture of C_7 and xylene (1:1) is chosen as the injected solvent to investigate the different impacts of light solvent (C_7 in this study) and heavy solvent (xylene in this study) on the production performance. The injection rate of the solvent mixture is 0.6 cm³/min with the same steam injection rate as other runs.

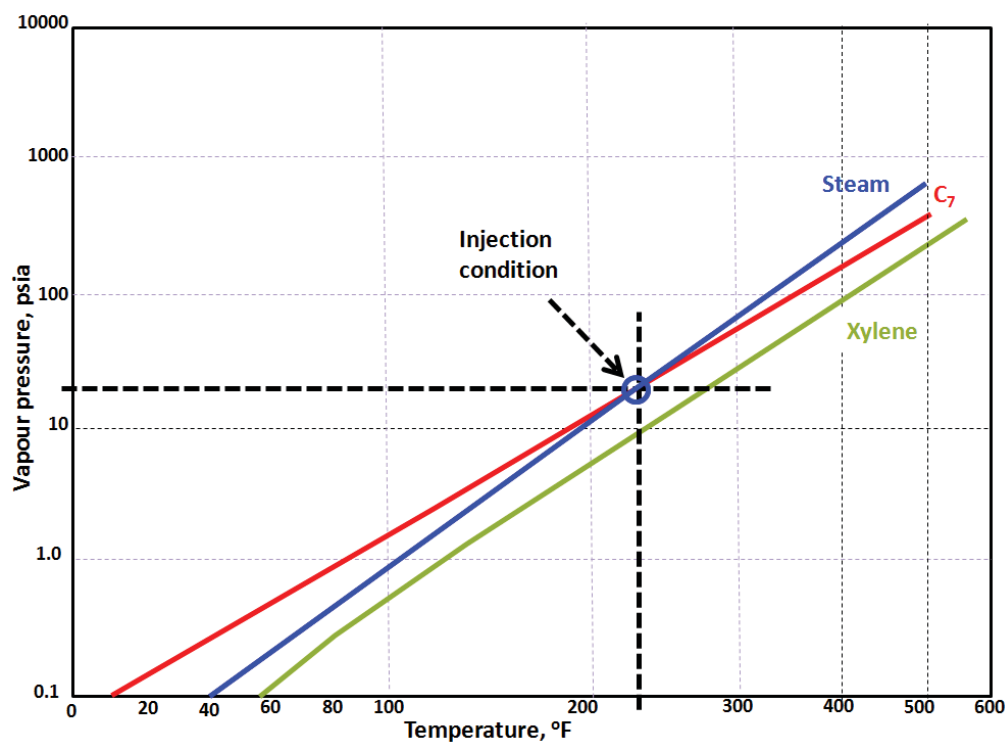


Fig. 39-Comparison of injected solvent vaporization temperature with steam temperature.

4.5 Experimental results and discussions

4.5.1 Production performance

The comparisons of oil production rate, cumulative oil productions and oil recovery factors, cumulative steam required for oil production (CSOR) and cumulative energy required for oil production (CEOR) are shown Fig. 40 to Fig. 43. respectively. It should be noted that the CEOR value is estimated based on the latent heat delivered by the injected fluid at the injection pressure 8 psig, and the heat delivered by xylene is calculated with the properties of octane (C₈).

From the comparisons, the difference between the production performances of Run 0 and Run 1 is very small, which indicates the repeatability of conditions. The slight difference of production performance between Run 0 and Run 1 is probably due to the timing of manually opening and closing the producer.

The oil production rates of all experimental runs from high to low generally follow the order of Run 3, Run 2, and Run 0 (Run 1). Under the experimental conditions, the higher the production rate (Fig. 40), the larger are the cumulative oil production volume and the recovery factor (Fig. 41); and the lower is the CSOR value (Fig. 42), the lower is the CEOR value (Fig. 43). Compared to pure steam injection runs (Run 0 and 1), coinjecting C_7 (Run 2) with steam increases the ultimate recovery factor of oil inside the cell from 25% to 29% , and decreases the ultimate CSOR 2.2 to 1.9 and the ultimate CEOR from 4892 J/cm^3 to 4326 J/cm^3 ; coinjecting C_7 and Xylene (Run 3) increases the ultimate recovery factor of oil from 25% to 34% , and decreases the ultimate CSOR 2.2 to 1.6 and the ultimate CEOR from 4892 J/cm^3 to 3629 J/cm^3 .

Comparison of the runs in the early production period indicates a significant “gas blanket effect” phenomenon for Run 2. The gas blanket represents the accumulation of solvent in the vapor phase along the vapor-bitumen interface, which works as a heat insulator to impede the heat transfer from the high-temperature vapor chamber to the surrounding low-temperature bitumen. The first production sample collected during Run 2 is much lower than during other runs (Fig. 40). The reason is that more C_7 stays in the vapor phase for Run 2 and the viscosity reduction effect is lower because of the gas blanket effect. Therefore, during the early period of Run 2, the cumulative oil production

and recovery factor are lower (Fig. 41), but the CSOR and CEOR values are much higher than in other runs (Fig. 42 and Fig. 43).

There is a general trend of decreasing oil production rate for all runs (Fig. 40) after the vapor chamber reaches the top of the cell. At the beginning, the oil production rate increases as the vapor chamber expands vertically. Once the vapor chamber reaches the top of the cell, the production rate starts to decrease because of the increasing trend of heat loss through overburden along with lateral expansion of the vapor chamber. The trend of decreasing oil production rate from high to low follows the sequence of Run 3, Run 2 and Run 0 (Run 1). At the top area of the vapor chamber, more solvent condenses to the liquid phase once the solvent front meets the top of the cell. The solvent in the liquid phase can better displace and reduce oil viscosity more efficiently than the solvent in the vapor phase. The phase change of solvent at the top area helps to offset the heat loss impact through overburden, which results in a smaller decreasing trend of oil production rate than pure steam injection runs (Run 0 and Run 1). The production performance for Run 3 is better than Run 2, which is due to the different solvent type and ratio injected in respective runs. This will be discussed in more in following section.

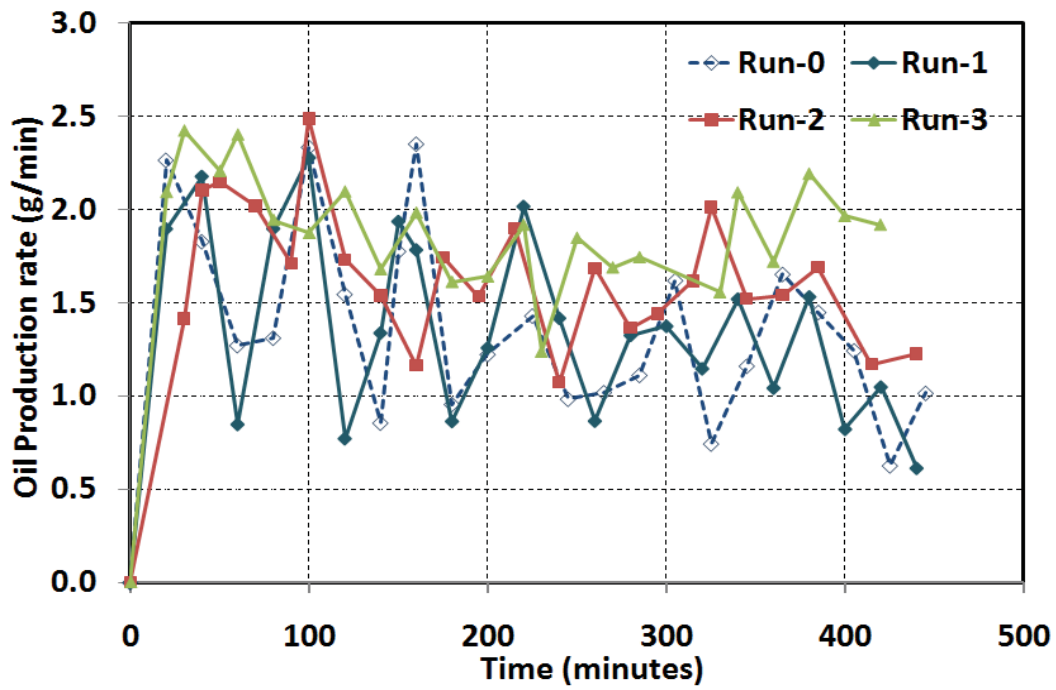


Fig. 40-Comparison of oil production rates among experimental runs.

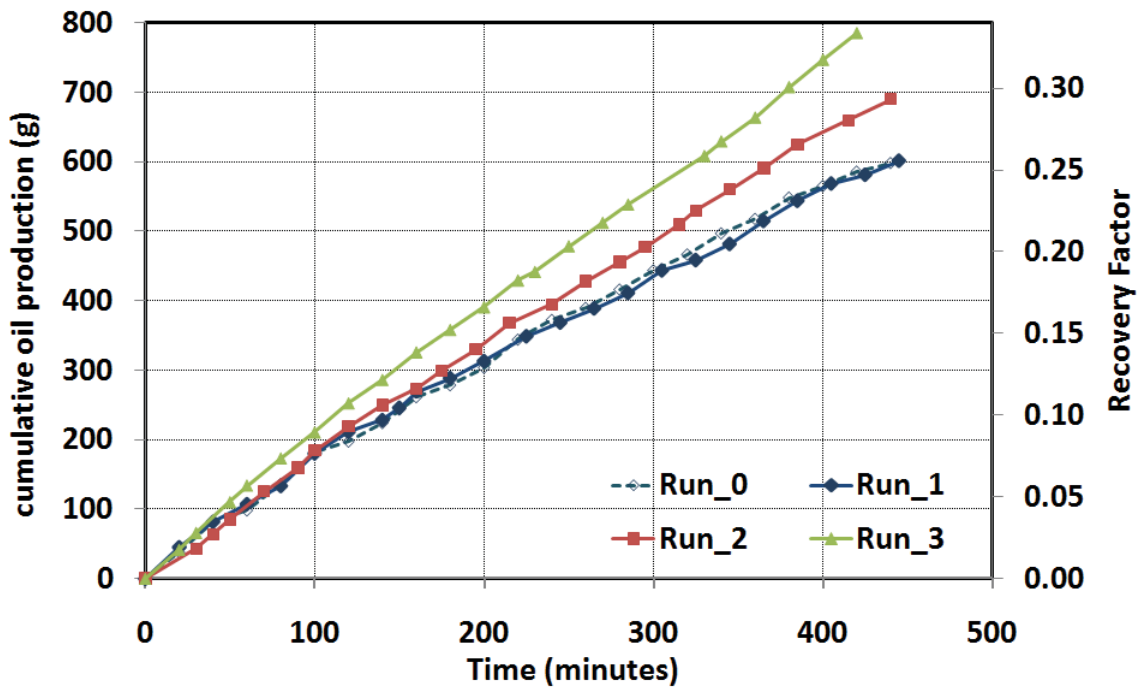


Fig. 41-Comparison of cumulative oil productions and oil recovery factors among experimental runs.

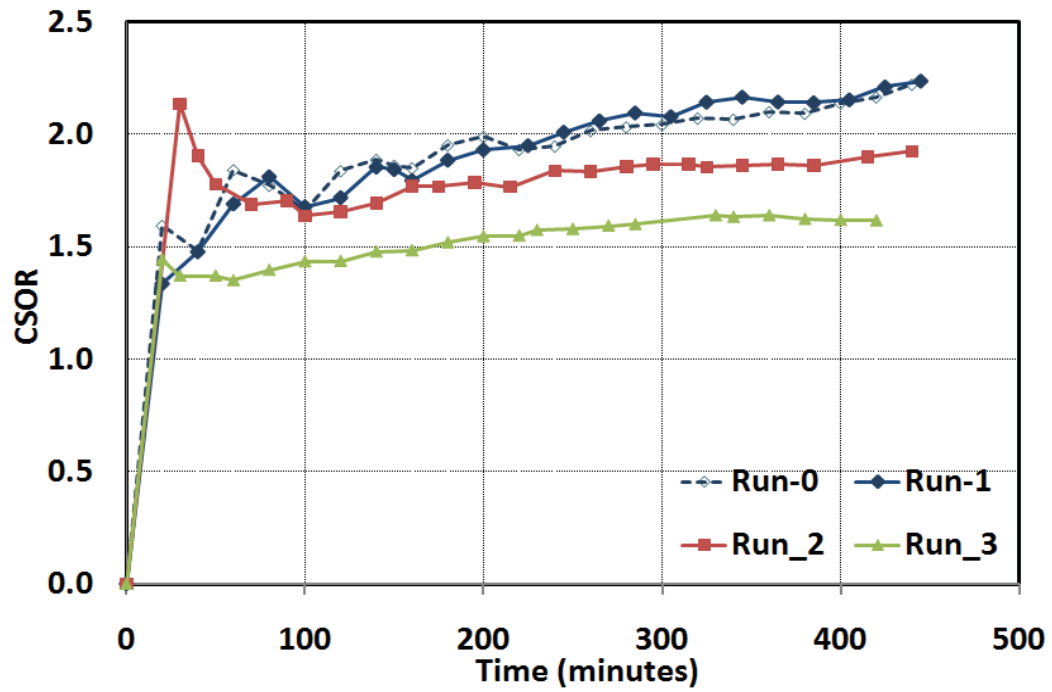


Fig. 42-Comparison of CSOR among experimental runs.

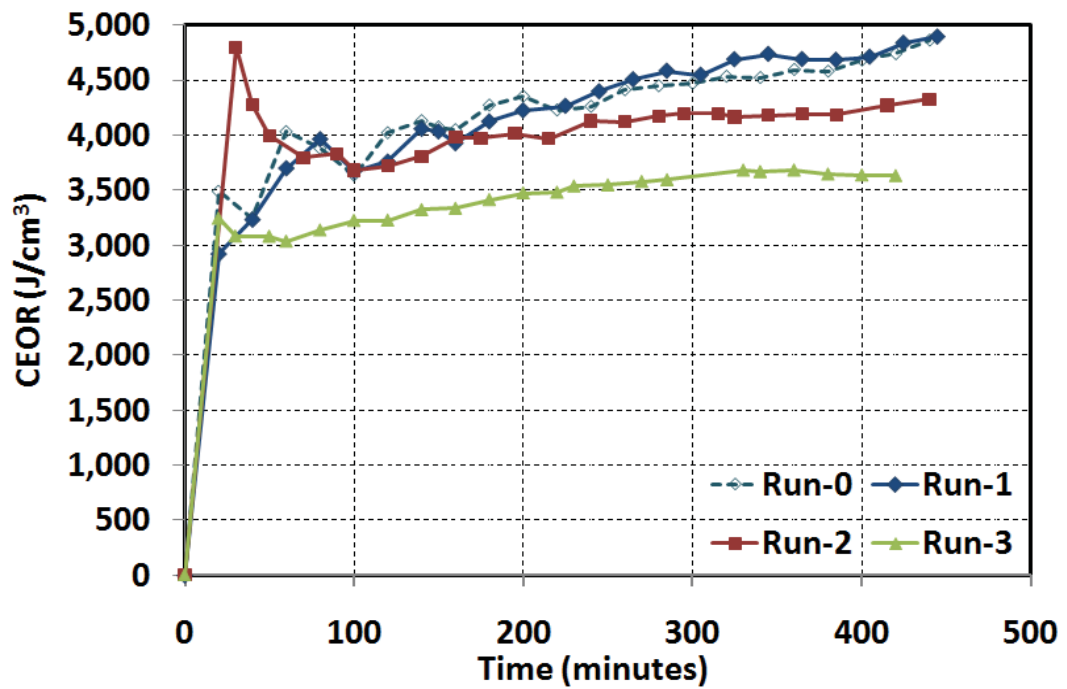


Fig. 43-Comparison of CEOR among experimental runs.

4.5.2 Discussion

The temperature distributions captured by the infrared camera at 4 and 7 hours for all experimental runs are shown in Fig. 44. Both Run 2 and Run 3 show larger vapor chambers than Run 1, which indicates the solvent coinjection improves the vapor chamber propagation. The top area of the vapor chamber for Run 2 forms at much lower temperature than for Run 1 and Run 3, which indicates that vapor C_7 accumulates due to the different traveling fronts of solvent and steam.

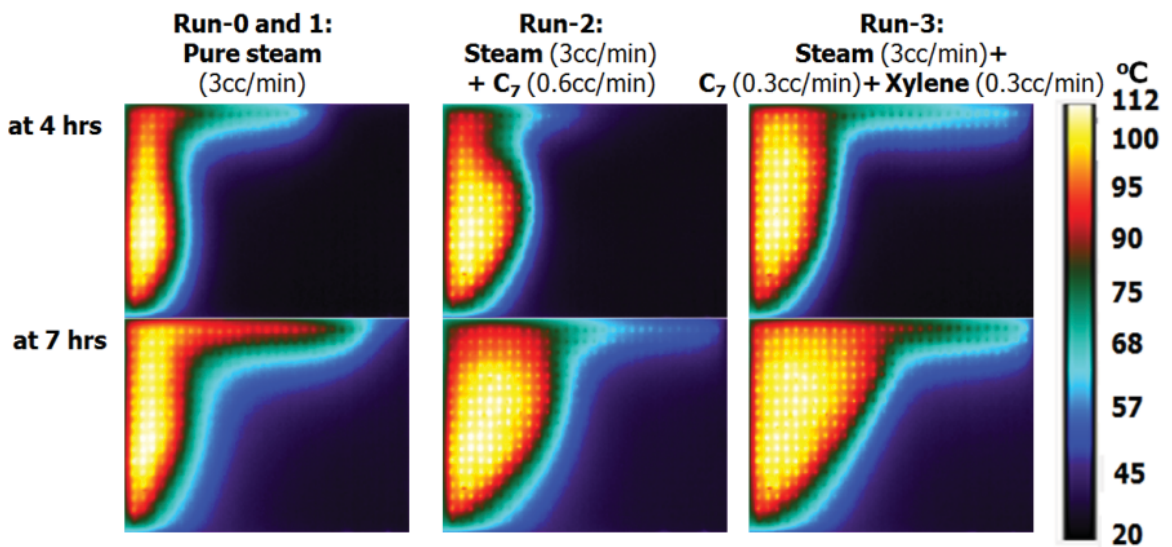


Fig. 44-Comparison of temperature distribution at 4 and 7 hours among experimental runs.

The accumulation of C_7 at the top area reduces the heat loss through the overburden, which is more obvious from the comparison of the lateral propagation of the vapor chamber along the the top edge for Run 1 than for Run 2. Since the injection ratio of the

lighter solvent, C_7 , for Run 2 is higher than for Run 3, more C_7 accumulates along the fluid interface for Run 2 than for Run 3. The accumulation of vapor C_7 along the edge of the fluid interface may impede the heat transfer from the high-temperature vapor chamber to the adjacent low-temperature bitumen.

The accumulation of volatile components inside the vapor chamber has several negative impacts on production performance: altering the condensing condition by partial pressure effect, reducing the heat transfer from vapor chamber to surrounding oil, impeding the heavier hydrocarbon entering into the reservoir, and blocking the contact between the heavier hydrocarbon and bitumen. Considering the in-situ GOR, the detail analysis of partial pressure effect similar as in Gates (2007) is very important to optimize the solvent injection process.

Fig. 45 compares the vapor pressures of solvent and steam for Run 2 and for Run 0 (Run 1). The blue bold circle indicates the saturation temperature of steam at the 8-psig injection pressure for Run 0 (Run 1). Under Run 2, the injection fluid includes about 16.7 vol% C_7 , the partial pressure of steam is reduced from the injection pressure to a lower value, and hence the saturation temperature of steam is reduced to a lower value, which is indicated by the blue dashed circle. The vaporization temperature of C_7 is shown by the red circle at its respective vapor pressure, which is much lower than the temperature of steam. Therefore, the traveling front of C_7 is faster than the steam front. C_7 in the vapor phase starts to accumulate at the top and along the edge of the vapor chamber. Once steam meets the low-temperature fluid interface, steam will condense

earlier than the C_7 vapor. The vapor pressure of C_7 is increased further and finally the C_7 vapor accumulates along the edge of the vapor chamber to build a thick gas blanket.

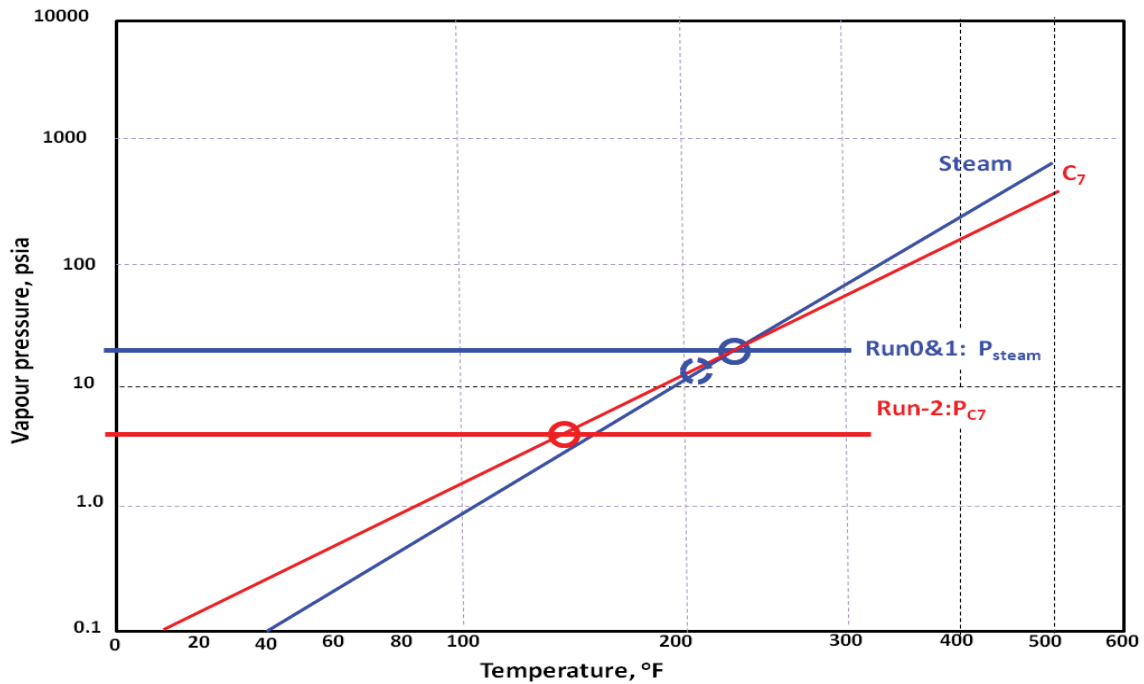


Fig. 45-Comparison of vapor pressure under Run 2 and Run 0 (Run 1).

Fig. 46 compares the vapor pressure for Run 3 and for Run 0 (Run 1). Similar discussion as for Fig. 45 can be applied to Fig. 46. The top orange curve of the band shown in this figure is the bubble-point curve of the solvent mixture used in Run 3, and the bottom green curve of the band represents the dewpoint curve of the solvent mixture.

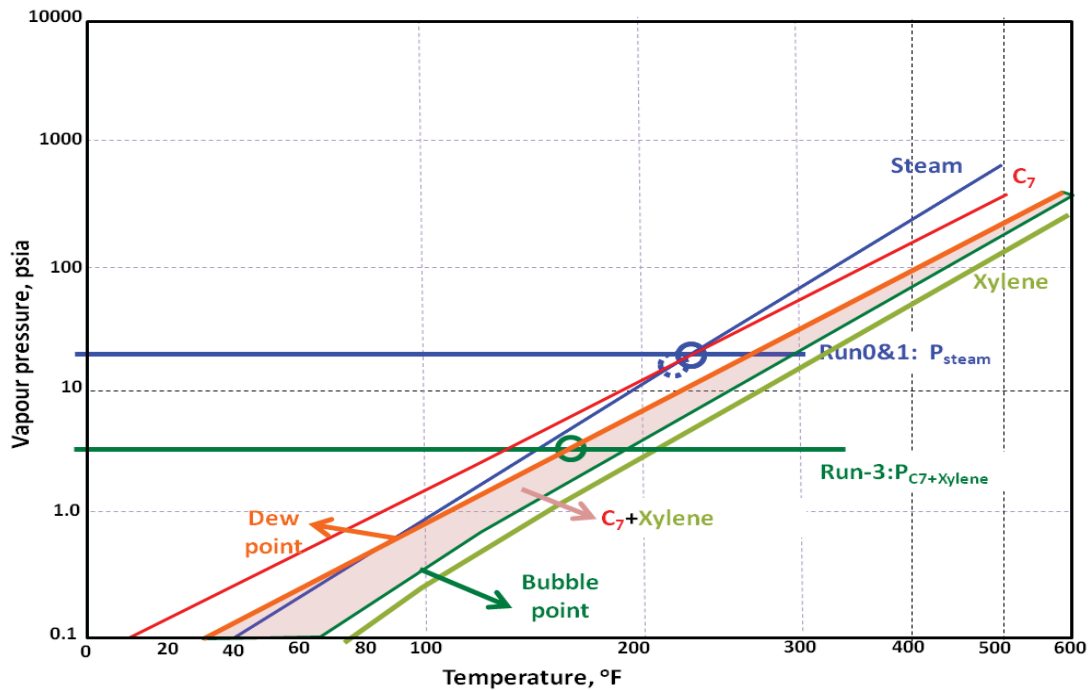


Fig. 46-Comparison of vapor pressure under Run 3 with under Run 0 (Run 1).

The vapor pressure of the solvent mixture for Run 3 is slightly lower than for Run 2 because the injection ratio of C₇ is smaller for Run 3. Therefore, the saturation temperature of the steam is slightly higher than for Run 2, as indicated by the blue dashed circle in Fig. 46. Considering the dynamic condensation process along the fluid interface, the vaporization temperature of the solvent mixture for Run 3 is on the bubble-point curve, as indicated by the green circle in Fig. 46. From the comparison between Fig. 45 and Fig. 46., the difference of the vaporization temperatures between the solvent mixture and steam is less for Run 3 than for Run 2, so the gas blanket effect for Run 3 is expected to be smaller than for Run 2. The resistance to impede heat transfer from the high-temperature vapor chamber to the surrounding low-temperature bitumen is less for Run 3 than for Run 2. From Fig. 44, the temperature at the top area of the vapor chamber

for Run 2 is much less than for Run 3, which indicates more vapor solvent accumulates at the top area for Run 2 than for Run 3.

The relative condensation time of steam and solvent may play another role in affecting the oil flow along the fluid interface. Since the bubble-point of the solvent mixture for Run 3 is higher than the vaporization point of C_7 for Run 2, the solvent mixture for Run 3 is more ready to condense than the C_7 vapor for Run 2. Earlier solvent condensation from vapor to liquid can reduce the viscosity and residual oil saturation of bitumen more efficiently, decrease the dilution effect of water condensate, and increase the mobility of the oil phase.

For a solvent mixture coinjection process in the field, the solvent should be injected at a temperature near its dewpoint to vaporize most components to enter the reservoir, and the production should be operated at a temperature lower than its bubble-point to reduce the breakthrough of injection fluid. Under the condition of Run 3 in the laboratory, xylene is injected and retained inside the vapor chamber by the production control. The density of xylene is lower than that of the condensate, so xylene mainly accumulates at the top of the liquid leg between the injector and producer. When the producer is opened, the condensate at the bottom of the liquid leg is produced first and most of xylene is retained inside the cell. Theoretically, liquid solvent can flush out all residual oil and mix with the oil phase very efficiently. Liquid xylene can accelerate the near-wellbore flow by increasing the mobility of the oil phase and reducing the residual oil saturation in the wellbore vicinity significantly. In addition, the near-wellbore flow may be

accelerated by xylene as it breaks the emulsion and asphaltene precipitation buildup at the producer vicinity.

5. CONCLUSIONS AND RECOMMENDATIONS

5.1 Conclusions

Simulation and experimental research have been performed to better understand the phase behavior and the drainage mechanisms of solvent and steam injection under SAGD process. The following main conclusions may be drawn from the simulation study:

1. In the vapor chamber, the properties and therefore effect of the injected solvent and steam are dependent of their respective vapor pressure. Considering the in-situ gas oil ratio (GOR), the detail analysis of partial pressure effect is very important to design a successful solvent coinjection process.

2. Co-injecting a solvent or solvent mixture with steam near its vaporization point at low concentration can take advantage of the solvent solubility without losing too much the benefit of heat derived from steam.

3. The flow resistance at the end of shale barriers and the extra heat absorbed by the residual water inside the unproductive shale barrier are the main reasons for the shale barrier effects. Long continuous shale barriers located vertically above or near the wellbore delay production performance significantly.

4. Coinjecting a multicomponent solvent can flush out the oil at different areas with different drainage mechanisms from vaporized and liquid components. Additional injector application at the top of the reservoir results only in marginal improvement.

5. High-temperature solvent injection at the solvent condensing condition can take advantages of both the heat and dilution effect of the solvent to reduce the oil viscosity efficiently with no steam required.

Under our laboratory conditions, the oil production rates decrease generally in the following order: Run 3, Run 2, and Run 0 (Run 1). Compared to pure steam injection runs (Run 0 and 1), coinjecting C_7 (Run 2) with steam increases the ultimate recovery factor of oil inside the cell from 25% to 29% , and decreases the ultimate CSOR 2.2 to 1.9 and the ultimate CEOR from 4892 J/cm^3 to 4326 J/cm^3 ; coinjecting C_7 and Xylene (Run 3) increases the ultimate recovery factor of oil from 25% to 34% , and decreases the ultimate CSOR 2.2 to 1.6 and the ultimate CEOR from 4892 J/cm^3 to 3629 J/cm^3 . For a longer experimental time, the difference among different types of runs will be more significantly. Based on analysis of the experimental results, the following conclusions may be drawn:

1. Properly designed steam-solvent injection can improve SAGD performance, resulting in lower steam and energy requirements.
2. Phase changes of solvent and steam occur at their respective vapor pressures instead of at the total injection pressure. Differences in partial vapor pressures result in different relative condensation times along the vapor-bitumen interface.
3. Light hydrocarbons (C_7 in Run 2) can be vaporized by steam and delivered to the entire vapor-bitumen interface to reduce the bitumen viscosity but may build a thick gas blanket that decreases the heat transfer.

4. Coinjecting a suitable multicomponent solvent mixture including solvent in vapor (C_7 in Run 2) and liquid phases (C_7 and xylene in Run 3) may enhance the production performance by altering the condensation dynamics of the light hydrocarbon (C_7).

5.2 Recommendations

1. A large high pressure laboratory model is needed for further study.
2. A visualized physical model is needed to better understand the mechanism of emulsion and asphaltene precipitation at the near wellbore area.
3. Further simulation study is needed to investigate the diffusion and dispersion mechanisms for history matching.
4. Further study is needed to investigate importance of near wellbore flow. Surfactant coinjection may accelerate the near wellbore flow as xylene impact in this study.
5. The uneven phase behavior inside the vapor chamber suggests further optimization study for field operation strategy.
6. The high temperature diluent process requires more technical study and economic evaluation.

REFERENCES

- Beach, I. and Purdy, D. 1997. A Canadian Alliance for Heavy Oil Recovery. Paper SPE -37525-MS presented at the 1997 SPE International Thermal Operation & Heavy Oil Symposium, Bakersfield, California, 10-12 February.
- Belgrave, J.D.M., Nzekwu, B., and Chhina, H.S. 2007. SAGD Optimization with Air Injection. Paper SPE 106901, presented at the SPE Latin American and Caribbean Petroleum Engineering Conference, Buenos Aires, Argentina, 15-18 April.
- Butler, R.M. and Mokrys, I.J. 1991. A New Process (VAPEX) for Recovering Heavy Oils Using Hot Water and Hydrocarbon Vapour. *JCPT* **30** (1):97-106.
- Butler, R.M. and Mokrys, I.J. 1993a. In-situ Upgrading of Heavy Oils and Bitumen by Propane Deasphalting: The VAPEX Process. Paper SPE 25452 presented at SPE Production and Operations Symposium, Oklahoma City, Oklahoma, 21-23 March.
- Butler, R.M. and Mokrys, I.J. 1993b. Recovery of Heavy Oils Using Vaporized Hydrocarbon Solvents: Further Development of the VAPEX Process. *JCPT* **32**(6): 56-62.
- Butler, R.M. and Mokrys, I.J. 1993c. Closed Loop Extraction Method for the Recovery of Heavy Oils and Bitumens Underlain by Aquifers: The VAPEX Process. *JCPT* **37**(4): 41-50.
- Butler, R. M. 1994. *Horizontal Wells for the Recovery of Oil, Gas and Bitumen*. Petroleum Society Monograph. The Petroleum Society of the Canadian Institute of Mining, Metallurgy and Petroleum, Calgary, Canada.
- Butler, R. M. 1997. Steam and Gas Push (SAGP). Paper No. 97-137 presented at the 48th Annual Technical Meeting of Petroleum Society, Calgary, Canada, 8-11 June.

- Butler, R. M. 1999. The Steam and Gas Push (SAGP). *JCPT* **38**(3): 54-61.
- Butler, R., Jiang Q., and Yee C.T. 2000a. The Steam and Gas Push (SAGP)-2: Mechanism Analysis and Physical Model Testing. *JCPT* **39**(4): 52-61.
- Butler, R., Jiang Q., and Yee C.T. 2000b. The Steam and Gas Push (SAGP)-3: Recent Theoretical Developments and Laboratory Results. *JCPT* **37**(8): 51-60.
- Butler, R., Jiang Q., and Yee C.T. 2001. The Steam and Gas Push (SAGP)-4: Recent Theoretical Developments and Laboratory Results Using Layered Models. *JCPT* **40**(1): 54-61.
- Chen, Q., Gerristen, M.G., and Kovsky, A.R. 2007. Effects of Reservoir Heterogeneities on the Steam-Assisted Gravity Drainage Process. Paper SPE 109873 presented at the SPE Annual Technology Conference & Exhibition, Anaheim, California, 11-14 November.
- Chung, K. H. and Butler, R. M. 1987. Geometrical Effect of Steam Injection on the Formation of Emulsions in the Steam-assisted Gravity Drainage Process. Paper SPE 87-38- 22 presented at the 38th Annual Technical Meeting of Petroleum Society, Calgary, 7-10 June.
- ConocoPhillips, 2009. Challenged Resources. <http://www.conocophillips.com/Tech/upstream/challenged/index.htm>, 20 May, 2009.
- Deng, X. 2005. Recovery Performance and Economics of Steam/Propane Hybrid Process. Paper SPE 97760 presented at International Thermal Operations and Heavy Oil Symposium, Calgary, Alberta, Canada, 1-3 November.
- Elliot, K.T. and Kovsky, A.R. 1999. Simulation of Early-time Response of Single-Well Steam Assisted Gravity Drainage (SW-SAGD). Paper SPE 54618 presented at SPE Western Regional Meeting, Anchorage, Alaska, 26-28 May.

- Farouq-Ali, S. M. 1997. Is There Life after SAGD. *JCPT* **36**(6): 20–23.
- Frauenfeld, T.W., Deng, X., and Jossy, C. 2006. Economic Analysis of Thermal Solvent Processes. Paper SPE 2006-164 presented at the Petroleum Society's 7th Canadian International Petroleum Conference (57th Annual Technical Meeting), Calgary, Alberta, Canada, June 13 – 15.
- Frauenfeld, T.W., Jossy, C., and Wang, X. 2007. Experimental Studies of Thermal Solvent Oil Recovery Process for Live Heavy Oil. *JCPT* **46** (11): 40-46.
- Frauenfeld, T.W., Jossy, C., Bleile, J., Krispin, D., and Ivory, J. 2009. Experimental and Economic Analysis of the Thermal Solvent and Hybrid Solvent Processes. *JCPT* **48**(11): 55-62.
- Gates, I.D. 2007. Oil Phase Viscosity Behavior in Expanding-solvent Steam-assisted Gravity Drainage. *JPSE* **59** (2007) 123–134.
- Hein, F. J., and Marsh, R. A. 2008. Regional Geologic Framework, Depositional Models and Resource Estimates of the Oil Sands of Alberta, Canada. Paper 2008-320 presented at the World Heavy Oil Congress 2008, Edmonton, Canada, 10-12 March.
- Ivory, J., Frauenfeld, T.W., and Jossy, C. 2010. Thermal Solvent Reflux and Thermal Solvent Hybrid Experiments. *JCPT* **49**(1): 23-31.
- Kimber, K.D. and Farouq Ali, S.M. 1989. Verification of Scaling Approaches for Steam Injection Experiments. *JCPT* **28** (1) 40.
- Kimber, K.D. and Farouq Ali, S.M. 1991. Scaled Physical Modeling of Steam-Injection Experiments. *SPE* **11**: 467-469.
- Kimber, K.D., Farouq Ali, S.M. and Puttagunta, V.R. 1988. New Scaling Criteria and Their Relative Merits for Steam Recovery Experiments. *JCPT* **27**(4) 86.

- Kisman, K. E. and Yeung, K. C. 1995. Numerical Study of the SAGD Process in the Burnt Lake Oil Sands Lease. Paper SPE 30276 presented at the SPE International Heavy Oil Symposium, Calgary, Alberta, Canada, 19-21 June.
- Law, D. H. S. and Nasr, T. N. 2000. Field-scale Numerical Simulation of SAGD Process with Top-water Zone. Paper SPE 65522 presented at Petroleum Society of CIM International Conference on Horizontal Well Technology, Calgary, Alberta, Canada, 6-8 November.
- Li, W. and Mamora, D. D. 2010. Drainage Mechanism of Steam with Solvent Co-injection under Steam-assisted Gravity Drainage (SAGD) Process. Paper SPE-130802-PP presented at the SPE International Oil & Gas Conference and Exhibition in China (IOGCEC), Beijing, China, 8-10 June.
- Mehrotra, A.K. and Svrcek, W.Y. 1986. Viscosity of Compressed Athabasca Bitumen. *CJCE* **64**: 844-847.
- Nasr, T.N. and Ayodele, O.R. 2005. Thermal Techniques for the Recovery of Heavy Oil and Bitumen. Paper SPE 97488-MS-P presented at SPE International Improved Oil Recovery Conference in Asia Pacific, Kuala Lumpur, Malaysia, 5-6 December.
- Nasr, T.N. and Ayodele O.R. 2006. New Hybrid Steam-solvent Processes for the Recovery of Heavy Oil and Bitumen. Paper SPE 101717 presented at SPE International Petroleum Exhibition and Conference, Abu Dhabi U.A.E, 5-8 November.
- Nasr, T. N. and Isaacs, E. E. 2001. Process for Enhancing Hydrocarbon Mobility Using a Steam Additive. United States Patent, US 6230814.
- Nasr, T. N., Beaulieu, G., Golbeck, H., and Heck, G. 2003. Novel Expanding Solvent-SAGD Process "ES-SAGD". *JCPT* **42**(1):13-16.

- Nenniger, J. and Nenniger, E., 2008. Method and Apparatus for Stimulating Heavy Oil Production. Canadian Patent 2351148.
- Oballa, V. and Buchanan, W. L. 1996. Single Horizontal Well in Thermal Recovery Processes. Paper SPE 37115 presented at the SPE International Conference on Horizontal Well Technology held in Calgary, Canada, 18-20 November.
- Poling, B.E., Prausnitz, J.M., and O'Connell, J. 2000. *The Properties of Gases and Liquids*, 5th edition, McGraw-Hill, USA.
- Polikar, M., Cyr, T.J., and Coates, R.M. 2000. Fast-SAGD: Half the Wells and 30% Less Steam. Paper SPE 65509 presented at the SPE/Petroleum Society of CIM International Conference on Horizontal Well Technology, Calgary, Alberta, Canada, 6-8 November.
- Pooladi-Darvish and M., Mattar, L. 2002. SAGD Operations in the Presence of Overlying Gas Cap and Water Layer: Effect of Shale Layers. *JCPT* **41** (6): 40–51.
- Pujol, L. and Boberg, T.C. 1972. Scaling Accuracy of Laboratory Steam Flooding Models. Paper SPE 4191 presented at the California Regional Meeting of the SPE of AIME, Bakersfield, California, 8-10 November.
- Richardson, J. G., Harris, D. G., Rossen, R. H. and Hee, G. V. 1978. The Effect of Small, Discontinuous Shales on Oil Recovery. *JPT* **30**: 1531–1537.
- Sasaki, K., Akibayashi, S., Yazawa, N., Doan, Q. T., and Farouq Ali, S. M. 2001. Experimental Modeling of the SAGD Process: Enhancing SAGD Performance with Periodic Stimulation of the Horizontal Producer. *SPEJ* **3**:89-97.
- Shu, W.R. 1984. A Viscosity Correlation for Mixtures of Heavy Oil, Bitumen, and Petroleum Fractions. *SPEJ* **6**:277-282.

- Slinghal, A. K. and Card, Colln. C. 1988. Monitoring of Steam Stimulation in the McMurray Formation, Athabasca Deposit, Alberta. SPE-14215-PA, *JPT* **40** (4): 483-490.
- Stalder, J. L. 2005. Cross SAGD (XSAGD)-An Accelerated Bitumen Recovery Alternative. Paper SPE 97647 presented at the SPE International Thermal Operating and Heavy Oil Symposium, Calgary, 1-3 November.
- Stegemeier, G.L., Laumbach, D.D., and Volek, C.W. 1980. Representing Steam Processes with Vacuum Models. *SPEJ* **6**:151-154.
- Thomas, S. 2008. Enhanced Oil Recovery: An Overview, *Oil & Gas Science and Technology* **63**(1): 9-19. DOI: 10.2516/ogst: 2007060.
- Yang, G. and Butler, R. M. 1992. Effects of Reservoir Heterogeneities on Heavy Oil Recovery by Steam-Assisted Gravity Drainage. *JCPT* **31** (8):37-43.
- Zhao, L. 2004. Steam Alternating Solvent Process. Paper SPE 86957 presented at the International Thermal Operations and Heavy Oil Symposium and Western Regional Meeting, Bakersfield, California, 16 -18 March.
- Zhao, L., Law, D.H., and Coates, R. 2003. Numerical Study and Economic Evaluation of SAGD Wind-Down Methods, *JCPT* **42**(1):53-57
- Zhao, L., Nasr, T.N., Hyang, H., Beaulieu, G., Heck, G., and Golbeck, H. 2004. Steam Alternating Solvent Process: Lab Test and Simulation. Paper SPE 2004-044 presented at the Petroleum Society's 5th Canadian International Petroleum Conference, Calgary, Alberta, Canada, 8-10 June.

VITA

Name: Weiqiang Li

Permanent address: 3116 TAMU, Richardson Building
Texas A&M University, College Station, Texas, 77843

Education: B.S. Thermal and Energy Engineering
Shandong University, China, 1997
M.S. Petroleum Engineering
Texas A&M University, College Station, 2007

Member: Society of Petroleum Engineers

Email address: weiqiang.li.us@gmail.com